TECHNICAL REPORT STANDARD TITLE PAGE

1. Report No.	2. Government Accession No.	3. Recipient's Catalog No.

4. Title and Subtitle
IN-PLANE SEISMIC RESISTANCE OF TWO-STORY CONCRETE MASONRY COUPLED SHEAR WALLS

5. Report Date
September 1989

6. Performing Organization Code

7. Author(s)
Kenneth Mark Merryman, Gilberto Leiva, Nicholas Antrobus, and Richard E. Klingner

8. Performing Organization Report No.
PMFSEL 89-3

9. Performing Organization Name and Address
Phil M. Ferguson Structural Engineering Laboratory
The University of Texas at Austin
10100 Burnet Road
Austin, TX 78758

10. Work Unit No.

11. Contract or Grant No.
ECE-8611860

12. Sponsoring Agency Name and Address
National Science Foundation
Washington, D.C.

13. Type of Report and Period Covered

14. Sponsoring Agency Code

15. Supplementary Notes

16. Abstract

To study the in-plane resistance of multi-story masonry coupled walls, 6 full-scale reinforced masonry specimens, each two stories high, are being constructed and tested in the laboratory as part of the U.S.-Japan Masonry program (TCCMAR). All specimens are of fully grouted hollow concrete masonry. Three specimens are pairs of walls, coupled by floor slabs with and without lintels. Three other specimens are single walls with door and window openings. In this paper, the design, construction, and testing of two of the coupled wall specimens are described. The specimens were loaded vertically by constant loads representing gravity loads on the shear wall's tributary area, and horizontally by quasi-static, reversed cyclic shear loads applied in the plane of the walls at the two floor levels. Test results are presented, discussed, and compared with analytical predictions of specimen performance. Implications of the results for design and test procedures are discussed.

17. Key Words	18. Distribution Statement
structural engineering, testing, lateral forces, walls, cyclic loading, masonry, buildings, earthquake engineering	

19. Security Classif. (of this report)	20. Security Classif. (of this page)	21. No. of Pages	22. Price
Unclassified			

Form DOT F 1700.7 (8-69)

IN-PLANE SEISMIC RESISTANCE OF TWO-STORY CONCRETE MASONRY COUPLED SHEAR WALLS

by

Kenneth Mark Merryman
Gilberto Leiva
Nicholas Antrobus
and
Richard E. Klingner

Report on a Research Project
Sponsored by
National Science Foundation
Grant No. ECE-8611860

Phil M. Ferguson Structural Engineering Laboratory
Department of Civil Engineering
BUREAU OF ENGINEERING RESEARCH
THE UNIVERSITY OF TEXAS AT AUSTIN

September 1989

This report presents the results of a research project which was part of the U.S. Coordinated Program for Masonry Building Research. The program constitutes the United States part of the United States - Japan Coordinated Masonry Research Program conducted under the auspices of the Panel on Wind and Seismic Effects of the U.S.-Japan Natural Resources Development Program (UJNR).

This material is based on work supported by the National Science Foundation under the direction of Program Director Dr. A.J. Eggenberger.

Any opinions, findings, and conclusions or recommendations expressed in this publication are those of the authors and do not necessarily reflect the views of the National Science Foundation and/or the United States Government.

ACKNOWLEDGEMENTS

The research described here is part of the U.S. Coordinated Program for Masonry Building Research (TCCMAR), and is supported by the National Science Foundation (Grant No. ECE-8611860). The work was carried out at the Phil M. Ferguson Structural Engineering Laboratory, Balcones Research Center, The University of Texas at Austin under the direction of Dr. Richard E. Klingner.

The authors thank the past and present undergraduates who worked on this project: Alex Gonzales, David Franzen, Mohamed Alyusuf, Tom Estrel, and David Dorr, without whose hard work the completion of this research could not have been possible.

The authors thank all the Ferguson Lab staff members for their assistance on this project. Special thanks to Blake, Dick, Wayne L., Pat, Wayne F., and Alec for their help on the floor, and to Irene, Laurie, Sharon, Maxine, Jean and Jennifer for help in answering numerous questions.

Table of Contents

List of Tables

List of Figures

1. INTRODUCTION

1.1 General

This research is concerned with the in-plane seismic resistance of two- story concrete masonry coupled walls. It is part of the U.S. Coordinated Program for Masonry Building Research directed by the Technical Coordinating Committee for Masonry Research (TCCMAR).

The U.S. Coordinated Program for Masonry Building Research, funded by the National Science Foundation, consists of a set of separate but coordinated tasks, intended to address the basic issues of masonry material and structural response to gravity and seismically induced loads. The program is divided into 10 tasks: 1) materials; 2) mathematical models; 3) walls; 4) intersections; 5) floors; 6) construction; 7) small-scale models; 8) design methods; 9) full-scale building; and 10) design recommendations and criteria development [1].

Task 3 (Walls) is divided into sub-tasks dealing with in-plane and out- of-plane loading. The in-plane load section, Task 3.1, consists of tests on: a) single-story panels without floor joints or openings; b) three-story walls without floor joints or openings; and c) two-story walls with openings and floor joints. This research is part of Task 3.1(c).

In Task 3.1(c) of the TCCMAR Program, 6 full-scale reinforced masonry walls, each two story high, will be constructed in the laboratory. All specimens will be of fully grouted hollow concrete masonry. Three specimens will be single walls with door and window openings and three specimens will be pairs of walls, coupled by various floor systems with and without lintels.

This research will involve the two coupled walls without lintels (Type 2 Specimen). The two floor systems investigated are floors spanning perpendicular to the shear walls (cast-in-place slab system) and floors spanning parallel to the shear walls (precast plank slab system). The Type 2 specimens represent a pair of coupled shear walls in a two-story building.

1.2 Scope and Objectives

1.2.1 Objectives of TCCMAR Task 3.1(c). The overall objectives of Task 3.1(c) are to examine how the in-plane seismic resistance of multistory concrete masonry walls is affected by floor-wall joints, wall openings, and floor elements.

1.2.2 Objectives of Previous TCCMAR Task 3.1(c) Research. The objectives of previous research in TCCMAR Task 3.1(c) were to:

a) design the two-story concrete masonry coupled shear wall specimens,

b) design and construct the loading apparatus and test setup; and

c) design the instrumentation of the first specimen.

That previous research was largely carried out by Antrobus, and is described in Reference 2. Material from that reference has been used for Chapters 2, 4, and 5 of this thesis with modifications for the specific scope of this research.

1.2.3 Objectives of this TCCMAR Task 3.1(c) Research. The specific objectives of this research are:

a) to verify the behavior of the lateral loading system test setup;

b) to examine the cyclic shear resistance of the coupled wall systems;

c) to examine the behavior of the floor-wall joint connection for a cast-in-place slab system and for a precast plank slab system;

d) to examine the coupling effectiveness (under reversed cyclic loads) of the floor systems without lintels;

e) to compare experimental results with predicted behavior of coupled shear walls; and

f) since this project is a coordinated research, to make the test results available to the other researchers in the TCCMAR program, and to the engineering community at large.

2. BACKGROUND

2.1 General

In this chapter, coupled wall behavior will be discussed briefly (Section 2.2). The behavior of reinforced concrete coupled walls will first be reviewed. The behavior of reinforced masonry coupled walls will then be discussed. In Section 2.3, the materials composing the masonry coupled walls will be briefly discussed.

2.2 Coupled Walls

2.2.1 General. Structural walls often require openings to accommodate windows and doors. When the openings are arranged in a pattern that allows interaction of two or more walls through slab and/or beams, the system is termed a "coupled wall." The performance of coupled walls is governed by the characteristics and behavior of the individual walls and the coupling system, and of the interaction between them.

2.2.2 Coupled Wall Behavior. A single cantilever wall must resist gravity loads and lateral forces. Coupled walls must resist gravity loads, lateral forces, and also the additional actions due to the coupling system. Under lateral load, the coupling system develops shears and moments, and transmits these to the walls. With reference to Figure 2.1, the equilibrium equation of the coupled wall system is:

$$M_o = M_1 + M_2 + L * T$$

where M_o is the total base overturning moment, M_1 and M_2 are the moments at the base of each wall about the plastic centroids of the walls, L is the length between the plastic centroids of the coupled walls, and T is the total shear force transferred by the coupling system between the walls.

Figure 2.1 compares the flexural resisting mechanisms of: (a) a solid cantilever wall; (b) coupled walls with strong coupling beams; and (c) coupled walls with weak coupling beams. The walls and the coupling system contribute some of the total overturning moment. At ultimate, the shear transferred between the walls varies with the strength of the coupling system. If the coupling system is weak, the amount of shear transfer will be small (Fig. 2.1(c)). The L*T parameter is small compared to M_1 and M_2, and the walls behave almost as independent cantilever walls with a slight increment in axial load induced by the coupling system. With strong coupling beams, the shear transferred by the coupling system is large

Lime gives workability and water retentivity, and contributes to tensile bond strength. The sand acts as an inert filler. The water is used as a mixing vehicle, and also creates plastic workability and initiates cementitious action. Both the plastic and hardened properties of the mortar are significant.

The properties of plastic mortar are related primarily to its construction suitability. The most important of these are workability and water retentivity. As specified in ASTM C270-87a, workability is measured using a flow test, and water retentivity of mortar is expressed as the ratio of flow after suction to initial flow.

While compressive strength is not the only important property of hardened mortar, it is the only one currently specified in ASTM C270-87a.

2.3.2 Typical Concrete Masonry Units. Concrete masonry units are typically made with zero-slump Portland cement concrete and lightweight aggregate. The concrete is vibrated under pressure in multiple-block molds and then steam-cured.

Concrete masonry units can be produced for load bearing and non-load bearing applications and can be made as solid or hollow units. Load- bearing concrete masonry units are covered in specification ASTM C90-86 (Hollow and Solid Load-Bearing Concrete Masonry Units), which prescribes the classification, materials, dimensional variations, and sampling and testing of the units.

A concrete masonry unit's relevant mechanical properties are its compressive strength, tensile strength, absorption, initial rate of absorption (IRA), modulus of elasticity, shrinkage and coefficient of thermal expansion. Testing for compressive strength and absorption is covered in ASTM C140-75 (Sampling and Testing Concrete Masonry Units). The procedure for determining a unit's initial rate of absorption is covered in ASTM C67 (Sampling and Testing Brick and Structural Clay Tile). Testing for modulus of elasticity and tensile strength are not covered in ASTM specifications. Testing of the drying shrinkage of concrete block is explained in ASTM C426-70 (Drying Shrinkage of Concrete Block).

2.3.3 Typical Masonry Grout. Masonry grout is used to fill some or all of the cells in hollow-core units, and between the wythes of a multi-wythe wall. As specified in ASTM C476-83 (Grout for Masonry), masonry grout is composed of Portland cement, sand, pea gravel, and water; it can also contain hydrated lime and additives.

Grout workability is achieved by the use of sufficient water to achieve a 10- to 12-inch slump. In spite of this high initial water content, subsequent compressive strength is satisfactory because the grout loses water to the units after placement. The problem of high shrinkage due to this water content is resolved by using water-retention agents.

The primary mechanical property of hardened grout is its compressive strength, tested as defined in ASTM C1019-84 (Sampling and Testing Grout).

2.3.4 Typical Masonry Assemblages. Masonry units are bonded together with mortar to form a masonry assemblage, which then can be filled with grout if desired. The primary properties of the assemblage are its tensile bond strength, compressive strength, shear strength and durability.

Before grouting, tensile bond strength is dependent on the bond between the mortar and the units. It is influenced by the elapsed time between spreading the mortar and laying the masonry unit, the suction of the unit, the water retentivity of the mortar, the pressure applied to the masonry joint during placement, the tooling of the joint, the texture of the masonry units' bedded surfaces, and the curing conditions. After grouting, tensile bond strength is also influenced by the tensile strength of grout. Tensile bond strength can be measured using ASTM C1072 (Masonry Flexural Bond Strength), ASTM E518 (Flexural Bond Strength of Masonry) or ASTM E72 (Conducting Strength Tests on Panels for Building Construction).

Compressive strength of a masonry assemblage is usually measured using stack-bonded prisms following ASTM E447-80 (Test Method for Compressive Strength of Masonry Prisms). The prisms generally fail due to transverse splitting. Mortar, usually more flexible than the units, expands laterally under compression and places the units in transverse biaxial tension.

Shear strength of a masonry assemblage can be measured following ASTM E519 (Diagonal Tension in Masonry Assemblages). The test is conducted using a 4-foot-square panel, loaded in compression along one of its diagonals. The test places the specimen in a stress state of diagonal compression and is intended to simulate shear in a real structure.

The durability of masonry is primarily related to the freeze-thaw resistance of the units, the efflorescence characteristics of the units, the water permeance of the masonry assemblage, and the quality of workmanship [12].

The only durability test in ASTM for concrete masonry units is that for water permeance of the masonry assemblage. Water permeance testing is an attempt to simulate the effects of wind-driven rain. Water permeance is measured in terms of the amount of water passing through a wall under a standard pressure gradient, and is covered in ASTM E514 (Water Permeance of Masonry).

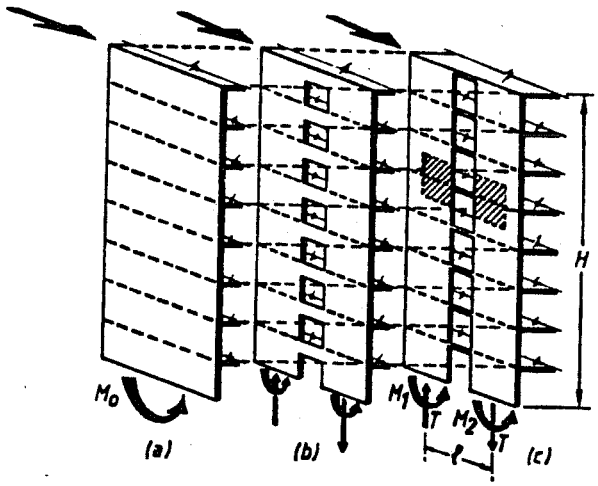

Figure 2.1 A Comparison of Flexural Resisting Mechanisms in Structural Walls [3].

in relation to M_1 and M_2 (Fig. 2.1(b)). The contribution of the of the L*T term to the total overturning moment is significant, and the coupled walls behave more like a single cantilever wall [3].

The failure modes of the coupled wall include: failure of the coupling system; flexural failure of the walls; shear failure of the walls; and sliding shear of the walls. Figure 2.2 illustrates the failure modes which could occur in the walls of a coupled wall system.

The coupling system can fail due to flexure or shear in the coupling beam, and also by failure of the connection between the coupling beam and the wall. For a slab coupling system, punching shear failure of the slab is another possibility.

Flexural failure of the walls involves crushing of the compression toe of a wall and/or the yielding of the vertical reinforcement of the wall.

Shear failure of the wall can involve diagonal tensile cracking of the walls, or shear sliding of the wall. Shear sliding can occur at the base, or along flexural cracks that extend across the wall length.

The walls should be designed to prevent a shear failure from occurring. A coupled wall system should be designed to have a ductile flexural failure of the walls. Design characteristics for the coupled wall system should include: a ductile coupling system to dissipate

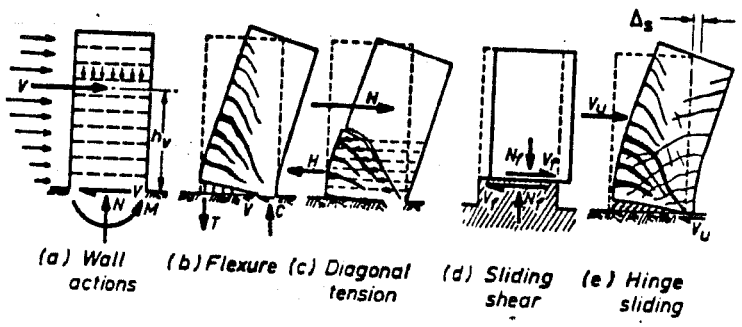

Figure 2.2 Failure Modes in Cantilever Walls [3].

energy which would protect the walls from early damage; a stable hysteretic response; and plastic hinging of the walls' bases and of the coupling beams [4].

The flexural behavior of a reinforced masonry wall is similar to that of a reinforced concrete wall. Therefore, the theory developed for reinforced concrete members is also used for reinforced masonry walls [5,6,7]. However, shear behavior of reinforced masonry walls differs from that of reinforced concrete walls. Extensive research is addressing the shear resisting mechanisms of reinforced masonry walls [8,9]. At present, the shear strength design equations for reinforced concrete walls are generally used for shear design of reinforced masonry walls [5,6,10].

2.3 Typical Masonry Materials

2.3.1 Typical Masonry Mortar. The primary purpose of mortar is to bond units into an integral assemblage [11]. The mortar separates the units and also holds them together. Material properties and proportions for mortar are defined in ASTM specification C270-87a (Mortar for Unit Masonry).

Masonry mortar generally is composed of Portland cement, lime, sand, and water. Portland cement contributes to the compressive strength and high early strength of mortar.

3. SPECIMENS' DESCRIPTION AND DESIGN

3.1 Description of Specimens

3.1.1 General. As shown in Figure 3.1, the three Type 2 specimens are coupled walls. The specimens rest on a reinforced concrete base beam. The specimens have one central door opening 3.33 ft (1015 mm) wide and 8.0 ft (2440 mm) high without a lintel over the opening. They are two-story concrete block walls 8.0 ft (2440 mm) high, 6 inches (150 mm) thick, and 16.67 ft (5080 mm) long, with floors 8 inches (200 mm) thick, and extending 3.0 ft (914 mm) from the lateral faces of the wall.

Figure 3.1 Type 2 Specimens: Coupled Walls

The specimens are designed to represent an internal shear wall in a two-story building with a flat roof. The prototype shear walls are 16.67 ft (5080 mm) long, and are assumed to be 20 ft (6096 mm) apart. A possible location of the specimen within the

Figure 3.2 Prototype Building Floor Plan

prototype building is shown in Figure 3.2. The walls of the prototype building are assumed to be rigidly connected to an immovable foundation.

The coupled wall element designations are shown in Figure 3.3. The walls are denoted as first-story and second-story walls; and with the base of the coupled wall considered the first floor, the floors slabs are designated as second-story and roof.

The second-floor and roof are replicated in the models by a floor slab extending 3.0 ft (914 mm) from each face of the wall. It was assumed that the effective floor width contributing to the stiffness and strength of the wall would lie within this width [4].

Under gravity loads, the floor system can act in either of two different ways:

1) If the floors span perpendicular to the plane of the coupled walls, the tributary floor load is carried by the coupled walls in the prototype building.

2) If the floors span parallel to the plane of the coupled walls, the floor load is not carried by the coupled walls in the prototype building.

In either case, the floor loads on the prototype coupled walls must be accurately replicated in the test specimens.

Figure 3.3 Coupled Wall Element Designations

3.1.2 Overall Description of Specimen 2a. The floors, without lintels, were assumed to span perpendicular to the coupled walls (Fig. 3.4). In such a situation, it would be unrealistic in practice to construct a floor of precast planks, as the planks would have no bearing surface at the wall openings without lintels. Therefore, the floors were assumed to be of cast-in-place reinforced concrete, 8 inches (200 mm) thick.

3.1.3 Overall Description of Specimen 2b. The floors were assumed to span parallel to the shear walls, which have no lintels at the openings (Fig. 3.4). As is typical of such construction, the floors were assumed to be of precast, prestressed concrete planks, 6 inches (152 mm) thick, with a 2-inch (50 mm) thick reinforced topping of cast-in-place concrete.

3.2 Specimen Design and Details

3.2.1 General. The coupled wall system was considered as part of the prototype building (Fig. 3.2). The elements of the coupled wall system were designed using the general provisions of the 1985 Uniform Building Code [13] for gravity and seismic loads. Although the 1988 Uniform Building Code [10] is the most current code, the 1985 UBC is used throughout because the preliminary design was performed in September 1987. The desired behavior for the specimens was a ductile flexural failure. The wall shear reinforcement and slab transverse reinforcement were designed based on the flexural capacity of the specimens.

Figure 3.4 Actual Specimen Location in Prototype Building

3.2.2 Structural Design and Details of Walls. Vertical reinforcement was designed based on the seismic provisions of the 1985 Uniform Building Code [13] for Zone 4. The shear reinforcement was designed based on the flexural capacity of the specimens. A detailed explanation of the design is given in Appendix A of this thesis, and is taken from Reference 14.

Block Layout for All Specimens

The walls were constructed of hollow lightweight units measuring 6 inches thick by 8 inches high by 16 inches long (152 x 203 x 406 mm) for full units, and 8 in. long (203 mm) for half units (Fig. 3.5). All full units are open at one end. All courses with horizontal reinforcement were laid using bond-beam units with one open end. Units were laid in running bond as shown in Figures 3.6 and 3.7 for Specimen 2a and 2b, respectively.

Wall Reinforcement for All Specimens

Wall reinforcement is arranged as shown in Fig. 3.8 for Specimen 2a and Specimen 2b. Vertical reinforcement consisted of 5 #4 bars (13 mm) placed at 16 in. centers (406 mm) in each wall ($\rho_v = 0.00248$). Vertical reinforcement was lap spliced to dowels in the base, using a 40d lap (20 in. or 510 mm). Horizontal reinforcement in the first-story was #4 bars (13 mm) every course ($\rho_h = 0.00444$). Horizontal reinforcement in the second-story

Figure 3.5 Concrete Masonry Units: Full and Half Unit

was #4 bars in every other course ($\rho_h = 0.00222$). All horizontal bars were anchored to the end vertical bars with 180-degree hooks.

3.2.3 Structural Details of Floors.

Specimen 2a Floor Slab

Floors were made of cast-in-place concrete, 8 in. (203 mm) thick.

As shown in Figure 3.9, transverse reinforcement in the top of the slab consisted of #5 bars (16 mm) spaced at 10 in.(254mm) with a $\rho' = 0.00388$, and in the bottom of the slab, of #4 bars (13 mm) spaced at 10 in. (254 mm) with a $\rho = 0.00250$. Transverse reinforcement requirements were governed by the required flexural capacity, in the prototype building, of a continuous slab spanning 20 ft. (6096 mm) between the shear walls [2]. Longitudinal reinforcement requirements are governed by shrinkage and temperature steel requirements for the prototype building. Longitudinal reinforcement consisted of #3 bars (10 mm) spaced at 12 in. (305 mm). As shown in Fig. 3.9, additional longitudinal reinforcement, consisting of four #4 bars (13 mm), was placed in the slab directly over the shear walls to provide extra flexural strength in the portion of the slab which was envisioned to act as a coupling beam between the two walls ($\rho = \rho' = 0.00206$). These #4 bars were enclosed by #3 ties (10 mm) placed at 3-in. centers (76 mm) between the walls.

Figure 3.6 Specimen 2a Block Layout

Specimen 2b Floor Slab

As shown in Figure 3.10, floors consisted of two precast planks measuring 6 in. thick (152 mm), 16.67 ft. long (5080 mm) and 3 ft. wide (914 mm). An 8-in. thick beam (200 mm) was cast between the planks, and a 2-in. thick topping slab was cast over them.

Longitudinal reinforcement for the precast planks consisted of four GR 270 3/8 in. strands (10mm) running the length of the each plank ($\rho^* = 0.00152$). Longitudinal

Figure 3.7 Specimen 2b Block Layout

reinforcement requirements of the precast slab were based on the 1985 Uniform Building Code [13] gravity load requirements on the slab in the prototype building. As shown in Fig. 3.10, additional longitudinal reinforcement, consisting of four #4 bars (13 mm), was placed between the precast planks directly over the shear walls to provide extra flexural strength in the portion of the slab which acted as a coupling beam between the two walls. These #4 bars were enclosed by #3 ties (10 mm) placed at 3-in. centers (76 mm). Topping reinforcement, based on minimum shrinkage and temperature steel requirements for the prototype building,

Figure 3.8 Specimen 2a and 2b Wall Reinforcement

Figure 3.9 Specimen 2a Slab Reinforcement Detail

Figure 3.10 Specimen 2b Slab Reinforcement Detail

consisted of WWF 6 x 6 x 6/6 (152mm x 152mm x 5.2mm/5.2mm), placed approximately at the midheight of the 2-in. topping slab (for top reinforcement: $\rho = 0.00097$, for bottom reinforcement: $\rho' = 0.00090$).

3.3 Material Tests

3.3.1 General. In this section, results of tests conducted on the materials used to construct the masonry walls are described. Masonry components, concrete, and reinforcement were tested according to specifications mentioned in the subsequent sections. In order to obtain representative material properties, most tests were performed immediately after completion of the wall tests.

3.3.2 Concrete Masonry Unit Tests. To ensure basic material uniformity, all concrete units for this and other TCCMAR tasks were manufactured by Blocklite (Selma, California). The units were specified to be Type I units (moisture-controlled), and to conform to the requirements of ASTM C90 (Hollow Load-Bearing Concrete Masonry Units).

Unit weight of two full-sized hollow units was determined by measuring the weight of sand required to fill the unit holes. Knowing the bulk specific weight of the sand, the net volume of the unit was calculated as the difference between its gross volume and the sand volume. The units were 15-9/16 in. long, 5-5/8 in. wide, and 7-1/2 in. high. Their average unit weight was 99.0 lb/ft^3, and their average area ratio (net volume/gross volume) was 0.6. Complete results are given in Table 3.1.

Table 3.1 Results of Concrete Block Unit Weight Measurements

Unit	Weight (lb)	Gross Vol	Net Vol	Unit Weight (pcf)
1	22.72	0.380	0.228	99.6
2	22.64	0.380	0.230	98.3
Av				99.0

Table 3.2 Results of Concrete Block Unit Compressive Strength Tests

Unit	Load (Kip)	Compressive Strength (psi)	
		Gross Area	Net Area
1	74.25	848	1414
2	64.58	737	1230
3	79.88	912	1521
Av		830	1390
COV		11%	11%

To determine compressive strength, 3 units were tested in accordance with ASTM C140 (Sampling and Testing Concrete Masonry Units). Compressive strength was calculated using both the gross and the net area. Results are given in Table 3.2.

3.3.3 Mortar Tests. The mortar conformed to the proportion specification for Type S mortar as specified in ASTM C270 (Mortar for Unit Masonry). It was proportioned (by volume) to have 1 part of portland cement, 1/2 part hydrated lime, and 4-1/2 parts of masonry sand.

a) Portland cement conformed to Type I (general purpose) of ASTM C150 (Portland Cement).

b) Lime conformed to Type S of ASTM C207 (Hydrated Lime for Masonry Purposes).

c) Sand was natural, and was specified to conform to ASTM C144 (Aggregate for Masonry Mortar).

Tests were conducted using both laboratory and field mortars. Before building the specimens, flow tests were conducted on laboratory mortars, to establish a water content giving a flow of just over 110. Two-in. mortar cube specimens were taken from this mix and tested to provide an index of relative mortar strength and quality to enable a comparison to be made with similarly tested mortars used by other researchers. Results are summarized in Table 3.3.

During construction of each story of the specimens, flow tests were conducted on field mortars taken from the mason's board. Two-in. (51-mm) cube specimens were taken and tested in accordance with ASTM C780 (Preconstruction and Construction Evaluation of Mortars for Plain and Reinforced Concrete Masonry). In some cases, additional 3- x 6-in. (76- x 152-mm) cylinders and 2- x 4-in. (51- x 102 mm) cylinders were taken and tested. Results are summarized in Table 3.4.

Table 3.3 Laboratory Mortar Test Results

Specimens	Age (days)	Average Compressive Strength (psi)	Coeff. of Variation
3 2-in. cubes	14	3260	4%
3 2-in. cubes	31	3380	3%

Table 3.4 Field Mortar Test Results

Sample	Specimens	Age (days)	Average Compressive Strength (psi)	Coeff. of Var.
Sp-2a Story 1	3 2-in cubes	16	800	3%
	2 3-in cyl.	16	600	-
	3 2-in cubes	28	690	10%
	5 3-in cyl.	113 (test)	1150	5%
Sp-2a Story 2	3 2-in cubes	76 (test)	1230	2%
Sp-2b Story 1	9 2-in cubes	156 (test)	1640	13%
	4 2-in cyl.	156 (test)	1330	4%
Sp-2b Story 2	9 2-in cubes	100 (test)	1770	9%
	7 2-in cyl.	100 (test)	1650	10%

3.3.4 Grout Tests. The grout conformed to the coarse grout specification of ASTM C476 (Grout for Masonry). Proportions (by volume) were 1 part portland cement to 3 parts masonry sand to 2 parts pea gravel. To control water loss and shrinkage of the grout, Type 2 Grout-Aid, manufactured by Sika, was used at a dosage of one pound of Grout-Aid to one bag of cement. Sand and pea gravel conformed to ASTM C404 (Aggregates for Masonry Grout).

During the grouting of each story, 3-in. (76-mm) grout prisms were formed in absorptive molds in accordance with ASTM C1019. They were subsequently tested in accordance with ASTM C39 (Standard Method of Test for Compressive Strength of Cylindrical Concrete Specimens). Additional 2-in. and 3-in cylinders were taken from grout poured in hollow units using a core drill and were then tested. Results are summarized in Table 3.5.

Table 3.5 Grout Test Results

Sample	Specimens	Age (days)	Average Compressive Strength (psi)	Coeff. of Var.
Sp-2a Story 1	3 3-in. prism	28	5320	5%
	1 3-in. prism	104 (test)	5410	-
	5 3-in. cores	104 (test)	4040	19%
Sp-2a Story 2	3 3-in. prism	69 (test)	4690	8%
	4 3-in. cores	69 (test)	4420	10%
Sp-2b Story 1	4 3-in. prism	154 (test)	5480	6%
	3 2-in. cores	154 (test)	3250	9%
Sp-2b Story 2	4 3-in. prism	88 (test)	4930	10%
	3 2-in. core	88 (test)	2470	27%

3.3.5 Prism Tests. During the construction of each story the mason constructed several full unit prisms, each 3 units high. The prisms were grouted simultaneously with the walls, consolidated using the same mechanical vibrators, and cured under the same conditions as the walls. Compression tests were performed in accordance with ASTM E447 (Compressive Strength of Masonry Prisms). Results are summarized in Table 3.6.

3.3.6 Concrete Tests. All concrete used was generally in accordance with the requirements of ACI 318-83 [15]. Concrete for the base beams had a specified compressive

Table 3.6 Prism Test Results

Sample	Specimens	Age (days)	Average Compressive Strength (psi)	Coeff. of Var.
Sp-2a Story 1	3 prisms	104 (test)	2020	19%
Sp-2a Story 2	4 prisms	69 (test)	2340	8%
Sp-2b Story 1	4 prisms	154 (test)	3090	10%
Sp-2b Story 2	4 prisms	88 (test)	2510	14%

strength of 6,000 psi (41.4 MPa). Concrete for the floor slabs had a specified compressive strength of 4,000 psi (27.6 MPa).

During the pouring of each floor slab, 6-in. (152-mm) diameter cylinder specimens were taken in accordance with ASTM C31 (Making and Curing Concrete Test Specimens in the Field), and were subsequently tested in accordance with ASTM C39. Results are summarized in Table 3.7.

Table 3.7 Slab Concrete Test Results

Sample	Specimens	Age (days)	Average Compressive Strength (psi)	Coeff. of Var.
Sp-2a Floor 2	3 6-in. cyl.	7	4250	12%
	3 6-in. cyl.	90 (test)	5280	1%
Sp-2a Roof	5 6-in. cyl.	57 (test)	3660	9%
Sp-2b Floor 2	6 6-in. cyl.	117 (test)	5220	2%
Sp-2b Roof	5 6-in. cyl.	65 (test)	3670	6%

3.3.7 Reinforcement Tests. Reinforcement conformed to Grade 60 of ASTM A615 (Deformed and Plain Billet Steel Bars for Concrete Reinforcement).

Within each bar size, all reinforcement for each specimen was intended to be taken from the same heat. However, due to an oversight in ordering materials, the reinforcement in Specimen 2a came from multiple heats.

Specimens from each heat of reinforcement were tested in tension, and stress-strain curves were obtained. Deformations were measured using a Tinius-Olsen extensometer over a 8-in. gauge length. Only cases in which the specimen fractured within the gauge length were considered. Typical stress- strain curves are given in Fig. 3.11 - 3.14.

Figure 3.11 Typical Stress-Strain Curve for Specimen 2a & 2b Dowel Reinforcement

Figure 3.12 Typical Stress-Strain Curve for Specimen 2a Vertical Reinforcement

Figure 3.13 Typical Stress-Strain Curve for Specimen 2a Longitudinal Reinforcement of Slabs

Figure 3.14 Typical Stress-Strain Curve for Specimen 2b Reinforcement except Starter Rebars

4. CONSTRUCTION OF SPECIMENS

4.1 General

The specimens were constructed in the Phil M. Ferguson Structural Engineering Laboratory, located at the Balcones Research Center of the University of Texas at Austin. The general construction sequence is given in Section 4.2. Each step of the construction sequence is then discussed further in subsequent sections [2].

Many of the items in the construction sequence were not related to the specimens, but rather to the test setup: base beams, vertical and lateral loading frames, and sway braces. These items were designed to be used with both the Type 1 and the Type 2 specimens, and were designed in accordance with the predicted lateral load capacity of the Type 1 specimens, which was predicted to exceed that of the Type 2 specimens [2].

4.2 Construction Sequence

1) Two precast concrete base beams were constructed.

2) The first-story wall was built on one of the precast concrete base beams.

3) The formwork for the second-floor was erected.

4) The first-story walls were grouted.

5) For Specimen 2a, the steel for the second-floor slab was placed, and the second-floor slab was cast. For Specimen 2b, the precast planks for the second-floor slab were placed. The reinforcement was then placed and the second-floor slab was cast.

6) After checking the concrete compressive strength, the formwork was removed and the floor was re-shored.

7) The second-story wall was built.

8) The formwork was re-erected on the second-floor. The first-floor sway braces were attached, and temporary bracing was attached from the top of the second-story wall to the reaction wall.

9) The second-story wall was grouted.

10) For Specimen 2a, the reinforcement for the roof was placed, and the roof slab was cast. For Specimen 2b, the precast planks for the roof were placed. The reinforcement was then placed and the roof slab was cast.

11) After checking the concrete compressive strength, the formwork and re-shores were removed, and permanent sway bracing was attached to the roof slab.

12) The loading hardware was attached to the reaction wall.

13) The hydraulic actuators were attached to the loading hardware, and the necessary hydraulic connections were made.

14) After exercising the actuators to flush the lines, the servocontrollers were connected and calibrated.

15) The loading beams were connected to the specimen, and the actuators were connected to the loading beams.

16) The vertical loading frame was erected, and the necessary hydraulic connections were made.

17) The data acquisition system was connected and checked out.

4.3 Construction of Concrete Base Beams

The reinforced concrete base beam was constructed in two halves outside the laboratory. Both halves were poured at the same time using ready-mixed concrete. Three 6-in. (152 mm) diameter cylinders were taken during the pouring of the beams. The concrete was vibrated into place using electric vibrators. Each part had five #4 (13 mm) vertical dowels (starter bars) for the wall reinforcement. Horizontal reinforcement was left protruding, and a shear key was provided at one end.

After the two halves of the base beam had cured for 14 days, they were transported into the laboratory and placed in position with the 25-ton overhead travelling crane. The protruding longitudinal bars from each half were lapped and surrounded with ties. The two halves were then joined by casting a small make-up piece in the center.

To permit two specimens to stand at once in the laboratory, two concrete base beams were constructed and placed on the laboratory floor. The concrete base beams are shown in Figure 4.1. The foundation dowels for the first-story of the first two specimens were cast in place with the beams, and later cut to the predetermined length. The base beams were re-used for subsequent tests. After the first two specimens were tested and removed, the old foundation dowels were cut off flush with the base. For subsequent tests, holes were drilled 14 inches deep in the base beam, and new foundation dowels were inserted and secured with an epoxy-based structural adhesive.

Figure 4.1 Concrete Base Beams

4.4 Construction of Masonry Walls

All masonry walls were laid by an experienced mason in running bond, as shown in Figures 4.2 - 4.3. The first-story walls were constructed using bond beam units for every course. After the walls were built to their full height of 8.0 ft (2440 mm) and the first-story formwork was erected, all cores were grouted using a single lift. Grout was consolidated using 3/4-in. electric vibrators. The vibrators were placed in the cores and turned on. Grout was placed in the cores, and the vibrators were slowly withdrawn during the grouting operation. Grouting of the walls is shown in Figures 4.4 and 4.5. The second- story walls were similarly constructed, the only exception being that the horizontal reinforcement was only placed in every other course in bond beam units, and the alternate courses were built with full units.

For Specimen 2a in order to check for grout flaws and voids in the walls, nondestructive testing was performed on the walls prior to testing by a participating TCCMAR group [16]. The two test methods used were the Japanese "Beat-wall" mechanical pulse flaw detection system, and the through-wall ultrasonic pulse velocity method. Suspicious areas were marked to be checked after testing. When testing was completed, grout was exposed in the marked areas by chipping away the concrete masonry unit. No evidence of grout flaws or voids was found.

Figure 4.2 Construction of Masonry Wall

Figure 4.3 Completed Construction of Masonry Wall

Figure 4.4 Placing Grout in Masonry Walls

4.5 Construction of Slabs

4.5.1 Formwork for Slabs. Formwork consisted of 3/4-inch plywood on 2-x 4-inch joists spaced at 16 inches. The formwork was made in four sections (two for each side of the specimen), erected on 4- x 4-inch timber shores and bolted together. Each shore was topped by a steel screw jack, used for leveling the forms before pouring, for removing the forms after

Figure 4.5 Vibrating Grout in Masonry Walls after Placement

curing, and for preloading the re-shores against the underside of the finished slab. Pairs of shores, 3 ft. apart, were spaced at 4-foot centers. The formwork is shown in Figure 4.6.

4.5.2 Reinforcement for Slabs. For both specimens, a reinforcement cage was constructed to run the length of the wall at the slab-wall connection.

Figure 4.6 Formwork Setup for Roof Slab

For Specimen 2a, the slab reinforcement was placed in two layers, each supported on steel slab bolsters. Numerous plastic pipes were attached to the formwork and the reinforcement to provide bolt holes for the attachments to the lateral loading frame and the sway bracing. Figure 4.7 shows the reinforcement for Specimen 2a.

For Specimen 2b, the slab reinforcement consisted of welded wire fabric placed on top of the precast planks. The bolt holes for the attachments to the lateral loading frame

Figure 4.7 Specimen 2a: Slab Reinforcement

were drilled after casting the slab topping. Figure 4.8 shows the reinforcement for Specimen 2b.

4.5.3 Concrete Placement for Slabs. Concrete was placed using a bottom-opening bucket lifted into place by a travelling overhead crane. The concrete was vibrated into place with electric vibrators. Figures 4.9 shows a typical slab casting.

4.5.4 Re-shores for Slabs. When the concrete had reached an adequate strength, the screw jacks were released, and the formwork was unbolted and slid out sideways. After sliding 2-x 4-inch boards onto the jack heads, other 2-x 4-inch boards, 3-ft. long, were placed perpendicular to the first boards on the jacks. The jacks were then tightened, lightly loading the boards against the underside of the slab.

Figure 4.8 Specimen 2b: Slab Reinforcement

Figure 4.9 Typical Slab Casting

5. TEST SETUP, INSTRUMENTATION AND TESTING PROCEDURE

5.1 Test Setup

5.1.1 General. As shown in Figures 5.1 to 5.3, the overall test setup consisted of the following elements:

1) reaction system
2) precast base beams
3) vertical loading frames
4) lateral loading frame
5) sway bracing

Lateral loads, representing seismic loads, were applied to the outer edges of the floor and roof at the midpoints of each coupled wall by hydraulic actuators attached to steel frames mounted on the reaction wall. Simple steel link sway bracing was attached to the outer edges of the second-floor and the roof and anchored to the reaction wall running parallel to the specimen's in- plane centerline.

For Specimen 2a, vertical load was applied to represent floor and roof gravity loads transferred from the slabs to the coupled walls in the prototype building but not in the specimen. The vertical load was applied to the top of the second-story of each coupled wall by hydraulic actuators attached to a steel frame mounted on the reaction floor. The elements comprising the test setup are described in more detail in the following sections [2].

5.1.2 Reaction System. This consisted of a massive reinforced concrete floor and two walls, 19 ft. (5790 mm) high, and joined at right angles. The floor and walls have anchor bolt locations, each with four anchor bolts, on a 4-ft. (1219 mm) square grid. Each floor anchor bolt location has an allowable vertical loading of plus or minus 200 kips (890 kN), and each wall anchor bolt location has an allowable horizontal loading of plus or minus 100 kips (445 kN) [17].

5.1.3 Concrete Base Beam. The concrete base beam was connected to the testing floor using 12 prestressing rods, each consisting of a 1-1/4 in. (32 mm) diameter ASTM 193 B7 rod prestressed to 25 kips (111 kN). Prestressing provided adequate lateral frictional resistance between the base and the reaction floor without allowing any slippage or the imposition of shear forces on the threads of the tie-down rods.

Figure 5.1 Vertical Loading Frame (Specimen 2a only)

5.1.4 Vertical Loading Frame. For Specimen 2a, which represents a prototype in which the floors span perpendicular to the shear walls, the walls of the prototype building carry a tributary floor loading which exceeds the self-weight of the specimen plus the loading hardware. The floor loads considered are:

a) the floor dead load of 80 psf (391 kg/m^2)

b) a partition load of 20 psf (98 kg/m^2)

Figure 5.2 Lateral Loading Frame

Figure 5.3 Sway Bracing

c) a floor finish of 5 psf (24 kg/m^2)

d) an HVAC load of 8 psf (39 kg/m^2)

e) a live load of 50 psf (244 kg/m^2), reduced for tributary area in accordance with Section 2306 of the 1985 Uniform Building Code [13].

The summation of all these loads results in a total vertical load of 37.15 kips/wall (92.2 psi). The calculations are shown in Appendix A: Design Criteria. Each wall weighs 16.15 kips, and the loading system weighs approximately 1.6 kips. To produce a mean axial compressive stress of 92.2 psi at the base of the coupled walls, an additional vertical load of 19.4 kips must be applied to each wall.

This vertical load was applied by a steel frame located at the out-of- plane centerline of each of the two coupled walls (Fig. 5.1). A spreader beam was used to distribute the load into the top slab along the in-plane centerline of each of the coupled walls. The spreader beam was attached with a pinned coupling to a yoke going across the specimen. Using a long 1-inch diameter rod, one end of the yoke was connected to an anchor plate attached to the reaction floor. Using another long 1-inch diameter rod, the other end of the yoke was connected to a hydraulic actuator mounted on an anchor plate attached to the floor. The hydraulic actuators for each vertical loading frame were operated in parallel under control

of an Edison load maintainer, so that as the specimen rocked under the lateral loading, the vertical load was held constant. All connections between the spreader beam and the yoke, the yoke and the rods, and the rods and the anchor plates were designed as pinned to allow for up to plus or minus 6 in. (152 mm) of horizontal movement, and 1 in. (25 mm) of vertical movement of the wall during the test.

5.1.5 Lateral Loading Frame. Layout of the lateral loading frame is shown in Figure 5.2. Using the 1986 AISC Load and Resistance Factor Design Specifications [18], the frame was designed to withstand a live load equal to the maximum actuator capacity, multiplied by a load factor of 1.6.

Lateral loads were applied to the specimens using 4 two-way hydraulic actuators, each with a capacity of 112 kips (498 kN). The stationary ends of the actuators were attached to a steel frame bolted to the reaction wall, and oriented perpendicular to the plane of the specimens. The other end of each actuator was attached to the center of a steel beam with a pinned connection at each end. The pinned connections were bolted to the outer edge of each floor slab at the out-of-plane centerline of each coupled wall. The purpose of the pinned connections was to allow for independent vertical, horizontal and rotational movements of each of the coupled walls during the test.

5.1.6 Sway Bracing. The sway bracing, shown in Figure 5.3, was designed to control out-of-plane movement of the specimens during testing. Four simple braces connected one outer corner of each floor slab with the reaction wall running parallel to the in-plane centerline of the specimen. The steel double angle braces were each designed to resist a load of 10% of one actuator's maximum load, again using a load factor of 1.6.

5.2 Instrumentation

5.2.1 General. The Ferguson Laboratory's data acquisition system has 140 channels of instrumentation. The system was configured to read up to 60 quarter-bridge and 80 full-bridge devices. Selected channels were monitored during each test. Data from all channels were read at discrete load points throughout each test, and were stored in digital form. They were then reduced and plotted using standard microcomputer spreadsheet programs. The instrumentation is shown in Figures 5.4 to 5.7 for Specimen 2a, and in Figures 5.8 to 5.11 for Specimen 2b. Numbers in those figures refer to channel numbering used for each gauge. The functions of the instrumentation are described in the following sections.

5.2.2 Measurement of Applied Loads. Lateral loads were measured using load cells placed on the actuators at each floor level, and were monitored continually during testing.

Figure 5.4 Specimen 2a: Displacement Transducers

For Specimen 2a, vertical loads were controlled using the Load Maintainer, were continually monitored using a load cell placed on one rod (Fig. 5.1), and were checked with the pressure gauge on the Load Maintainer.

5.2.3 Measurement of Overall Lateral Displacements. Wall lateral displacements were measured using linear potentiometers at each end of each floor level. At the south end of the roof slab, three linear potentiometers were connected to the specimens. The first linear potentiometer was used to read displacement for the data acquisition system. The second

Figure 5.5 Specimen 2a: Strain Gauges on Vertical Reinforcement

was connected to a plotter to continuously monitor the top floor displacement during the test. The third was used for operating the test under load control.

For Specimen 2a (Fig. 5.4) and Specimen 2b (Fig. 5.8), Channels 30, 31, 61 and 62 were used to read the overall lateral displacement.

5.2.4 Measurement of Flexural Deformations in Walls. Flexural deformations were measured using 4 sets of linear potentiometers on both extreme fibers of each wall. Channels

Figure 5.6 Specimen 2a: Strain Gauges on Horizontal Reinforcement

1-16 and 32-47 were used as shown in Figure 5.4 for Specimen 2a, and in Figure 5.8 for Specimen 2b.

5.2.5 Measurement of Shearing Deformations in Walls. Shearing deformations were measured using one set of crossed linear potentiometers on each story of each wall. Channels 17-20 and 48-51 were used to monitor these potentiometers, as shown in Figure 5.4 for Specimen 2a, and in Figure 5.8 for Specimen 2b.

Figure 5.7a Specimen 2a: Strain Gauges for Second Story Slab

Figure 5.7b Specimen 2a: Strain Gauges for Roof Slab

Figure 5.8 Specimen 2b: Displacement Transducers

5.2.6 Measurement of Slip. Relative horizontal movement between the base beam and the laboratory floor was measured by a linear potentiometer. Channel 63 was used to monitor this movement as shown in Figure 5.4 for Specimen 2a and Figure 5.8 for Specimen 2b.

Relative horizontal movement between the walls and the base beam was measured by linear potentiometers just above the base beam. This movement was monitored with Channels 21 and 52, as shown in Figure 5.4 for Specimen 2a, and in Figure 5.8 for Specimen 2b.

Figure 5.9 Specimen 2b: Strain Gauges on Vertical Reinforcement

Relative horizontal movement between the walls and the slabs was measured by linear potentiometers above and below the second-floor slab, and by linear potentiometers below the roof slab. Channels 22-23 and 53-54, Figure 5.4 for Specimen 2a and Figure 5.8 for Specimen 2b, were used for the relative movement above and below the second-floor slab. Channels 24 and 55 were used for the linear potentiometers below the roof slab, as shown in Figure 5.4 for Specimen 2a, and in Figure 5.8 for Specimen 2b.

5.2.7 Measurement of End Rotations of Coupling Beams. Rotations were measured by a set of linear potentiometers placed at each end of each coupling beam. Channels 25-28

Figure 5.10 Specimen 2b: Strain Gauges on Horizontal Reinforcement

and 56-59 were used for the monitoring of these potentiometers, as shown in Figure 5.4 for Specimen 2a, and in Figure 5.8 for Specimen 2b.

5.2.8 Measurement of Strains in Reinforcement and Concrete. Strains were measured using electrical resistance strain gauges placed on the vertical reinforcement and horizontal wall reinforcement. The concrete slab had strain gauges on longitudinal reinforcement. Specimen 2a also had strain gauges placed on the concrete surface.

Figure 5.11a Specimen 2b: Strain Gauges for Second Story Slab

Figure 5.11b Specimen 2b: Strain Gauges for Roof Slab

Vertical reinforcement strain gauge locations and channel numberings are shown in Figure 5.5 for Specimen 2a, and in Figure 5.9 for Specimen 2b. Horizontal strain gauge locations and channel numberings are shown in Figure 5.6 for Specimen 2a, and in Figure 5.10 for Specimen 2b. Specimen 2a had strain gauges placed on the longitudinal steel across the slab width and on the surface of the concrete, as shown in Figure 5.7. Specimen 2b only had strain gauges placed on the longitudinal steel which formed the beam between the precast planks, as shown in Figure 5.11.

5.3 Testing Procedure

5.3.1 General. The loading history followed was based on the Sequential Phased Displacement (SPD) loading history [19] shown in Figure 5.12. The SPD loading history begins as a series of reversed cyclic loads to monotonically increasing maximum displacements up to a displacement denoted as the First Major Event (FME). The First Major Event corresponds to some significant predicted specimen behavior such as first flexural cracking of the walls. After reaching the FME, the SPD loading history can be visualized as a series of displacements to 1.0, 1.25, 1.50 and 2.0 times the FME displacement.

5.3.2 Loading Sequence. Due to the stiffness of the wall, testing began under load control. Base shears were keyed to the base shear corresponding to the First Major Event (FME). Once the lateral displacement at the top of the wall was large enough to be controlled, the loading system was switched to displacement control. The subsequent loading history was then based on the First Major Event displacement.

During the testing of Specimen 2a, the Sequential Phased Displacement loading history was modified slightly. As shown in Fig. 5.12, each series of displacements involved about 37 different load points, each requiring several minutes of data acquisition and echo-printing. Because the First Major Event corresponded to a very small displacement, many series of displacements were required to reach significant lateral drift levels. Testing took 4 days. To shorten the time somewhat, the displacement sequence for some parts of the testing was changed from (1.0, 1.25, 1.5, 2.0) to (1.0, 1.5, 2.0).

For Specimen 2b, the Sequential Phased Displacement loading history was again modified. Based on the knowledge obtained from testing Specimen 2a, the First Major Event was keyed to a larger displacement than for Specimen 2a. Also, the displacement sequence was modified to increase in increments of 100, 200, 400, 800, and 1600 percent of the First Major Event. Since the loading increments were increased, a reading was added at the midpoint between the last load series maximum point and the next load series maximum point.

5.3.3 Tasks Conducted at Each Load Point. At each load point, readings from all channels were scanned, stored and printed. During the first and last cycles at each displacement level, all cracks were marked and photographs were taken. Videotape recordings were made during the first cycle at each of the higher displacement levels. Also, for Specimen 2b, cracks were marked and photographs were taken at midpoint between the last load series maximum point and the next load series maximum point.

6. PREDICTION OF WALL BEHAVIOR

6.1 General

In this chapter, analyses to predict the behavior of the coupled shear wall specimens are described, and the results obtained are discussed. Two approaches were considered in analyzing the walls: a simple plastic analysis for the collapse mechanism; and a step-by-step nonlinear analysis of the walls under monotonically increasing lateral loads.

In all analyses, wall capacity was assumed to be controlled by flexural behavior. According to a capacity design philosophy, elements were provided with shear capacities larger than the shear forces associated with the development of the flexural strength of the system. The elements were also assumed to have enough deformation capacity to develop a collapse mechanism with no deterioration of strength. Deformations by sliding shear were not considered.

Since the flexural behavior of lightly reinforced concrete masonry elements is well described by the theory developed for reinforced concrete members [5,6,7], the wall specimens of this study were analyzed using the general methodology developed for reinforced concrete sections under eccentric axial load.

6.2 Material Properties

6.2.1 Properties of Reinforcing Steel. Results of tests on reinforcement are shown in Subsection 3.3.7 (Reinforcement Tests).

6.2.2 Properties of Prestressing Steel. Behavior curves given in the PCI Design Handbook [20] were used.

6.2.3 Properties of Masonry. Since the masonry component tests had not been performed at the time Specimen 2a was analyzed, an estimated value of 3000 psi for the masonry compressive strength f'_m was used. Based on the results of Specimen 2a material tests, a value of $f'_m = 2200$ psi was used for Specimen 2b. The behavior of the masonry was modeled using the curve given by Kent and Park [21].

6.2.4 Properties of Concrete. Based on 7-day compressive strength of 4250 psi, an estimated value of $f'_c = 5700$ psi was used for the concrete slabs of Specimen 2a. Since no test data were available at that time, the specified value of $f'_c = 4000$ psi was considered for Specimen 2b. For the precast planks, the specified f'_c of 5000 psi was used. The behavior of the concrete was modeled using the curve given by Kent and Park [21].

6.3 Simple Plastic Analysis

6.3.1 Collapse Mechanism. A simple plastic analysis of a flexural collapse mechanism was performed. This mechanism, shown in Fig. 6.1, assumes the development of plastic hinges at the ends of coupling elements and at the wall bases. The walls are assumed to rotate about their compression toes, and all deformations were assumed to be concentrated at the plastic hinges. The ultimate lateral load obtained from such a mechanism is an upper bound to the actual lateral capacity of the system [22].

Applying the principle of virtual work to the collapse mechanism, the following equation is derived:

$$M_o\delta\Theta = (M_1 + M_2)\delta\Theta + (2N_g - N_1 - N_2)(\ell_w/2)\delta\Theta + 2(M_{s1} + M_{s2})\delta\alpha \quad (1)$$

Where

M_o : Overturning moment capacity of the system

N_g : Externally applied axial load on each wall

N_1, N_2 : Total axial load at the wall bases

M_1, M_2 : Flexural capacity at the wall bases associated to axial forces N_1 and N_2

M_{s1}, M_{s2} : Flexural capacity of coupling elements

ℓ_w : Length of wall section

$\delta\Theta$: Virtual rotation of wall bases

$\delta\alpha$: Virtual rotation of coupling element end sections

ℓ : Distance between walls

For small rotations,

$$\delta\alpha = (1 + \ell_w/\ell)\delta\Theta \quad (2)$$

Equilibrium of vertical forces gives:

$$2N_g - N_1 - N_2 = 0 \quad (3)$$

Figure 6.1 Assumed Collapse Mechanism

The coupling system transmits an axial force N between the walls. This force, equal to the total shear associated with the flexural capacities of the coupling elements, is given by:

$$N = 2(M_{s1} + M_{s2})/\ell \tag{4}$$

Substituting Equations (2) to (4) into Equation (1), the expression of the overturning moment capacity of the system is obtained:

$$M_o = M_1 + M_2 + N(\ell + \ell_w) \tag{5}$$

The total lateral load capacity V_u is given by:

$$V_u = M_o/[h(2+\beta)] \tag{6}$$

Where

β : Ratio between load acting on 2nd floor and load acting on roof

h : Story height

As determined from equilibrium, the shear force taken by each wall is then:

$$V_1 = [(1 + \beta)/(2 + \beta)]\,[M_1 + N(\ell + \ell_w)/2]/h \tag{7}$$

$$V_2 = [(1 + \beta)/(2 + \beta)]\,[M_2 + N(\ell + \ell_w)/2]/h \tag{8}$$

6.3.2 Element Flexural Capacities.

Coupling Systems

The following assumptions were considered in computing the flexural capacity of the coupling systems:

a) Given the characteristics of the loading system, no axial load was assumed to act on the coupling elements.

b) The effective width was taken equal to the total width of the slabs.

c) The flexural capacity of elements was computed at a maximum concrete strain of 0.003.

d) The end sections of the coupling systems were assumed able to maintain their flexural capacity until the wall collapse mechanism was developed.

In the case of Specimen 2a (cast-in-place slab), the slab flexural capacity was calculated using the RCCOLA computer program [23]. The nominal flexural capacities were computed as $M_{s1} = M_{s2} = 760.1$ kip-in.

In the case of Specimen 2b (precast plank) the composite section was analyzed assuming plane sections. The nominal flexural capacities were M_{s1} = 1343 kip-in and M_{s2} = 478 kip-in.

Walls

The following assumptions were made in computing the flexural capacity of the walls:

a) Each wall was assumed to act under an axial load equal to the gravity loads plus the total shear force transmitted through the coupling system when the coupling elements had reached their flexural capacities.

b) Each wall's flexural capacity was assumed to correspond to a maximum masonry strain of 0.003.

d) The base sections of the walls were assumed to maintain their flexural capacities until the overall collapse mechanism had developed.

For the given values of the axial loads, the flexural capacities of the wall base sections were calculated using a microcomputer version of the RCCOLA computer program [23]. Nominal flexural capacities are given in Table 6.1.

Table 6.1 Nominal Flexural Capacities of Walls

Specimen	Grav Load	Coupl Shear	Total Axial Load		Flexural Capacity	
	N_g (Kip)	N (Kip)	N_1 (Kip)	N_2 (Kip)	M_1 (K-in)	M_2 (K-in)
2a	37.2	54.2	-17.0	91.4	3319	5510
2b	12.7	65.2	-52.5	77.9	2209	4764

6.3.3 Lateral Load Capacity. The lateral load capacity of each specimen, computed using Equation (7) for $\beta = 1$ (equal forces at each level), was as follows:

a) Specimen 2a: 101 kips

b) Specimen 2b: 102 kips

6.4 Nonlinear Step-by-Step Analysis

6.4.1 Geometric Modelling. The coupled walls were modeled and analyzed as planar frames (Fig. 6.2). Walls were represented by columns placed at the plastic centroids of the wall sections. Coupling elements were represented by beams rigidly connected to the columns. The beams were modeled with rigid ends equal in length to half of the wall length. Columns were assumed to be fixed at their bases.

Figure 6.2 Geometric Model for Nonlinear Step-by-Step Analysis

Since axial deformations of the walls were expected to be negligible, the position of the column elements with respect to the wall cross section was not expected to influence the inelastic response [3].

6.4.2 Element Properties. Material properties and behavior were as described in Chapter 2. The moduli of elasticity of the masonry and concrete were assumed to remain constant during the loading process, and were taken equal to $57{,}000\sqrt{f'_m}$ and $57{,}000\sqrt{f'_c}$ respectively (psi units).

For each level of axial load, the stiffnesses of the reinforced concrete and reinforced masonry member sections were calculated using the RCCOLA computer program [23]. This program analyzes reinforced concrete member sections under combined moment and axial load, for given concrete and steel stress-strain curves. A similar analysis was performed for the prestressed concrete elements.

In addition to the assumptions already mentioned in Section 6.3.2, it was assumed the inelastic action was concentrated in zero-length hinging regions at the bases of the walls and at the ends of the coupling beams.

6.4.3 Description of Nonlinear Analysis. The planar frame model of the coupled walls was subjected to an incremental collapse analysis under monotonically increasing lateral loads. Each increment in load was defined by the occurrence of a major event in one or more elements. A major event could be first flexural cracking of an element, yielding of the extreme flexural reinforcement of an element, or attainment of flexural capacity in an element. Each load increment was determined by performing an elastic analysis using the member properties calculated for that increment.

The steps followed during the analysis process are described in the following paragraphs:

a) The analysis was started with the coupled wall system under the actions of gravity loads. Elements were assumed to have the elastic properties corresponding to the gross masonry/concrete cross section. The increment in lateral load necessary to produce first flexural cracking (usually in the tension wall) was then calculated. In the case of Specimen 2a, a value of 40 psi was assumed for f_{mt}, the modulus of rupture of the masonry. Based on the results of the Specimen 2a tests, a much higher value $f_{mt} = 4\sqrt{f'_m} = 188$ psi was used for Specimen 2b.

b) The elastic properties of each cracked element were modified using that element's moment-curvature curve, for the axial load level corresponding to first cracking.

c) The load increment necessary to produce a new major event was calculated. The total lateral load, lateral displacements, and internal forces at the end of the new increment were given by the superposition of the initial values and those calculated at that increment.

d) The elastic properties of each element were modified using the moment-curvature curve for the axial load level corresponding to the end of the last increment.

e) Steps (c) and (d) were repeated until the collapse mechanism described in Section 3 was developed.

Results of these analyses, presented in the form of base shear versus lateral displacements, are shown in Tables 6.2 and 6.3, and Figures 6.3 and 6.4 for Specimens 2a and 2b respectively.

Table 6.2 Predicted Base Shear-Displacement History for Specimen 2a

Base Shear (Kip)	Top Sipl (in)	Event
13.0	0.012	Flex crack at base of tension wall
15.0	0.014	Flex crack at base of comp wall
50.9	0.070	Steel yielding at base of tens wall
53.3	0.074	Steel yielding at 2nd floor slab
63.3	0.11	Steel yielding at roof slab
72.7	0.19	Steel yielding at base of comp wall
87.2	0.59	Flexural capacity of compressed wall
98.0	1.59	Flexural capacity of tensioned wall collapse mechanism

Table 6.3 Predicted Base Shear-Displacement History for Specimen 2b

Base Shear (Kip)	Top Displ (in)	Event
21.6	0.020	Flex crack at base of tens wall
26.3	0.026	Flex crack at base of comp wall
34.5	0.041	Steel yielding at base of tens wall & Flex crack at 2nd floor slab top face
42.0	0.061	Flex crack at roof slab top face & Steel yielding at 2nd floor slab top face
43.4	0.066	Flex crack at top of 1st story tens wall & flex crack at top of 2nd story tens wall
49.3	0.095	Steel yielding at top of 1st st tens wall & Steel yielding at roof slab top face
53.8	0.12	Steel yielding at top of 2nd story tens wall
57.6	0.14	Flex crack at base of 2nd story tens wall
61.4	0.17	Flex crack of 2nd floor slab bot face
65.2	0.21	Steel yielding at base of comp wall
68.8	0.27	Steel yielding at base of 2nd st tens wall
74.2	0.40	Flex crack at top of 1st story comp wall Flex crack at top of 2nd story comp wall
75.8	0.44	Flex crack of roof slab bottom face
81.0	0.63	Flex capacity of 2nd floor slab (top face)
85.9	0.99	Flex capacity of roof slab (top face)
88.2	1.33	Flex capacity of comp wall base
91.0	4.26	Flex capacity of tens wall base Collapse mechanism

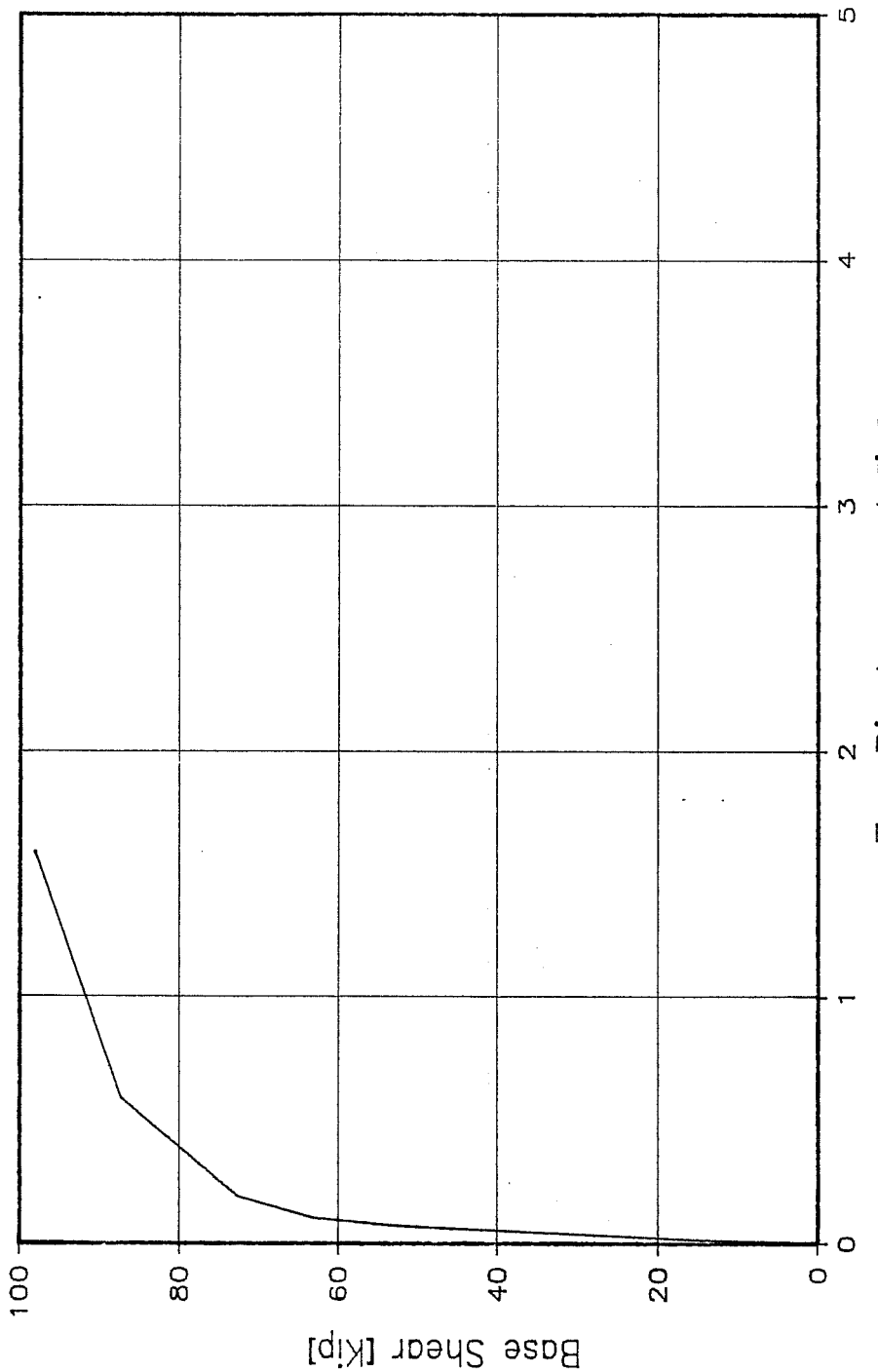

Figure 6.3 Specimen 2a: Predicted Base Shear versus Displacement Envelope

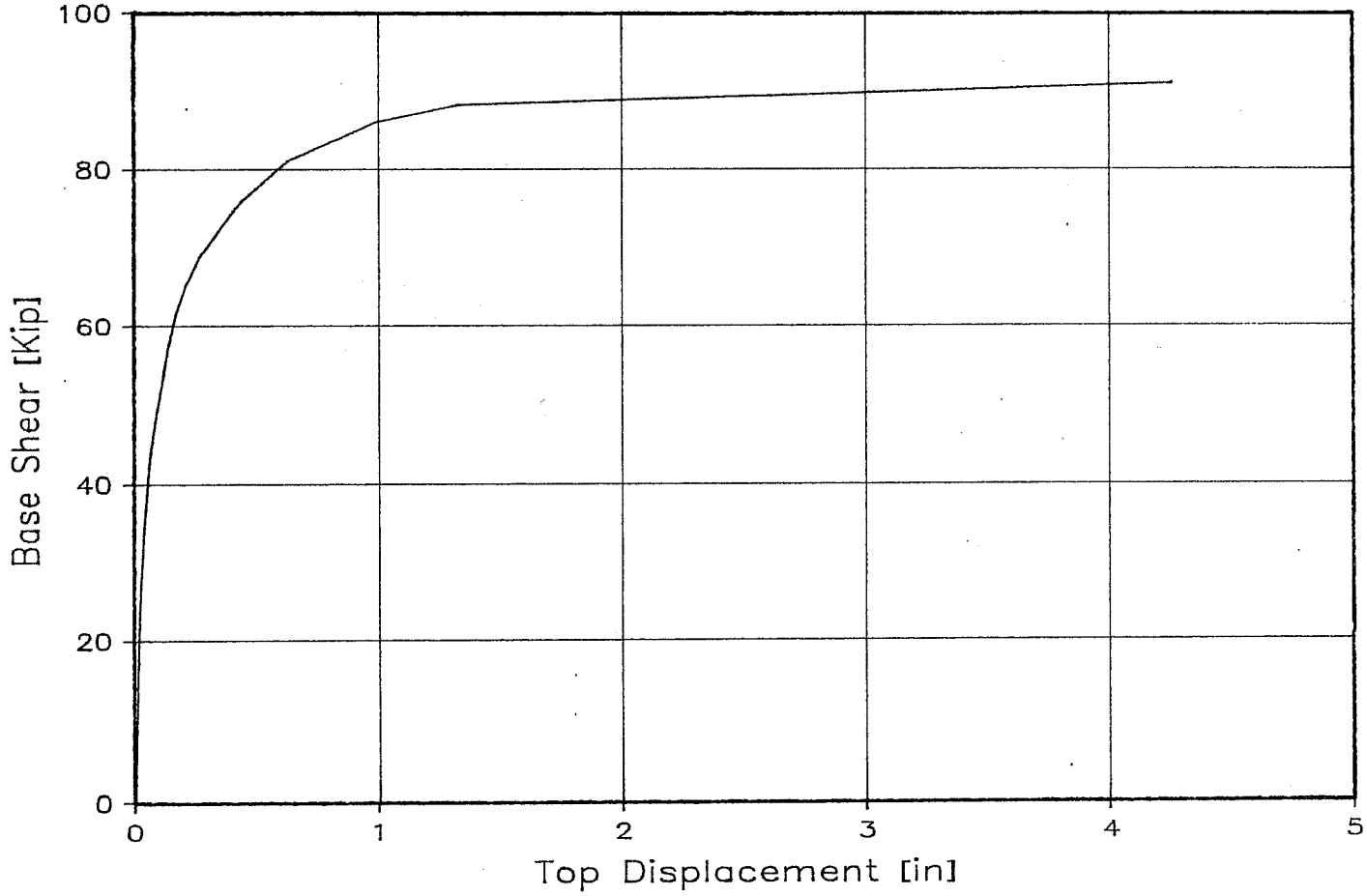

Figure 6.4 Specimen 2b: Predicted Base Shear versus Displacement Envelope

7. EXPERIMENTAL RESULTS

7.1 General

Experimental results are described based on visual observations, on the plot of top displacement versus base shear obtained directly during the test, and on readings from the data acquisition system. Events during the tests are described in terms of base shear and top displacement at each load point. The load points identify the scan number at which computer readings were taken.

The events described include cracking in the walls, cracking in the coupling elements, cracking in the joints between the wall and the coupling system, yielding of reinforcement, fracture of reinforcement, and sliding between the wall and the base.

7.2 Experimental Results for Specimen 2a

7.2.1 Test Summary, Specimen 2a. The Sequential Phased Displacement Loading history [19] was followed, with the modifications discussed in Section 4.4.

When testing Specimen 2a, vertical load was to be maintained at 19.4 kips per wall (92.2 psi at the wall base). Due to a problem with the calibration of the load cell, the vertical load was kept at only 12 kips per wall until Load Point 137. The calibration problem was then detected and corrected, and the load was increased to the proper level. This occurred at the same time the lateral loading system was switched from load to displacement control.

The First Major Event (FME), previously defined as first flexural cracking, occurred when the wall was being loaded in the north direction, at a base shear of 24.2 kips and a top displacement of 0.036 inches.

The maximum base shear reached was 95.9 kips with a top displacement of 1.69 inches for the north loading direction, and 84.7 kips with a top displacement of 1.64 inches for the south loading direction. Testing was continued to larger top displacements. The maximum top displacement obtained was 2.23 inches to the north with a base shear of 80.5 kips, and 2.17 inches to the south with a base shear of 63.5 kips.

After testing, the final wall state included crushing of the compression toes, tensile fracture of a longitudinal bar at the first-story of the north wall, and movement of the walls' bases both in-plane and out-of-plane. Figures 7.1 to 7.3 show the final state of the walls.

7.2.2 Lateral Displacement of the Wall, Specimen 2a. The displacement history of the top story is shown in Figure 7.4. The maximum displacement was in the north direction

Figure 7.1 Sp. 2a: First Story of North Wall at End of Test

at 2.23 inches, corresponding to a story drift of 1.09%. The maximum displacement in the south direction was 2.17 inches (1.06% story drift).

7.2.3 Load-Top Displacement History, Specimen 2a. The history of top displacement versus base shear for the entire test is shown in Figure 7.5. The envelopes of the history are shown in Figure 7.6.

7.2.4 Slip between Wall and Base, Specimen 2a. Slip of the walls relative to the base is shown in Figures 7.7 to 7.8. The base slip data was subjected to a series of corrections to obtain the final base slip history [24]. The corrections were needed due to problems encountered with the potentiometers during the test. These corrections are explained in Appendix B.

7.2.5 Strain in Longitudinal Reinforcement at Wall Bases, Specimen 2a. Figures 7.9 and 7.10 show the strain in wall longitudinal reinforcement at the base. Readings are peak values normalized by yield strain. The strain profile across the base remained linear up to yield, and then became nonlinear under increased loading.

7.2.6 Strain in Transverse Reinforcement, Specimen 2a. The transverse reinforcement strain gauge readings normalized by the yield strain value are shown in Figures 7.11 to 7.14. The plots show that the transverse steel did not yield.

Figure 7.2 Sp. 2a: First Story of South Wall at End of Test

7.2.7 Strain in Slab Longitudinal Reinforcement, Specimen 2a. Figures 7.15 and 7.16 show the strain profile across both slabs when the wall was being loaded northward. The figures show that the strain decreases as the distance away from the wall increases.

7.2.8 Detailed Test Description, Specimen 2a. Test observations are summarized in Tables 7.1 and 7.2, and are described in detail in the following paragraphs. Figures 7.17 to 7.21 show the progression of cracking during the test.

Figure 7.3 Sp. 2a: Base of South End of First Story of South Wall at End of Test

The First Major Event occurred at Load Point 39, as the wall was being loaded in the north direction, at a base shear of 24.2 kips and a top displacement of 0.036 inches. The crack formed at the base on the tension side of the first-story south wall. The crack extended about 12 inches along the wall. Loading southward at Load Point 43, the base shear was 24.3 kips, and the top displacement was 0.037 inches. At that point, flexural cracking occurred along the base of the tension side of the north wall. The crack extended along the wall about 4 inches. When the wall was further cycled at 100% of the First Major Event,

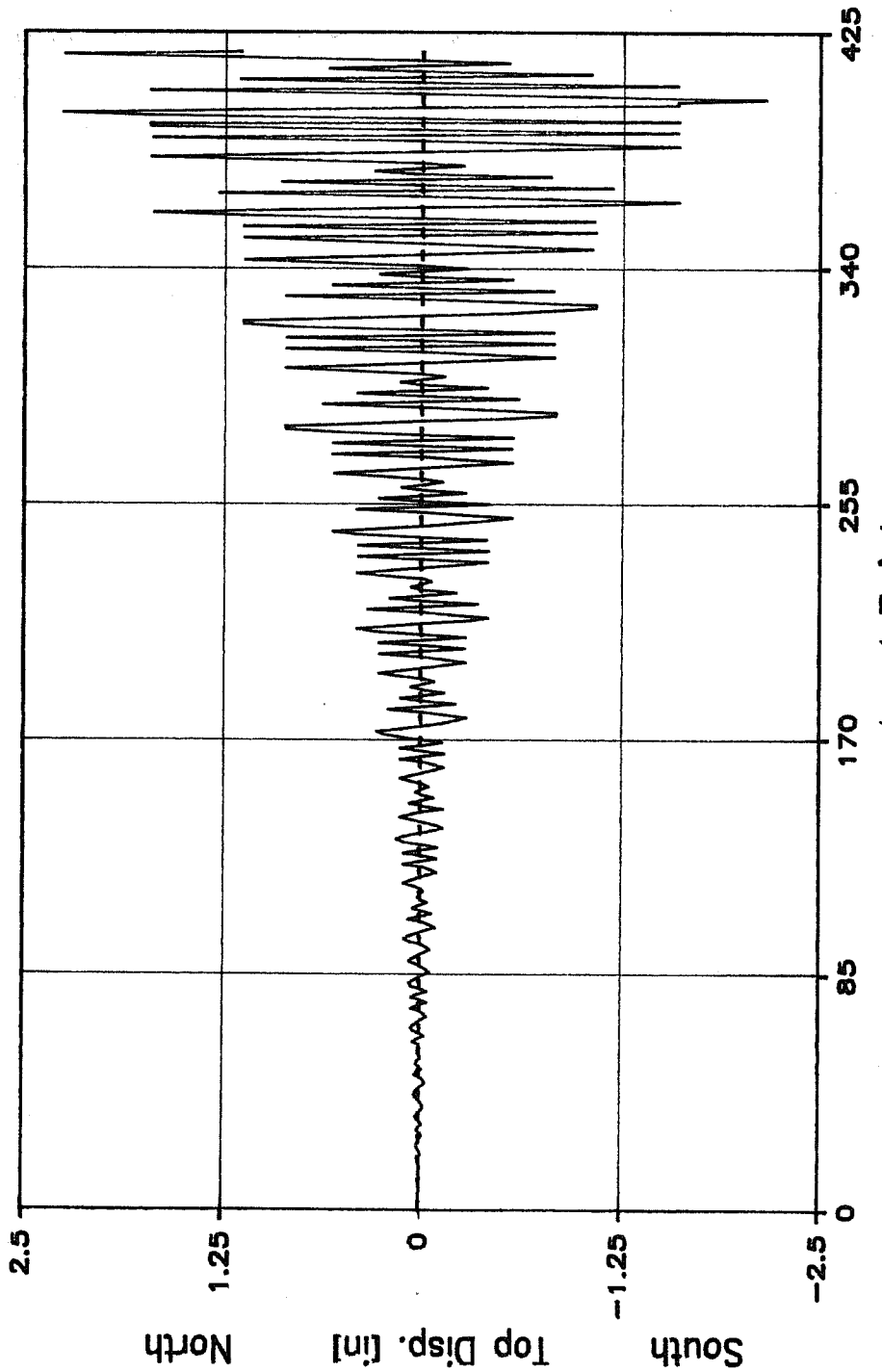

Figure 7.4 Sp. 2a: Top Displacement History

Figure 7.5 Sp. 2a: Base Shear versus Top Displacement History

Figure 7.6 Sp. 2a: Base Shear versus Top Displacement Envelope

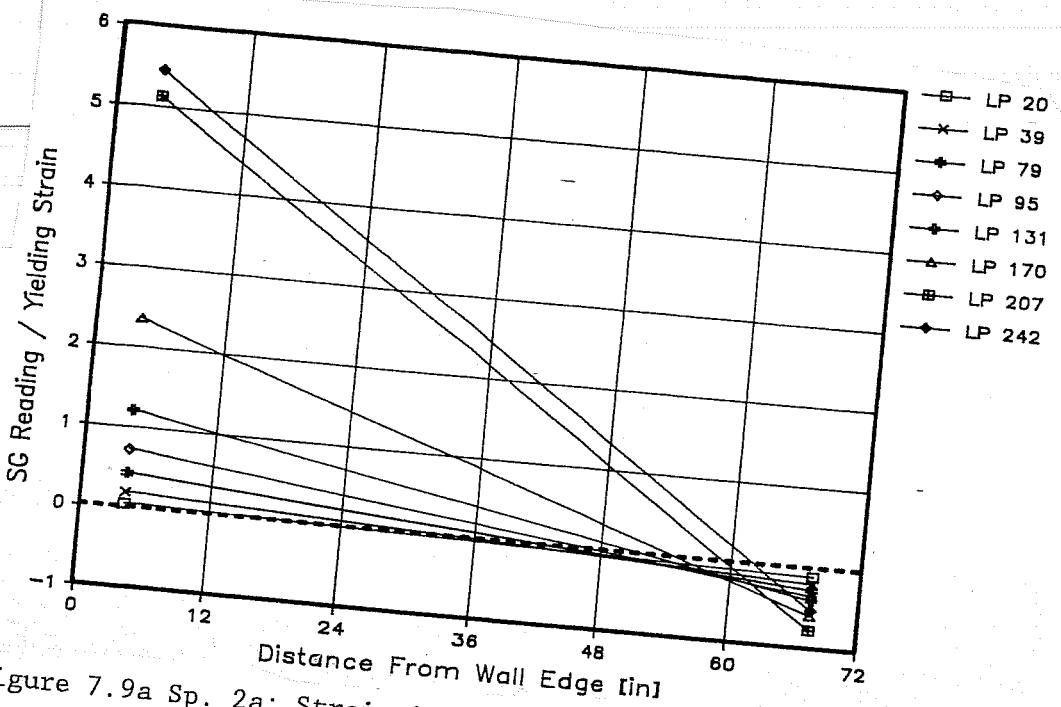

Figure 7.9a Sp. 2a: Strain in Longitudinal Reinforcement at Base of First Story North Wall - North Loading

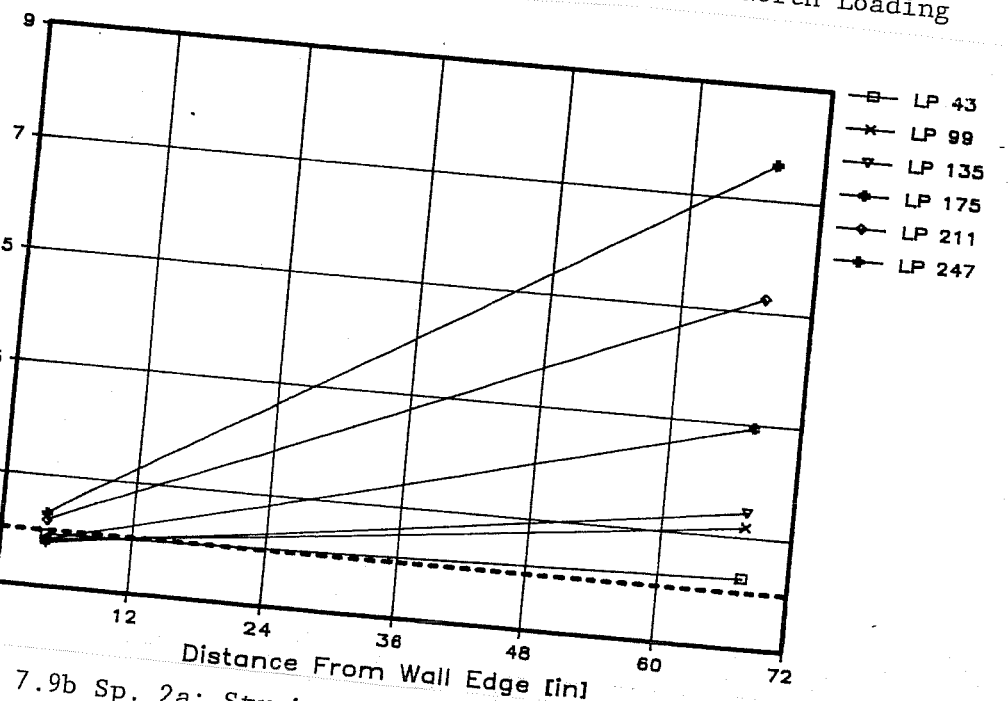

7.9b Sp. 2a: Strain in Longitudinal Reinforcement at Base of First Story North Wall - South Loading

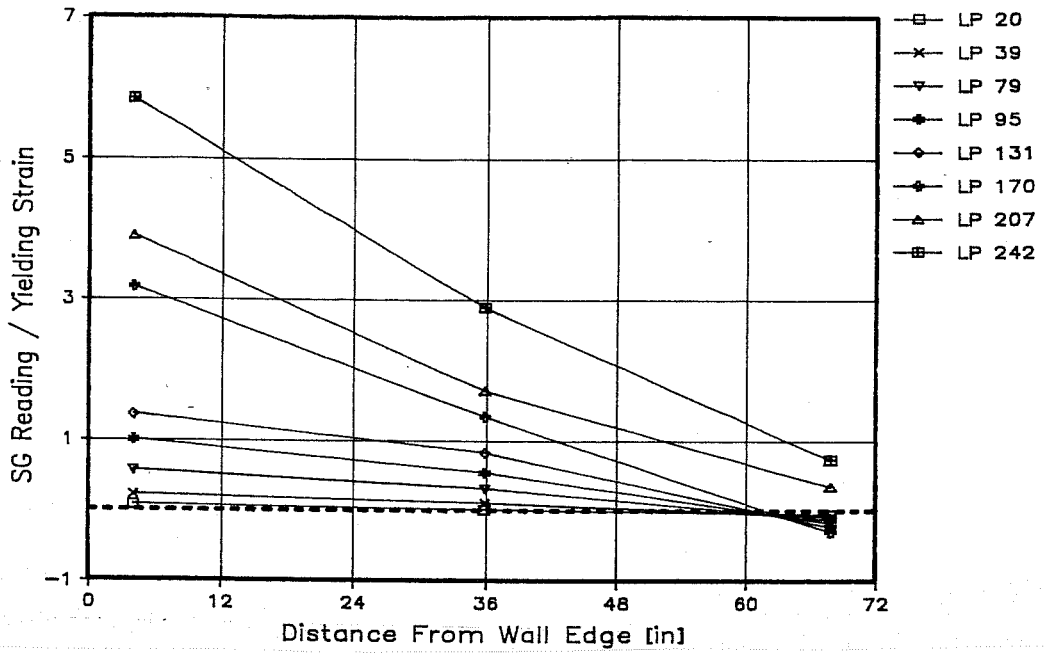

Figure 7.10a Sp. 2a: Strain in Longitudinal Reinforcement at Base of First Story South Wall - North Loading

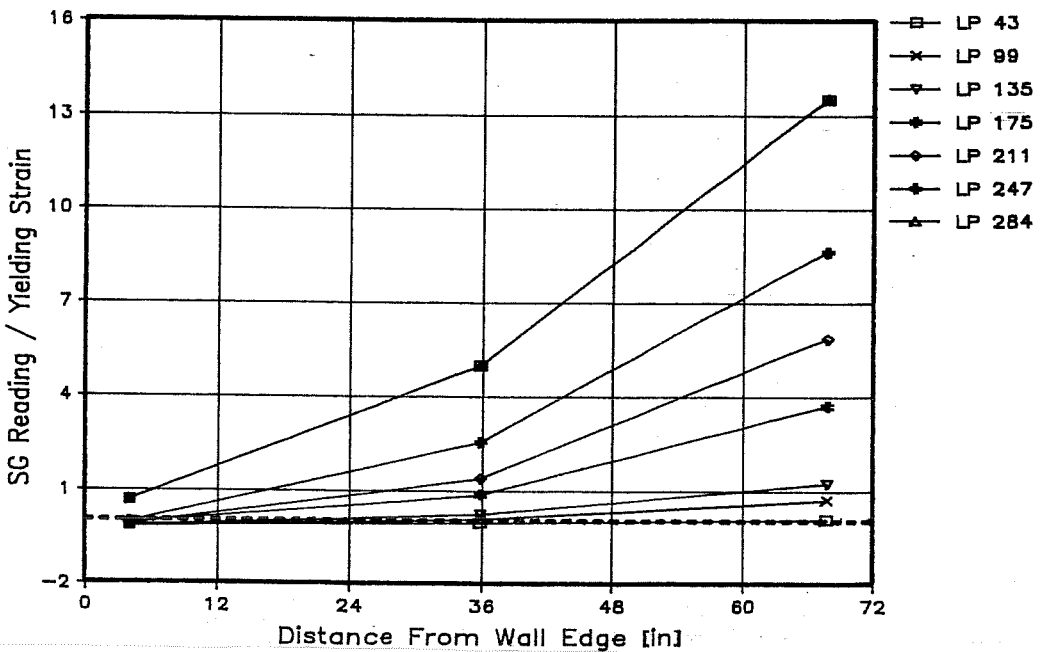

Figure 7.10b Sp. 2a: Strain in Longitudinal Reinforcement at Base of First Story South Wall - South Loading

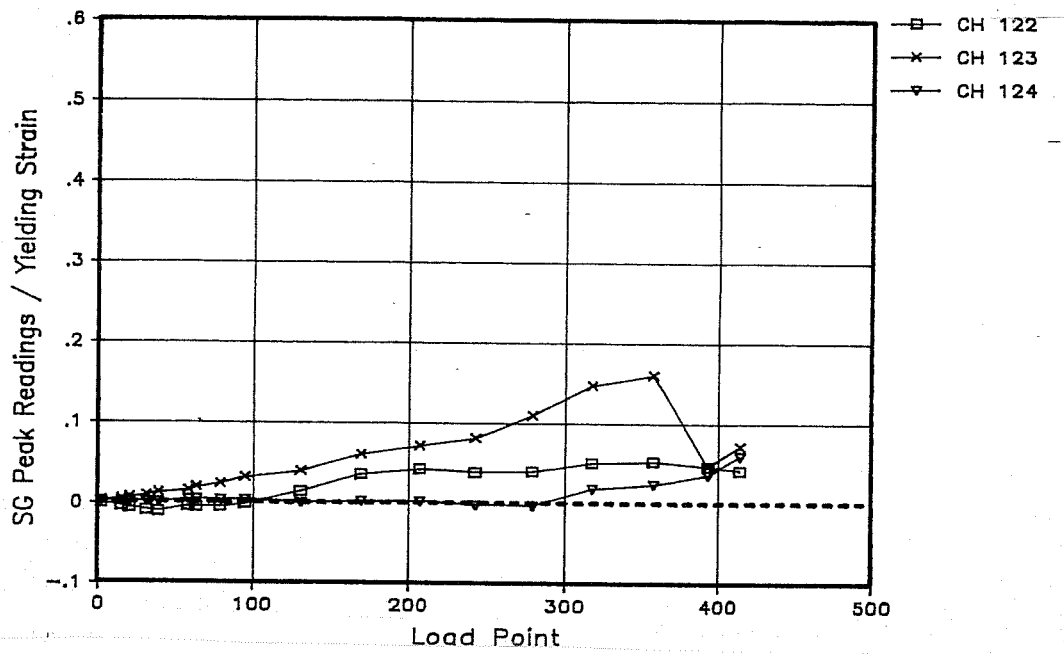

Figure 7.11a Sp. 2a: Strain in Transverse Steel for First Story North Wall - North Loading

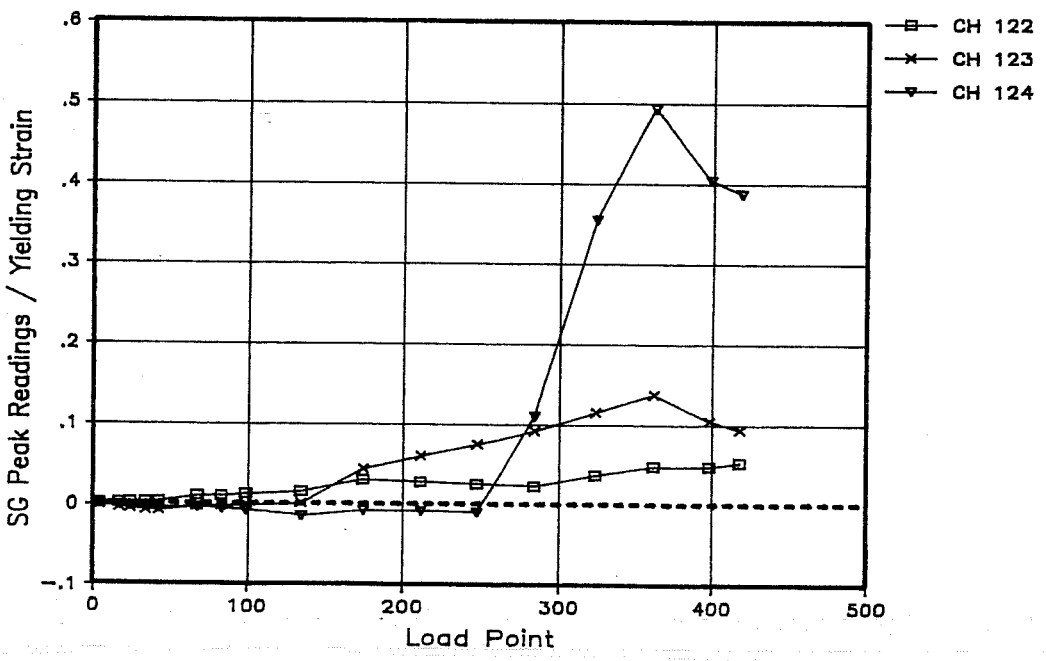

Figure 7.11b Sp. 2a: Strain in Transverse Steel for First Story North Wall - South Loading

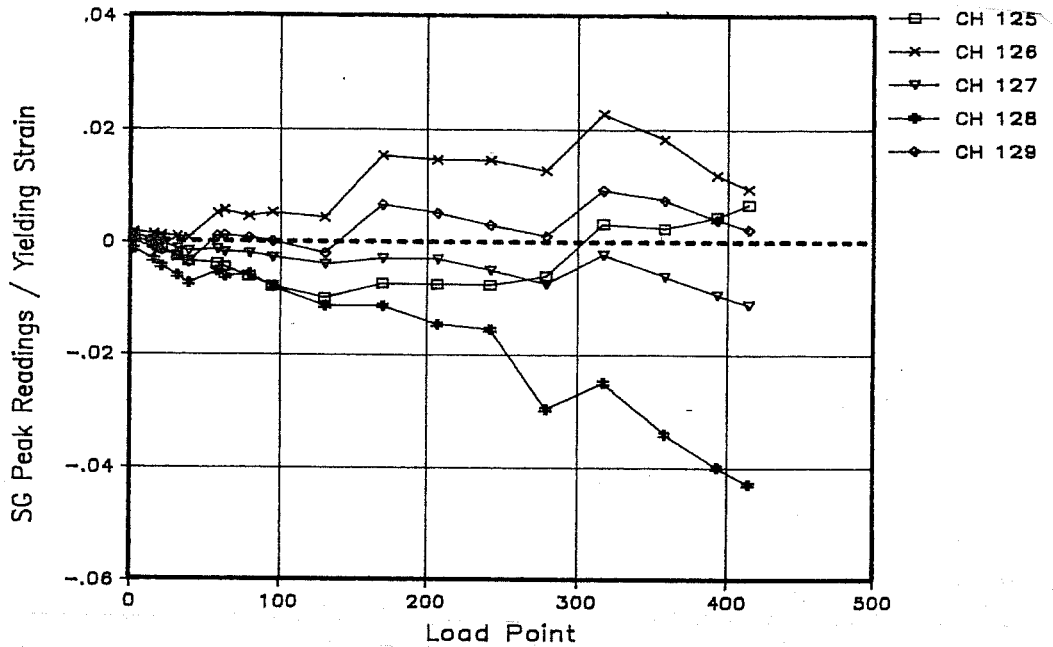

Figure 7.12a Sp. 2a: Strain in Transverse Steel for Second Story North Wall - North Loading

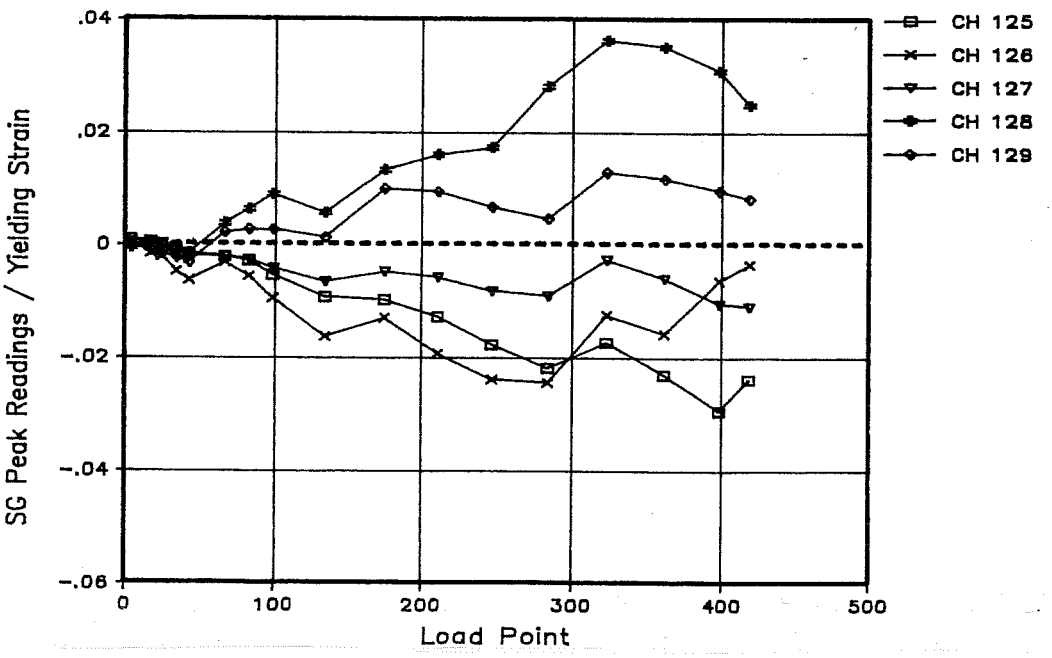

Figure 7.12b Sp. 2a: Strain in Transverse Steel for Second Story North Wall - South Loading

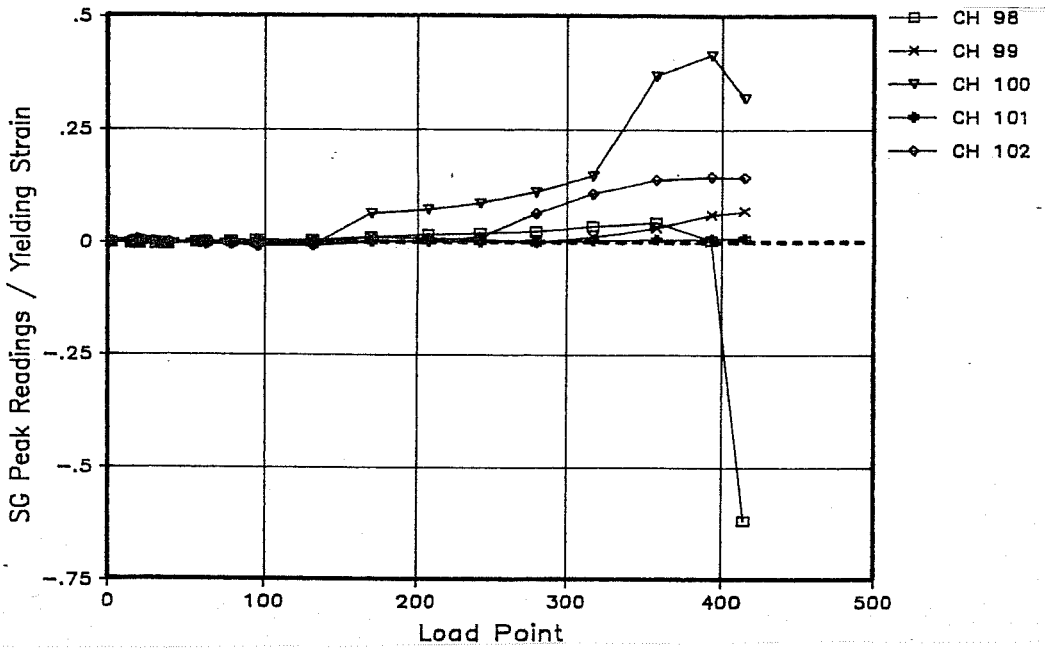

Figure 7.13a Sp. 2a: Strain in Transverse Steel for First Story South Wall - North Loading

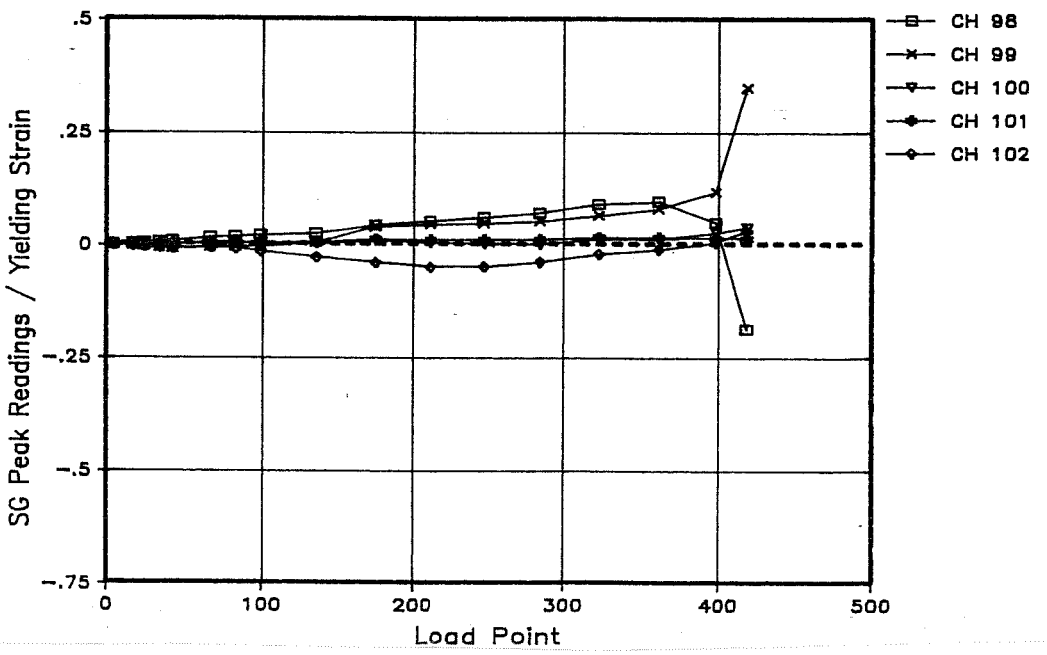

Figure 7.13b Sp. 2a: Strain in Transverse Steel for First Story South Wall - South Loading

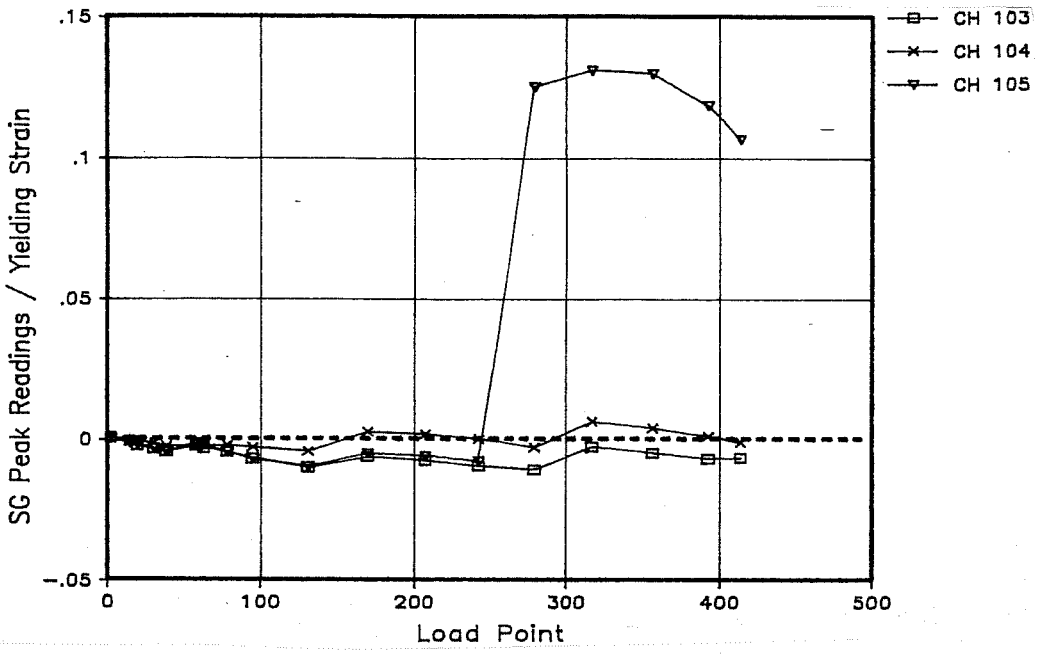

Figure 7.14a Sp. 2a: Strain in Transverse Steel for Second Story South Wall - North Loading

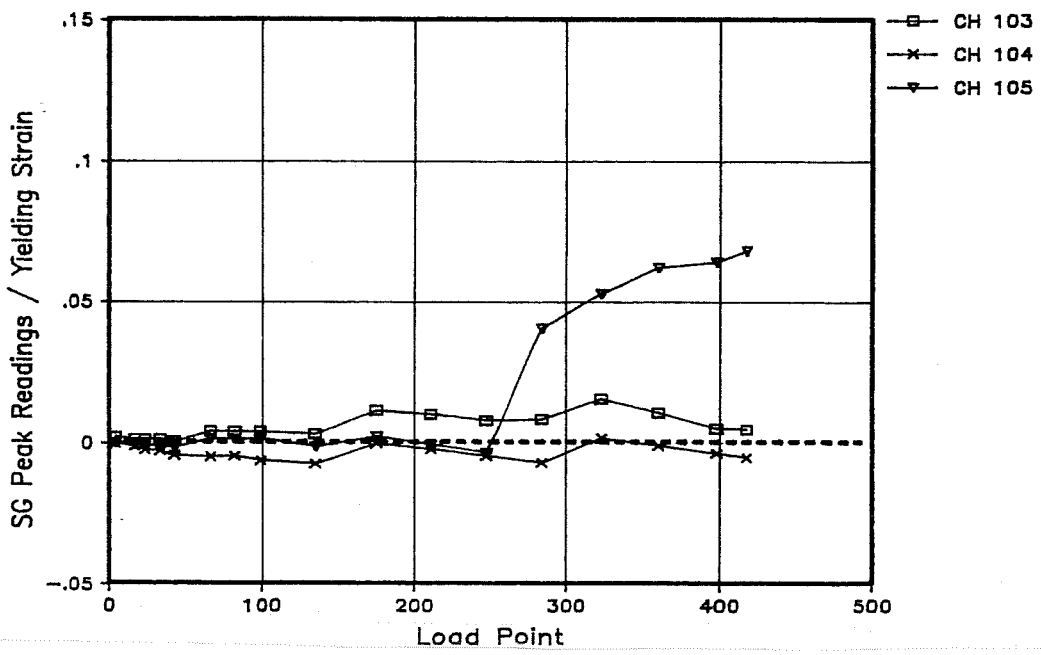

Figure 7.14b Sp. 2a: Strain in Transverse Steel for Second Story South Wall - South Loading

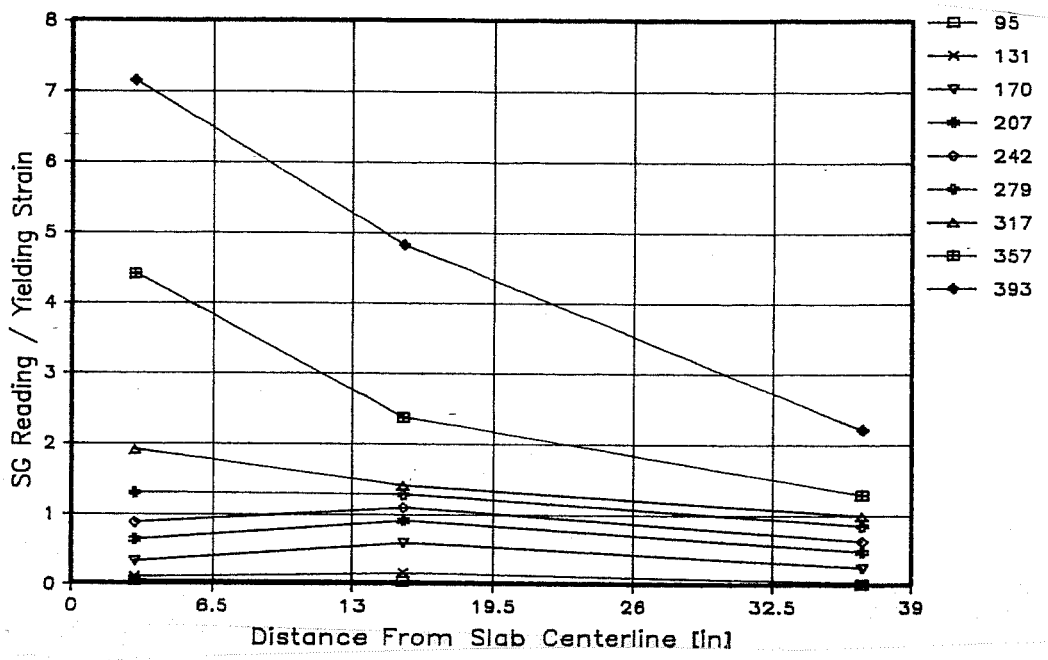

Figure 7.15 Sp. 2a: Strain in Longitudinal Reinforcement for Second Floor Slab - North Loading

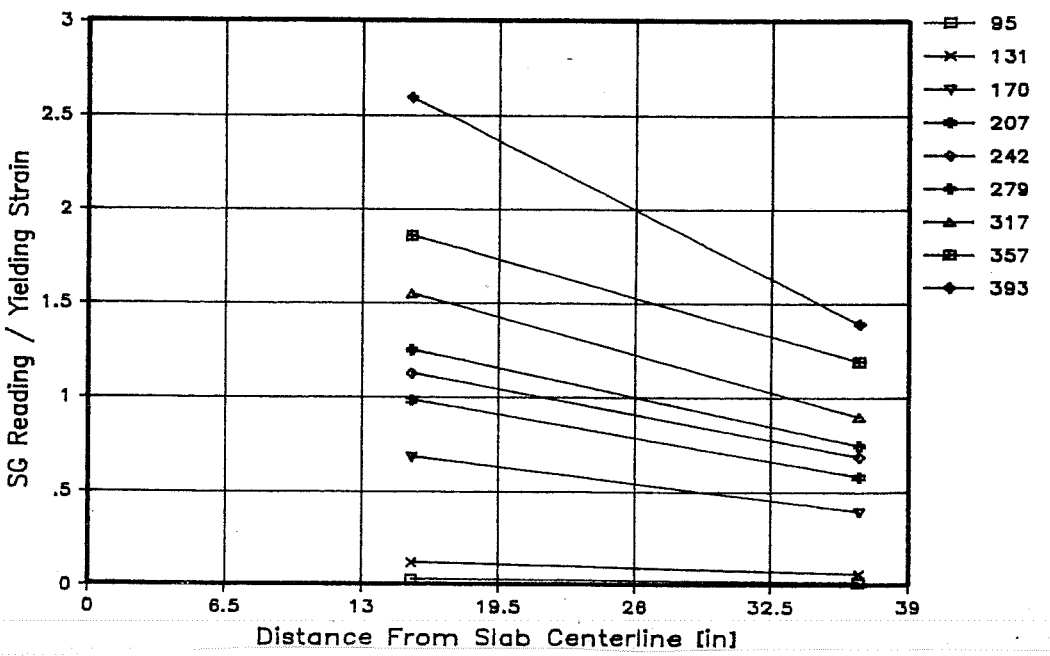

Figure 7.16 Sp. 2a: Strain in Longitudinal Reinforcement for Roof Slab - North Loading

Table 7.1 Observed Behavior of Specimen 2a
(September 10-14, 1988) Northward Loading.

Load Pt	Specimen Behavior	Base Shear		Top Displacement	
		kips	kN	inches	mm
39	Flexural cracking of tension wall	24.2	107.6	0.036	0.3
58	Flexural cracking of compression wall	24.2	107.6	0.045	0.4
95	Yield of longitudinal steel in tension wall	48.3	226.4	0.11	1.8
131	Cracking and yield of both slabs; yield of compression wall	58.5	260.2	0.16	4.1
169	Cracking of bottom of both slabs	62.4	277.6	0.24	6.1
170	Flexural cracking above lap splices	66.8	297.1	0.28	7.1
207	Diagonal cracks in tension wall	73.2	325.6	0.41	10.4
279	Diagonal cracks in compression wall	86.7	385.6	0.86	21.8
317	Toes of both walls start to crush; wide flexural cracks at wall bases and splices	89.4	397.7	1.13	28.7
357	Maximum load	95.9	426.6	1.69	42.9
384	Face shells spall at toe of compression wall	77.9	346.5	1.67	42.4
414	Extreme compression bar buckles in compression wall; walls slide on base	80.5	358.1	2.23	56.6

Table 7.2 Observed Behavior of Specimen 2a
(September 10-14, 1988) Southward Loading.

Load Pt	Specimen Behavior	Base Shear		Top Displacement	
		kips	kN	inches	mm
43	Flexural cracking of tension wall	24.3	108.1	0.037	0.9
99	Yield of longitudinal steel in tension wall	48.6	216.2	0.10	2.5
135	Cracking and yield of both slabs; yield of compression wall	54.5	242.4	0.14	3.6
247	Diagonal cracks in tension wall	71.2	316.7	0.57	14.5
284	Diagonal cracks in compression wall; toes of both walls start to crush	77.7	345.6	0.84	21.3
361	Maximum load	84.7	376.8	1.64	41.7
386	Face shells split at toe of compression wall	72.6	322.9	1.63	41.4
397	Fracture of extreme tension bar of tension wall	45.9	204.2	1.63	41.4
418	Longitudinal and lateral sliding of walls	63.5	282.5	2.17	55.1

the flexural cracking extended along the base. Slight hysteresis began to show in the plotted load-displacement curves.

The next loading series was at a base shear of about 200% of the First Major Event base shear. At Load Point 95, the base shear was 48.3 kips at a top displacement of 0.11 inches, under load to the north. Yielding of the longitudinal steel in the first-story south wall (tension wall) occurred as shown in Figure 7.10(a). The flexural crack at the base of the first-story south wall extended about two-thirds of the wall length. Slight flexural cracking began at the base of the second-story north wall. At Load Point 99, the wall was loaded southward with a base shear of 48.6 kips and a top displacement of 0.10 inches. The longitudinal steel in the first-story north wall yielded as shown in Figure 7.9(b). Flexural cracking began in the second-story walls. The plotted hysteresis loops became more oval in shape. At the last 200% FME load point cycle, flexural cracks widened at the base of the walls, and formed above the longitudinal reinforcement splice in both first-story walls. On the north side of the second-story south wall, contraflexure cracking was beginning below the roof slab.

During the next load series at a base shear of about 400% of the First Major Event base shear, each lower-story wall, when placed in compression due to overturning, experienced yield of the longitudinal steel on its tension side. At Load Point 131, this occurred at a base shear of 58.5 kips and a top displacement of 0.16 inches, as the wall was being loaded in the northward direction (Figure 7.9(a)). Vertical cracks became visible at the north wall compression toe. The crack widened at the base of the first-story south wall at the south side. First cracking and yielding occurred on the top face of both slabs. Flexural cracks formed completely across the top face of both slabs on the north opening edge, and began on the bottom face of the slabs at the south edge of the wall opening. The crack width in the slabs was about one-sixteenth to one-eighth of an inch.

As shown in Figure 7.15, yielding of the second-floor slab did not occur until Load Point 279, and as shown in Figure 7.16 yielding of the roof slab does not occur until Load Point 242. This yielding corresponds to a crack running across the slabs at the location of the strain gauges. Considering both the crack width and the fact that the strain gauges showed steel yielding at the gauge location, it is believed that the longitudinal slab steel yielded as soon as the slabs cracked. The slab cracking accounts for some of the loss in stiffness that appeared on the plotter at that point.

At Load Point 135, the base shear was 54.5 kips and the deflection was 0.14 inches, under load towards the south at about 400% of the First Major Event base shear. Both slabs cracked and yielded on the top face on the south side at this load level in the south loading

direction. Flexural cracking began on the bottom face of both slabs on the north edge of the wall openings.

At this point, the test setup was switched to displacement control.

The next loading series was at a displacement of about 800% of the First Major Event displacement of 0.036 inches. At Load Point 169, cracking continued on the bottom face of both slabs, while loading to the north at a base shear of 62.4 kips and a top displacement of 0.24 inches. At Load Point 170, the top displacement was 0.28 inches (about 800% of the First Major Event), and the base shear was 66.8 kips. At this level, flexural cracking occurred above the base longitudinal splices in the first-story walls. When loading southward at 800% of the First Major Event, similar cracking occurred. At Load Point 175, the base shear was 58.2 kips, and the top displacement was 0.28 inches.

At Load Point 207, approximately 1200% of the First Major Event displacement, diagonal shear cracking began in the first-story south wall. As shown in Figure 7.13(a), this was not accompanied by yielding of the transverse steel. The base shear was 73.2 kips, and the top displacement was 0.41 inches to the north. Flexural cracking began along the second-story base of the south wall.

When loading southward at a top displacement approximately 1600% of the First Major Event displacement, diagonal shear cracking began in the first-story north wall at Load Point 247. Figure 7.11(b) shows that the transverse steel did not yield. The base shear was 71.2 kips and the top displacement was 0.57 inches. Both slabs had developed additional cracking on their top and bottom faces.

The next event occurred at Load Point 279, when the base shear was 86.7 kips and the top displacement was 0.86 inches, approximately 2400% of the First Major Event displacement. Diagonal cracking began in the first-story north wall when loading to the north. At Load Point 284, when loading to the south at a base shear of 77.7 kips and a top displacement of 0.84 inches, diagonal cracks formed in the first-story south wall. The toes of both bottom walls started to crush when the walls were placed in compression. Cracks developed across the top and bottom faces of both slabs away from the wall opening edges and propagated towards the middle of each wall. While cycling at this level, a 1/4- inch crack would open at the base bed joint of the first-story north wall on the north edge.

During the next load series, at a displacement approximately 4800% of the First Major Event displacement, the maximum load was reached in both directions. In the north direction, the maximum base shear was 95.9 kips at a top displacement of 1.69 inches (Load Point 357). In the south direction, the maximum base shear was 84.7 kips at a top displacement of 1.64 inches (Load Point 361). New diagonal cracks formed on the south first-story

wall. During this loading series, the face shells spalled at the toe of both walls when these were in compression due to overturning.

At Load Point 397, when loading up to 6400% of the First Major Event towards the south, the base shear was 45.9 kips and the top displacement was 1.63 inches. The extreme tension bar (north) in the first-story north wall fractured, generating a loud noise. Fracture of this bar is shown in the top displacement-base shear history (Figure 7.5). At Load Point 414, the maximum top displacement to the north of 2.23 inches was reached and the base shear was 80.5 kips. The extreme compression bar (north) buckled at the base of the first-story north wall. At that time, both walls were sliding longitudinally on the base up to 0.5 inches as shown in Figures 7.7 and 7.8. They were also displacing laterally.

At Load Point 418, the walls were sliding both longitudinally and laterally. The maximum top displacement to the south of 2.17 inches was reached, and the base shear was 63.5 kips. Due to safety concerns regarding the lateral movement, the test was stopped.

The north wall had a final in-plane displacement at the base of 0.25 inches to the north. The south wall in-plane displacement at the base was 0.5 inches. The out-of-plane displacement for the north wall varied from 1/2 to 9/16 inches. The south wall displacement varied from zero to 3/4 inches.

7.3 Experimental Results for Specimen 2b

7.3.1 Test Summary, Specimen 2b. The Sequential Phased Displacement Loading history [19] was followed using the modifications discussed in Section 5.3.2. The history is shown in Figure 5.12.

Before the testing began, the specimen was accidentally loaded when the first-story ram on the east side began to extend after being connected to the load transfer beam. As shown in Figure 7.22, hairline diagonal cracks formed in each wall. The bed joint on the concrete base beam was cracked at the south end of the south wall. Local cracking also occurred in the roof slab near the south sway brace plate. This problem was due to a malfunction of the Pegasus Closed Loop Servocontroller System's servo system module. The module was replaced, and the problem did not re-occur.

Testing began under load control. The loading program began by cycling at progressively increasing load until the First Major Event was reached.

The First Major Event was to be defined as yielding of the first-story walls. Due to problems encountered while testing, however (discussed in Subsection 7.3.8) the First Major Event was actually defined as a base shear of 44 kips, and a top displacement of 0.20 inches.

Figure 7.22 Sp. 2b: Cracking Due to Pretest Loading

The maximum base shear was 88.1 kips, at a maximum top displacement of 3.46 inches for the north loading direction, and 78.3 kips at a maximum top displacement of 3.10 inches for the south loading direction.

The final wall state included loss of the compression toes for both walls when loading to the north, and crushing of the south wall compression toe when loading to the south. Both walls had residual in-plane and out-of-plane displacement. Figures 7.23 to 7.25 show the final state of the walls.

7.3.2 Lateral Displacement of the Wall, Specimen 2b. The top displacement history is shown in Figure 7.26. The maximum displacement was in the north direction at 3.46 inches, corresponding to a story drift of 1.70%. The maximum displacement in the south direction was 3.10 inches (1.52% story drift).

7.3.3 Load-Top Displacement History, Specimen 2b. The history of top displacement versus base shear for the entire test is shown in Figure 7.27. The envelope of the history is shown in Figure 7.28.

7.3.4 Slip between Wall and Base, Specimen 2b. The wall base slip relative to the base is shown in Figure 7.29 and 7.30.

Figure 7.23 Sp. 2b: First Story of North Wall at End of Test

7.3.5 Strain in Longitudinal Reinforcement, Specimen 2b. All pertinent figures show longitudinal strains normalized by yield strain for various load points. Figures 7.31 to 7.32 show the strain profile for the longitudinal bars at the bases of the north and south walls. Figures 7.33 to 7.34 show the strain profile for the longitudinal bars at the intersection of the top of the first- story walls and the second-floor slab. Figure 7.35 to 7.36 show the strain profile for the longitudinal bars at the bases of the second-story walls. Figures 7.37 to 7.38 show the strain profile for the longitudinal bars at the intersection of the top of the second-story walls and the roof slab.

Figure 7.24 Sp. 2b: First Story of South Wall at End of Test

7.3.6 Strain in Transverse Reinforcement, Specimen 2b. The transverse strain gauge readings normalized by the yield strain are shown in Figures 7.39 to 7.42.

7.3.7 Strain in Longitudinal Beam Reinforcement, Specimen 2b. The beam, lying between the precast planks of the floor slabs, had strain gauges placed as shown in Figure 5.11. Figures 7.43 to 7.44 show the strain gauge readings normalized by the yield strain value for the steel.

7.3.8 Detailed Test Description, Specimen 2b. Test observations are summarized in Tables 7.3 and 7.4, and are described in detail in the following paragraphs. The progression of cracking is shown in Figures 7.45 through 7.49.

Figure 7.25 Sp. 2b: Base of South End of First Story of South Wall at End of Test

The first loading cycles were at about 10 kips base shear. At Load Point 16, the base shear was 10.3 kips, and the top displacement was 0.017 inches loading to the south. A flexural crack formed at the south wall base.

During the 20-kip loading cycles, flexural cracking occurred in both first-story walls. At Load Point 25, the base shear was 21.2 kips and the top displacement was 0.055 inches to the south. The north wall formed a diagonal crack from the top north side to the third course up on the south side. This crack was an effect of the system malfunction before testing began. A flexural crack formed at the top of the first-story north wall at the opening. The first-story south wall formed flexural cracks along the north side. The cracks occurred along

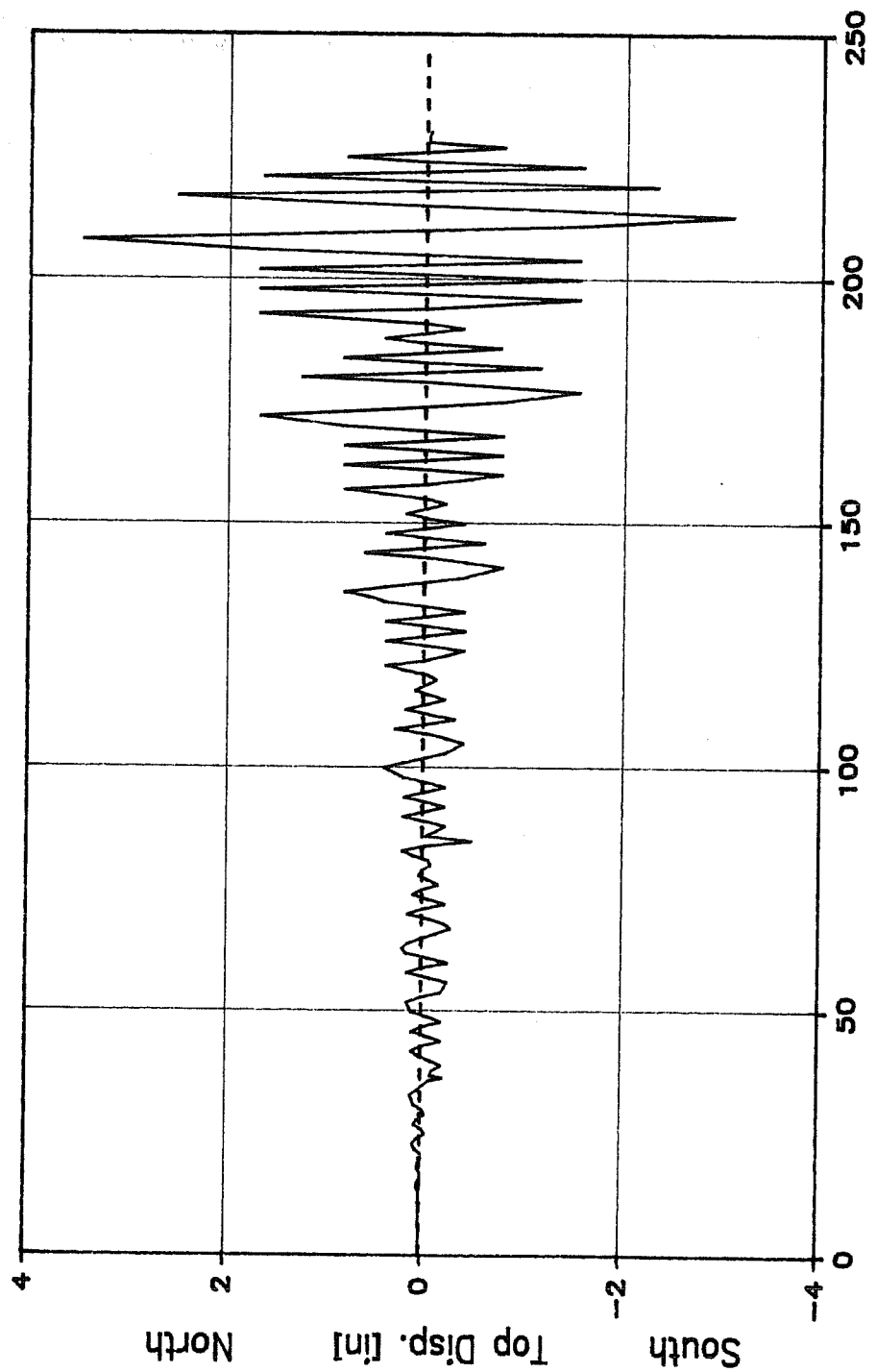

Figure 7.26 Sp. 2b: Top Displacement History

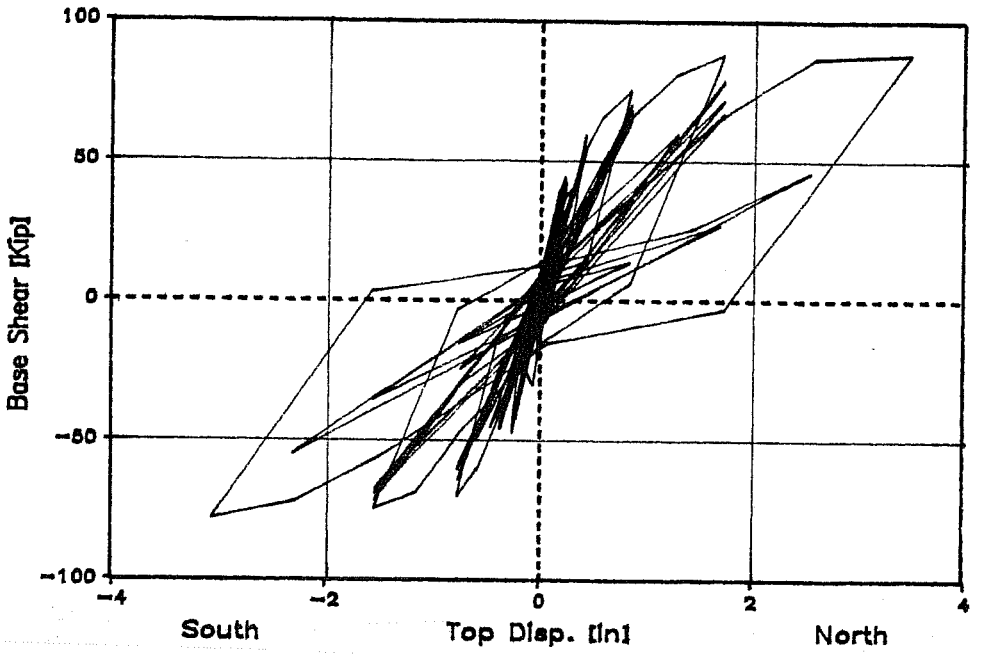

Figure 7.27 Sp. 2b: Base Shear versus Top Displacement History

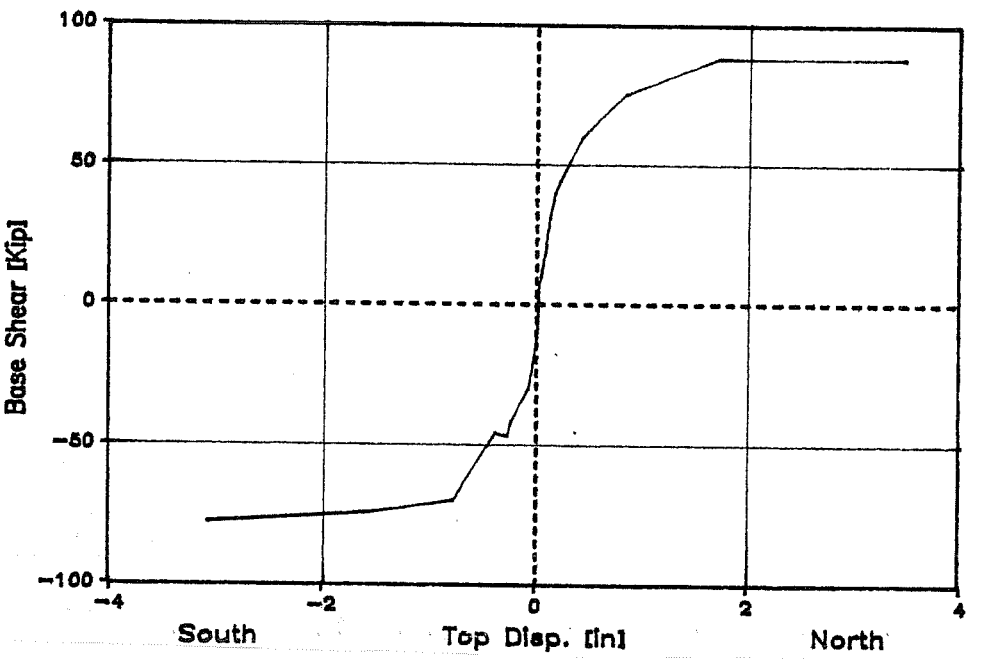

Figure 7.28 Sp. 2b: Base Shear versus Top Displacement Envelope

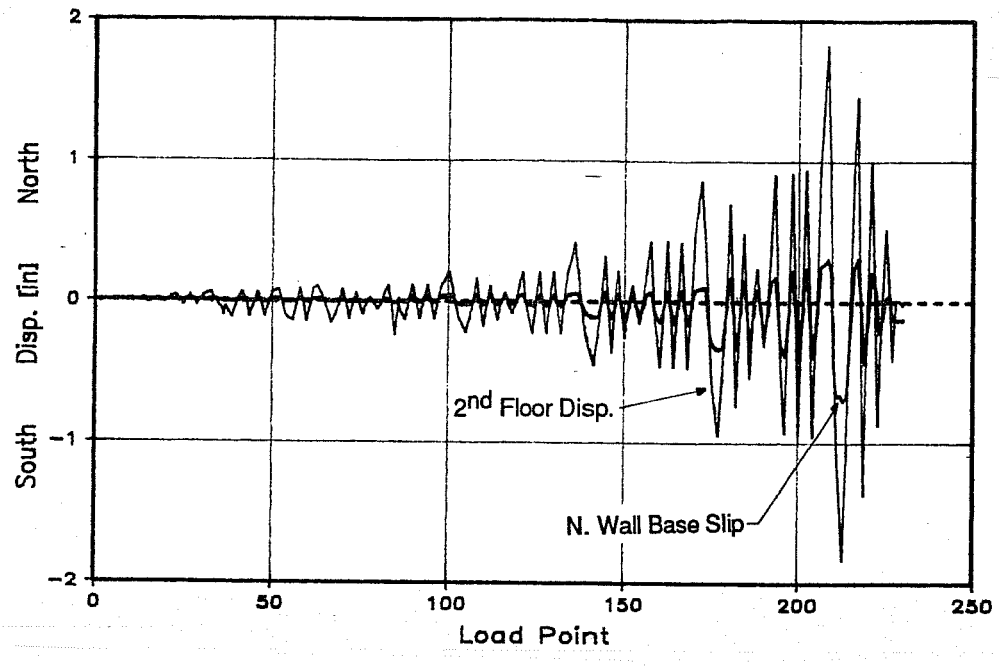

Figure 7.29 Sp. 2b: Slip at Base of First Story of North Wall

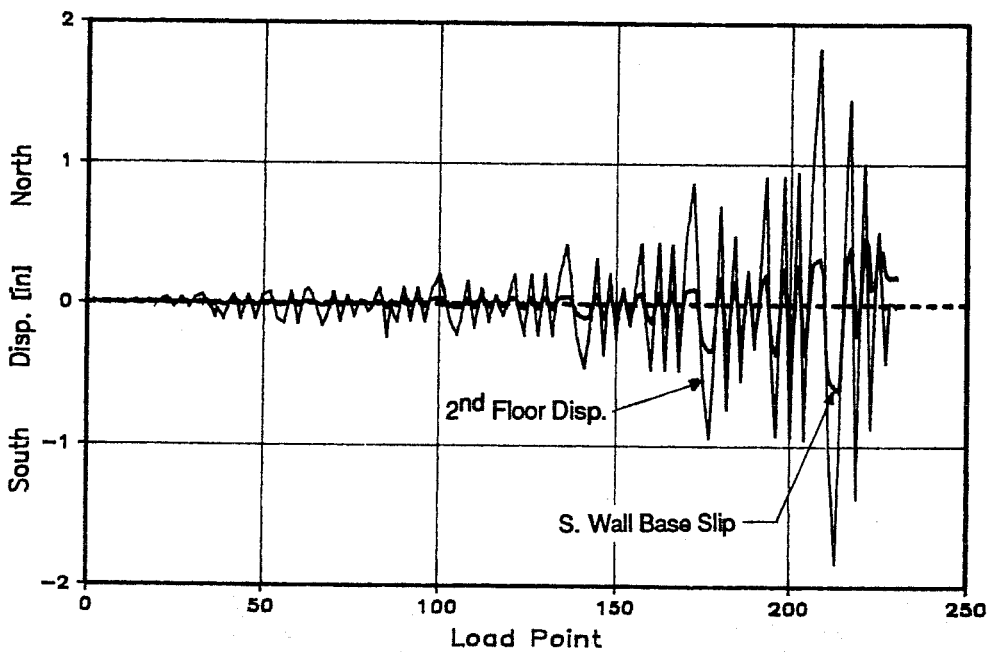

Figure 7.30 Sp. 2b: Slip at Base of First Story of South Wall

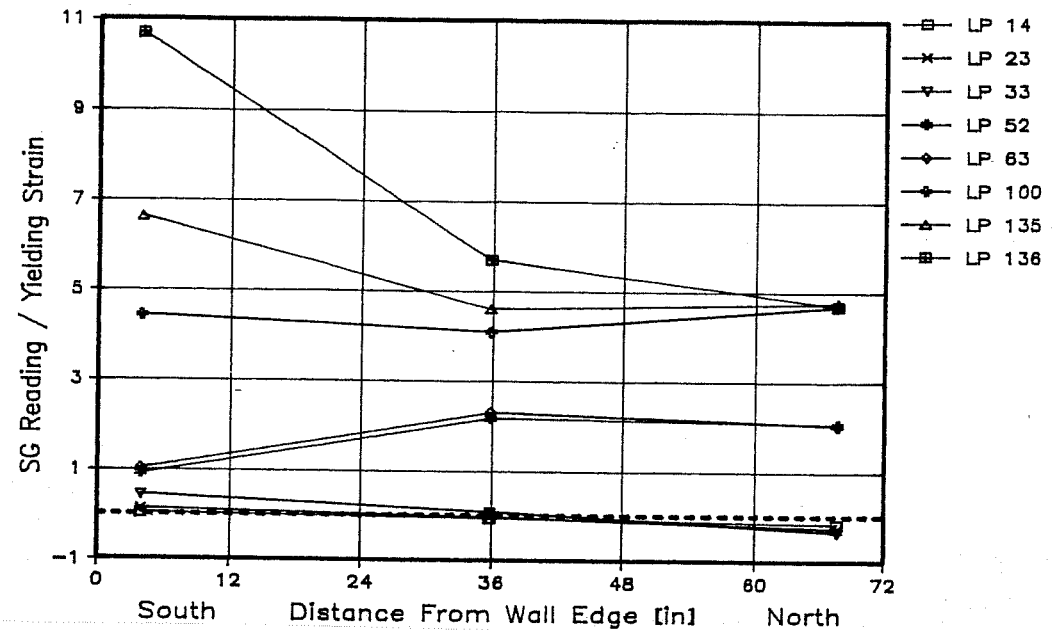

Figure 7.31a Sp. 2b: Strain in Longitudinal Reinforcement at Base of First Story North Wall - North Loading

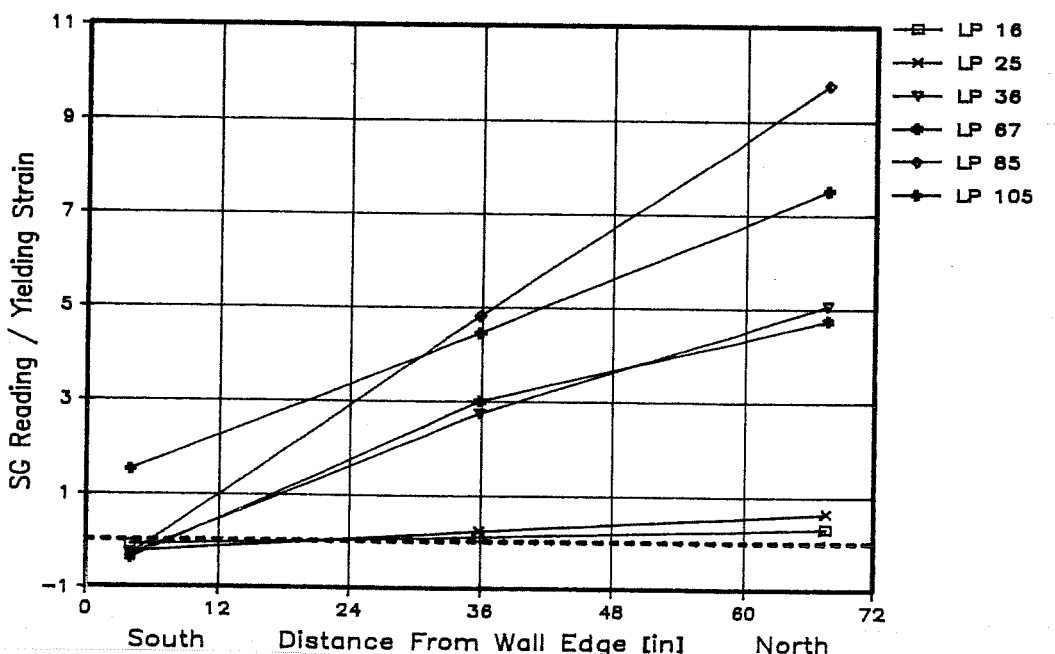

Figure 7.31b Sp. 2b: Strain in Longitudinal Reinforcement at Base of First Story North Wall - South Loading

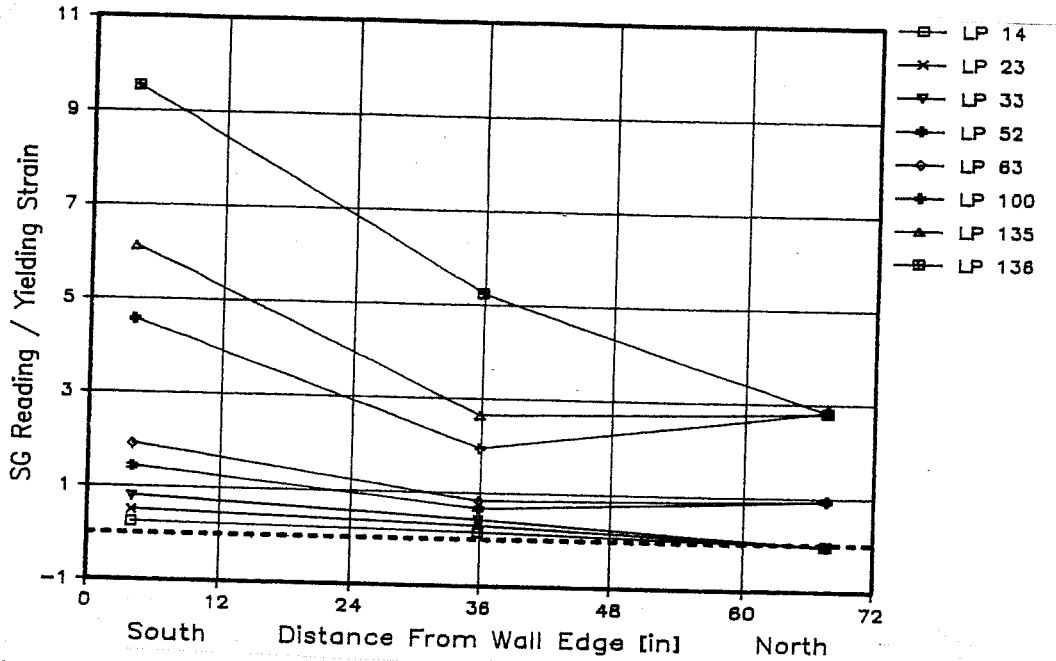

Figure 7.32a Sp. 2b: Strain in Longitudinal Reinforcement at Base of First Story South Wall - North Loading

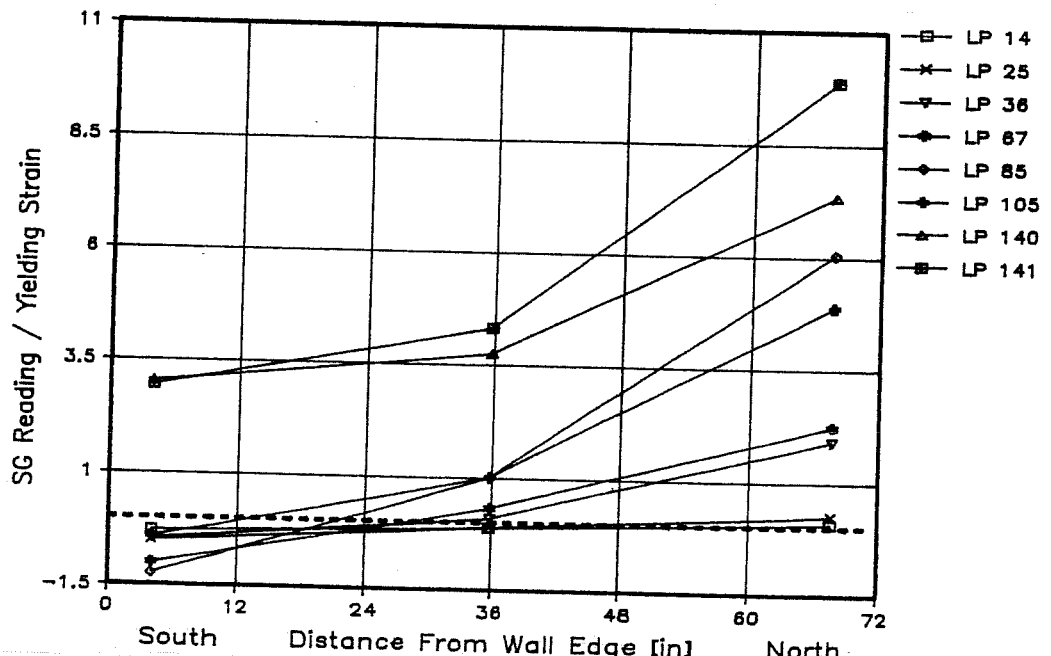

Figure 7.32b Sp. 2b: Strain in Longitudinal Reinforcement at Base of First Story South Wall - South Loading

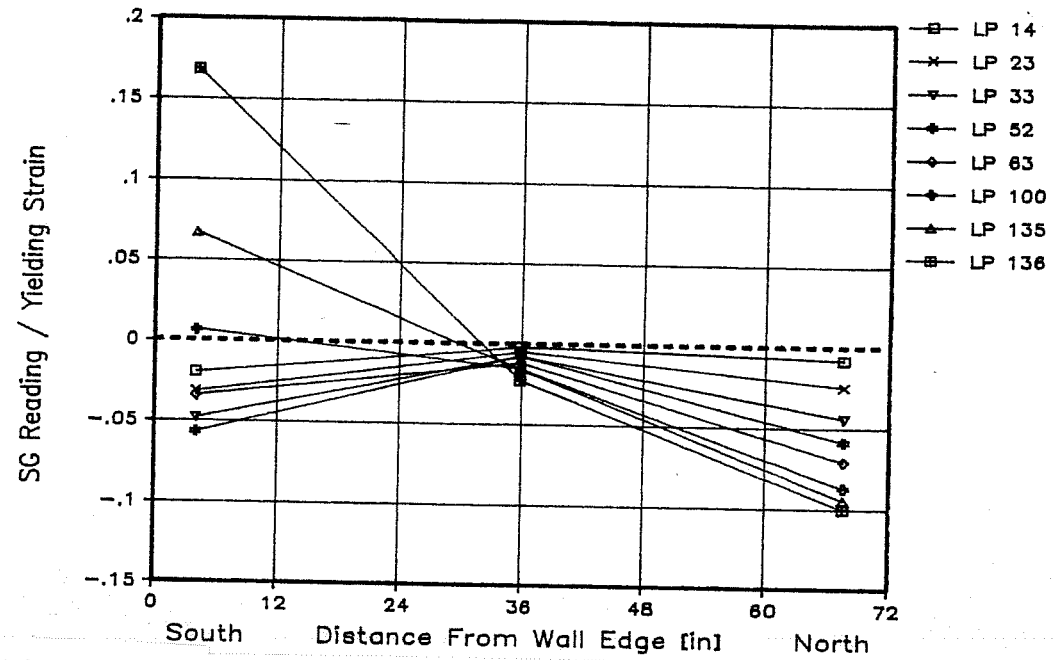

Figure 7.33a Sp. 2b: Strain in Longitudinal Reinforcement at Top of First Story North Wall - North Loading

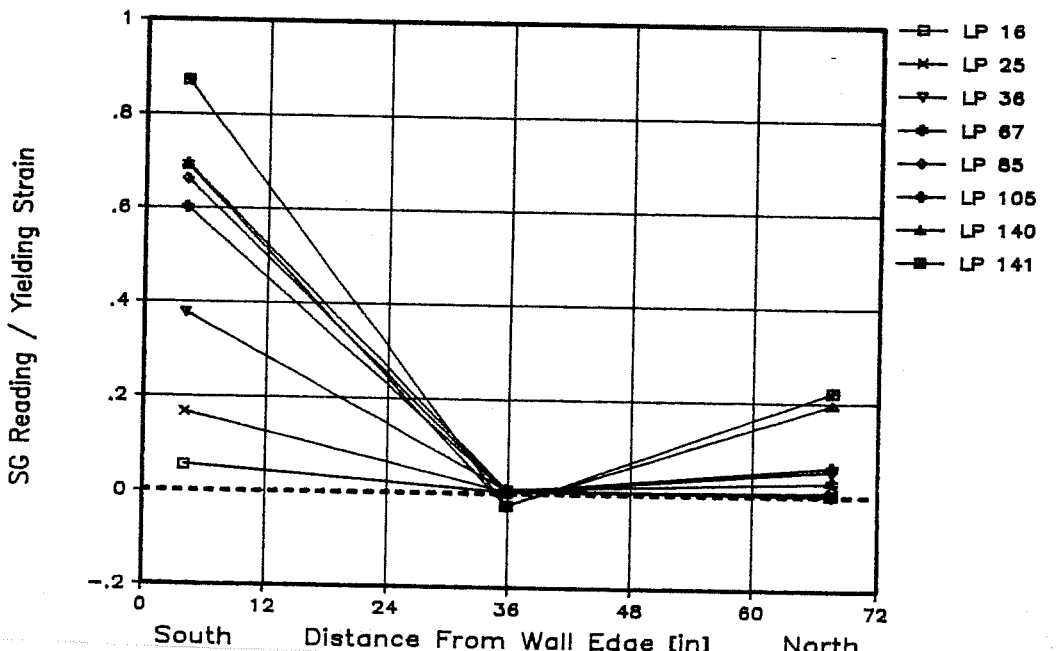

Figure 7.33b Sp. 2b: Strain in Longitudinal Reinforcement at Top of First Story North Wall - South Loading

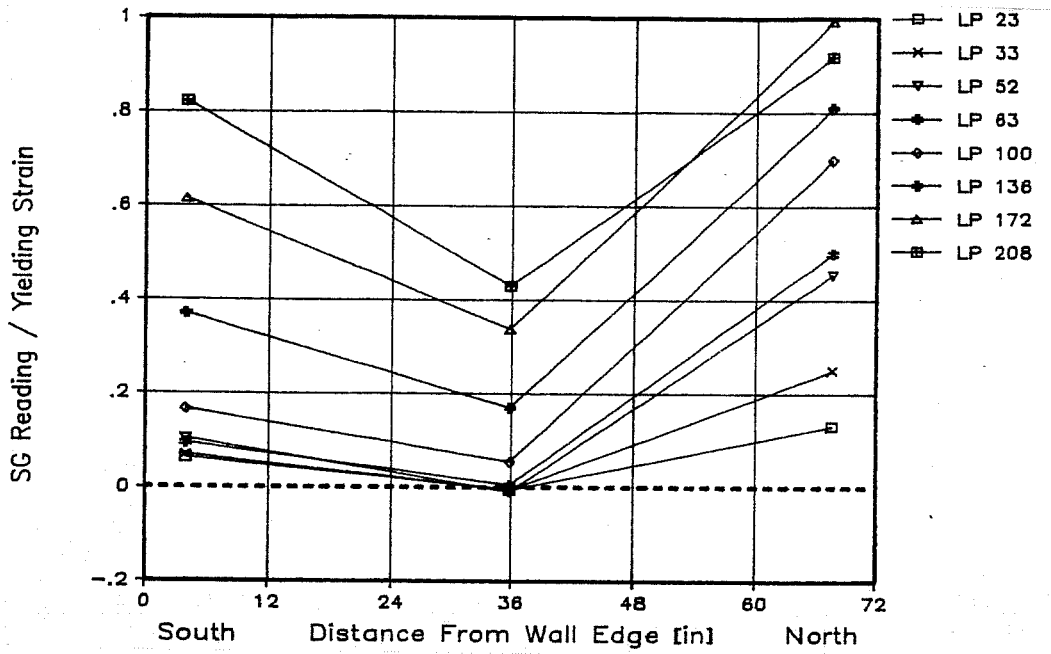

Figure 7.34a Sp. 2b: Strain in Longitudinal Reinforcement at Top of First Story South Wall - North Loading

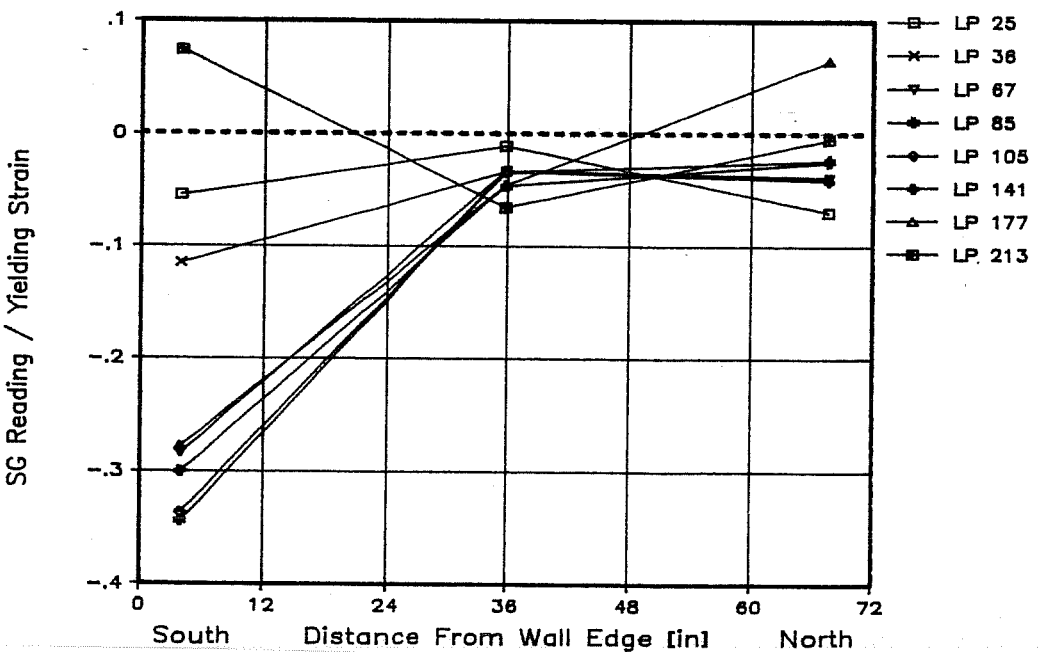

Figure 7.34b Sp. 2b: Strain in Longitudinal Reinforcement at Top of First Story South Wall - South Loading

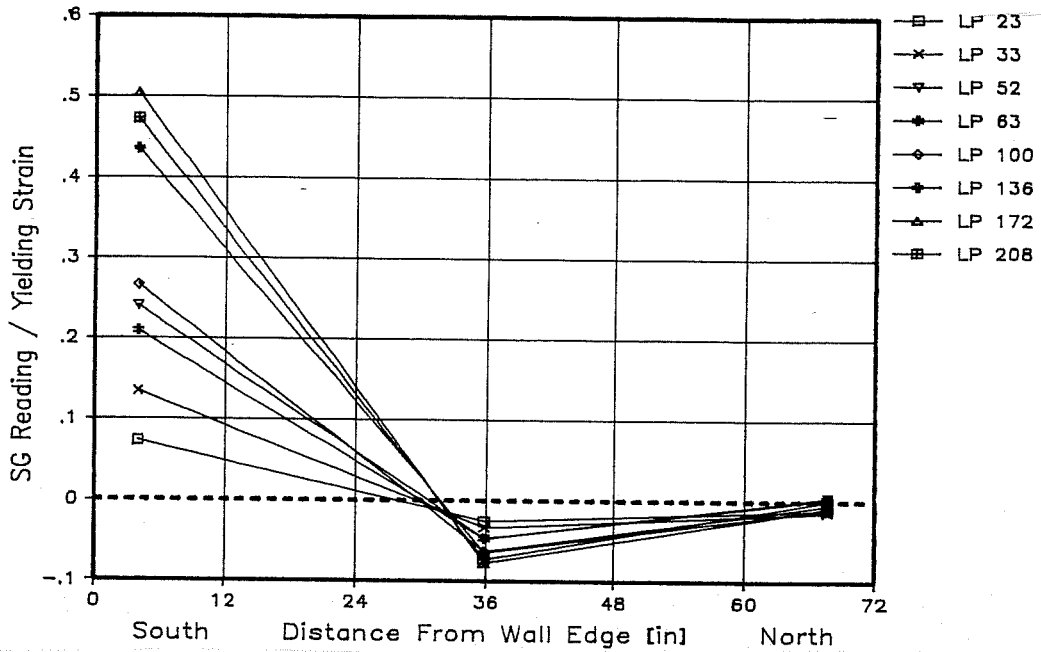

Figure 7.35a Sp. 2b: Strain in Longitudinal Reinforcement at Base of Second Story North Wall - North Loading

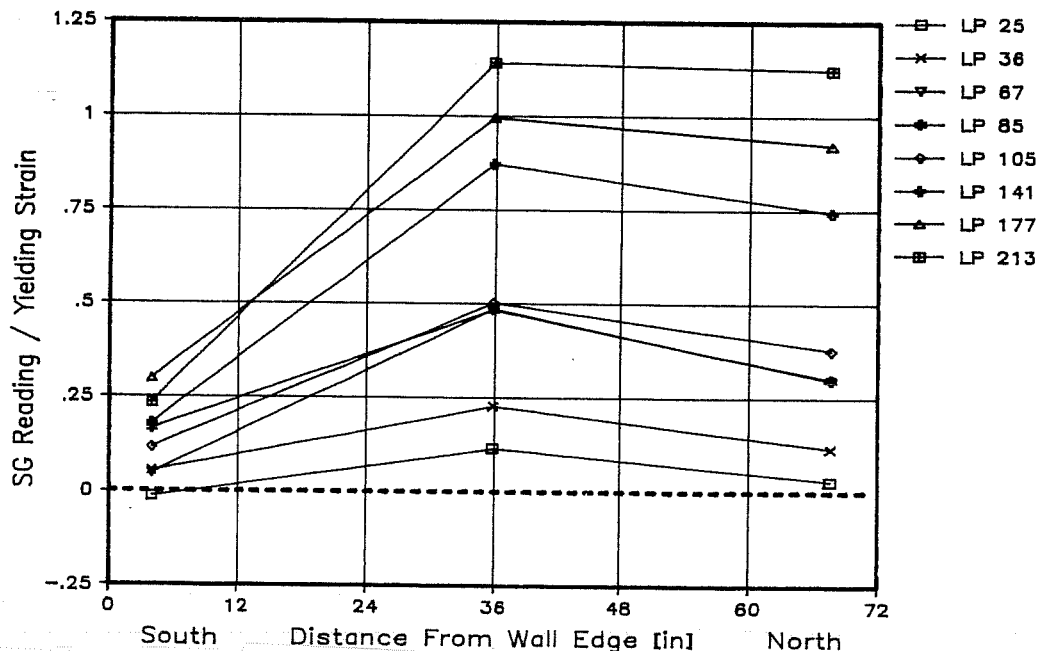

Figure 7.35b Sp. 2b: Strain in Longitudinal Reinforcement at Base of Second Story North Wall - South Loading

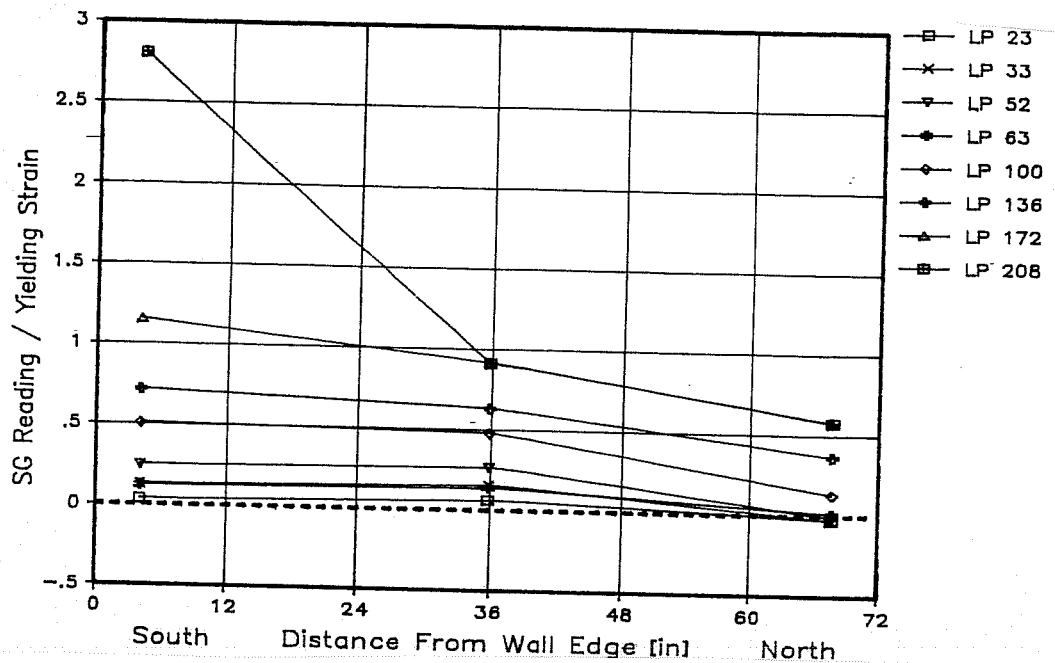

Figure 7.36a Sp. 2b: Strain in Longitudinal Reinforcement at Base of Second Story South Wall - North Loading

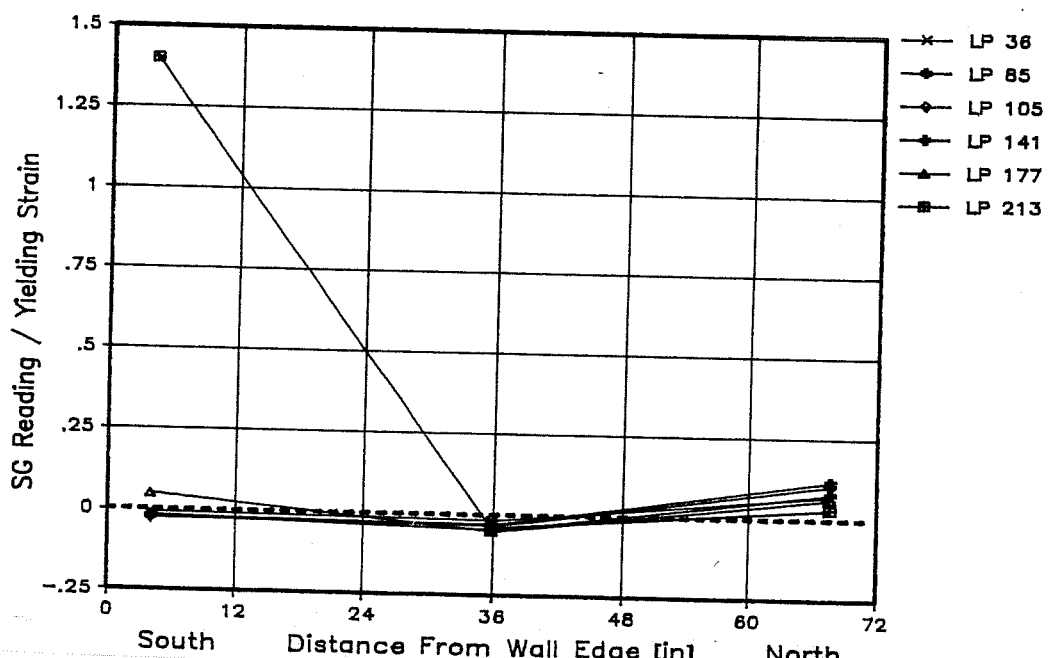

Figure 7.36b Sp. 2b: Strain in Longitudinal Reinforcement at Base of Second Story South Wall - South Loading

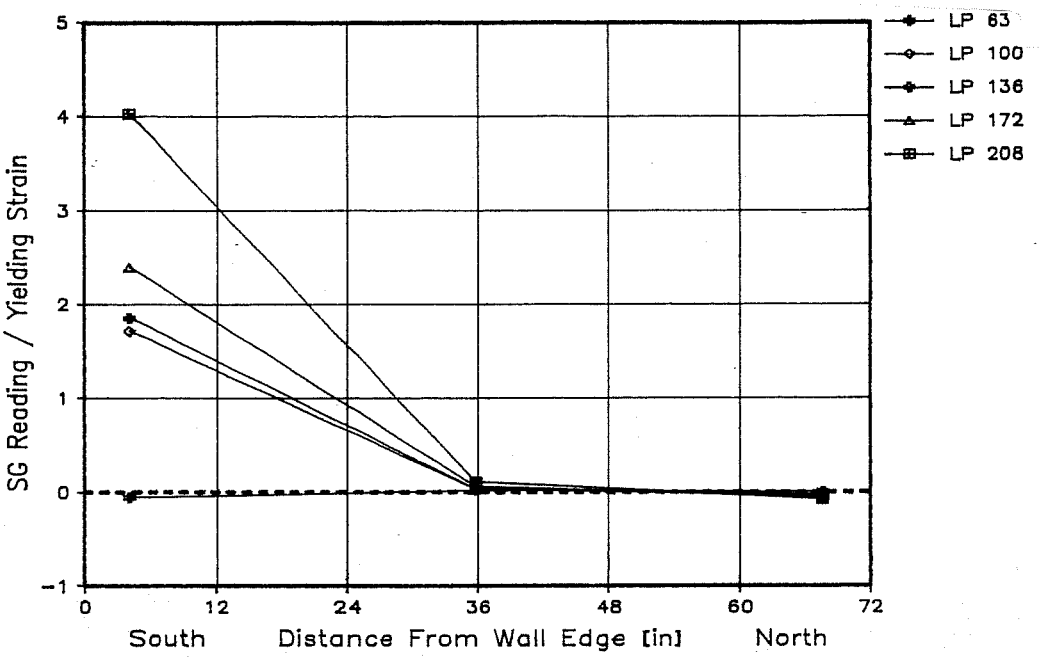

Figure 7.37a Sp. 2b: Strain in Longitudinal Reinforcement at Top of Second Story North Wall - North Loading

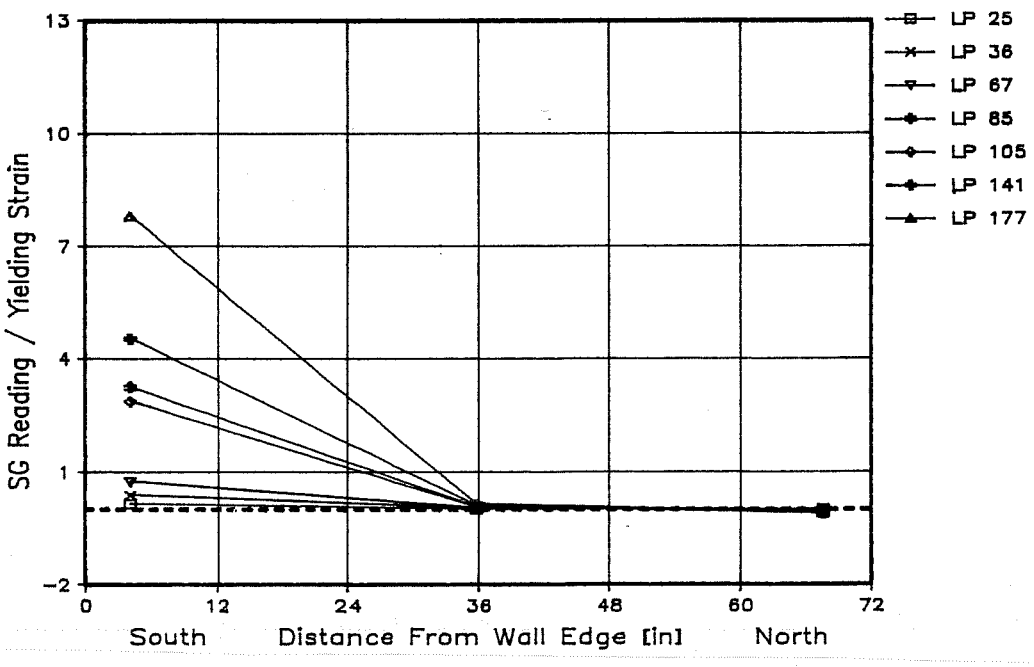

Figure 7.37b Sp. 2b: Strain in Longitudinal Reinforcement at Top of Second Story North Wall - South Loading

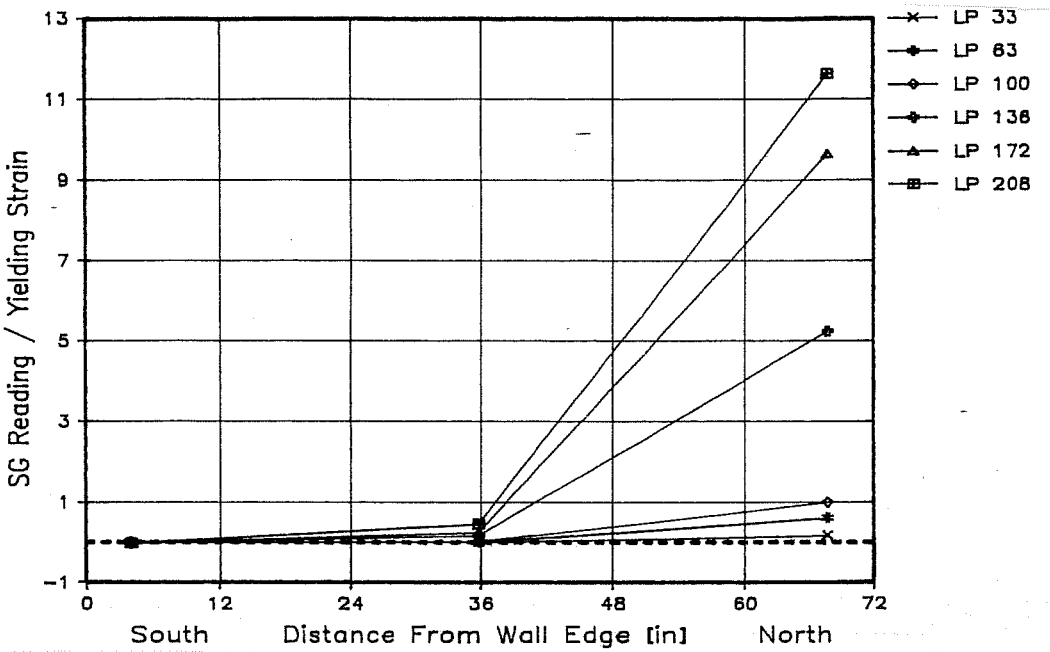

Figure 7.38a Sp. 2b: Strain in Longitudinal Reinforcement at Top of Second Story South Wall - North Loading

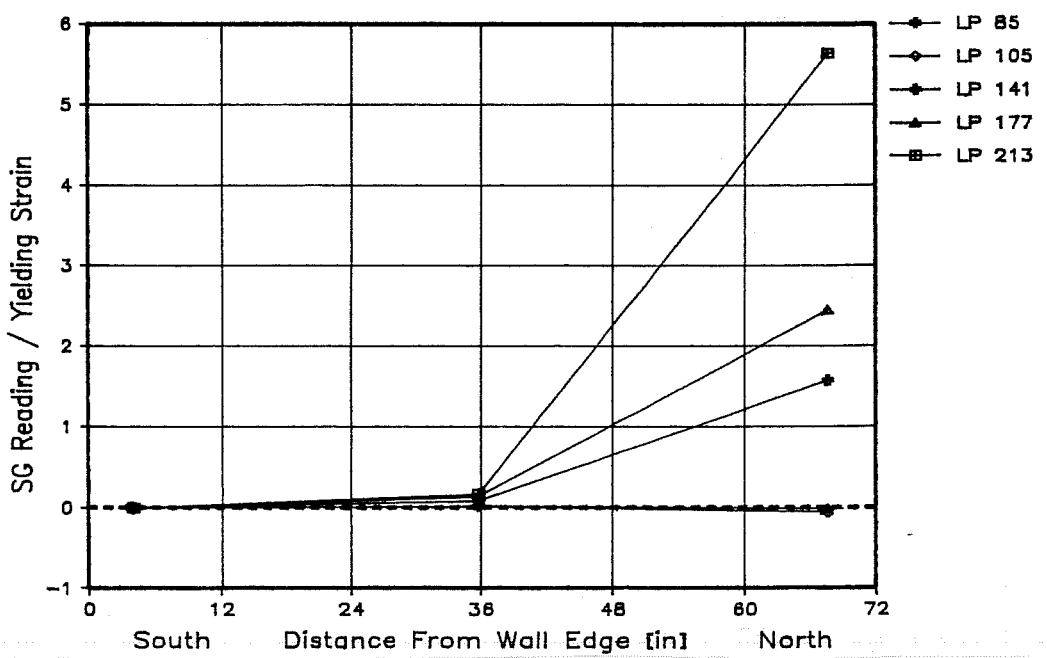

Figure 7.38b Sp. 2b: Strain in Longitudinal Reinforcement at Top of Second Story South Wall - South Loading

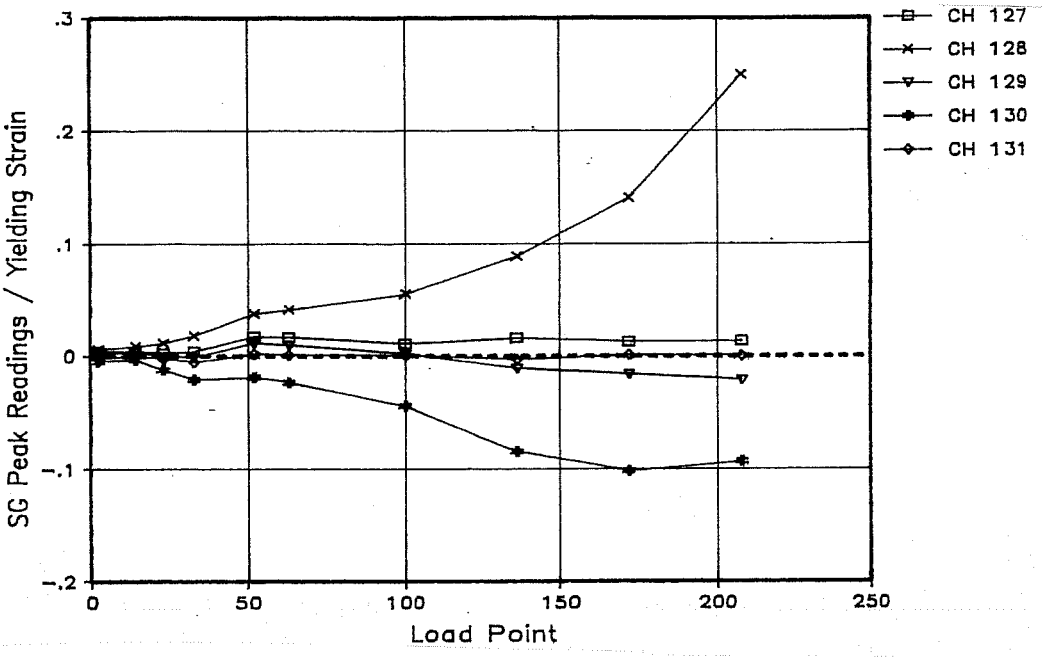

Figure 7.39a Sp. 2b: Strain in Transverse Steel for First Story North Wall - North Loading

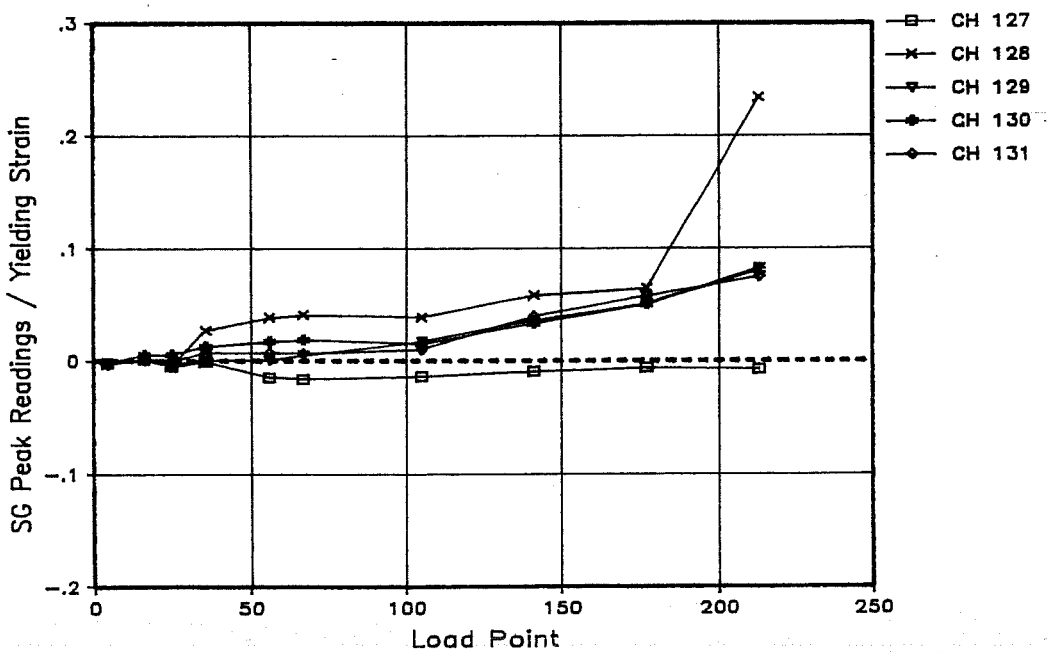

Figure 7.39b Sp. 2b: Strain in Transverse Steel for First Story North Wall - South Loading

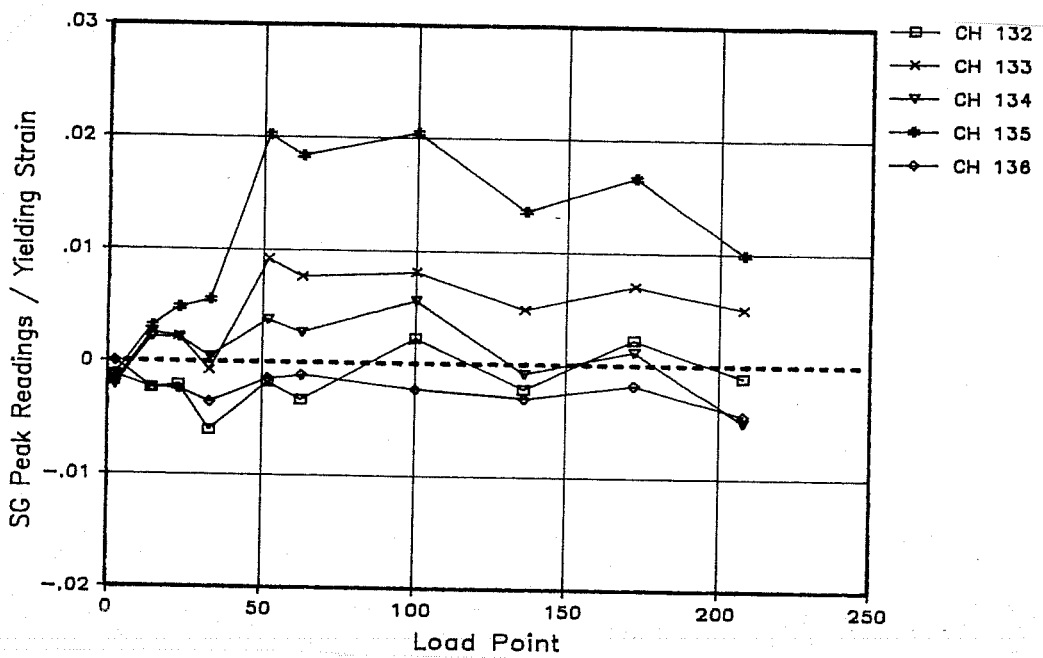

Figure 7.40a Sp. 2b: Strain in Transverse Steel for Second Story North Wall - North Loading

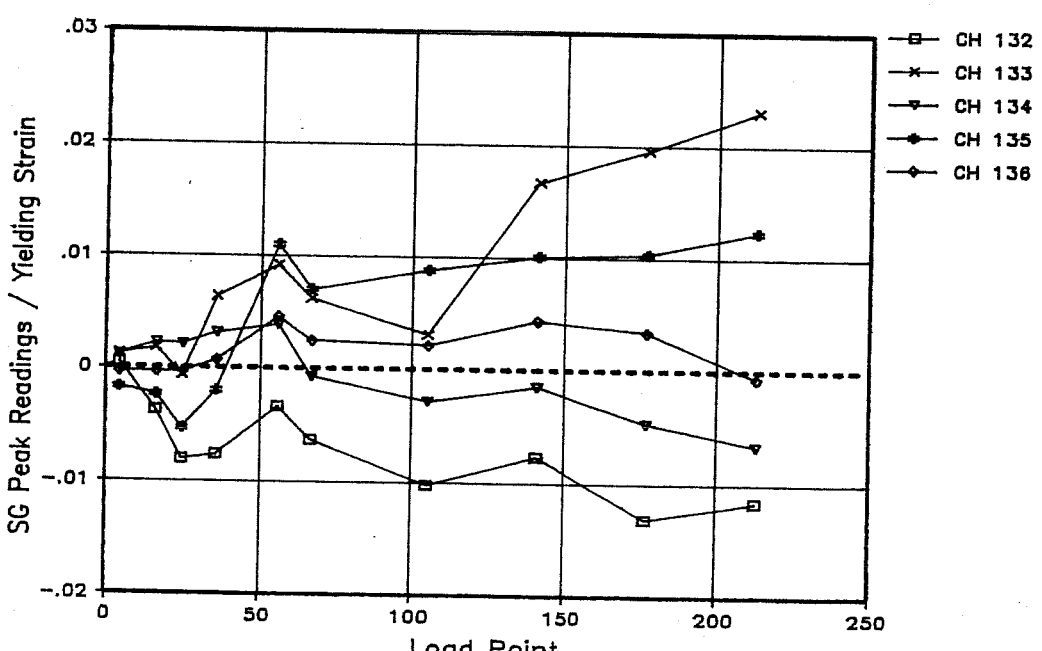

Figure 7.40b Sp. 2b: Strain in Transverse Steel for Second Story North Wall - South Loading

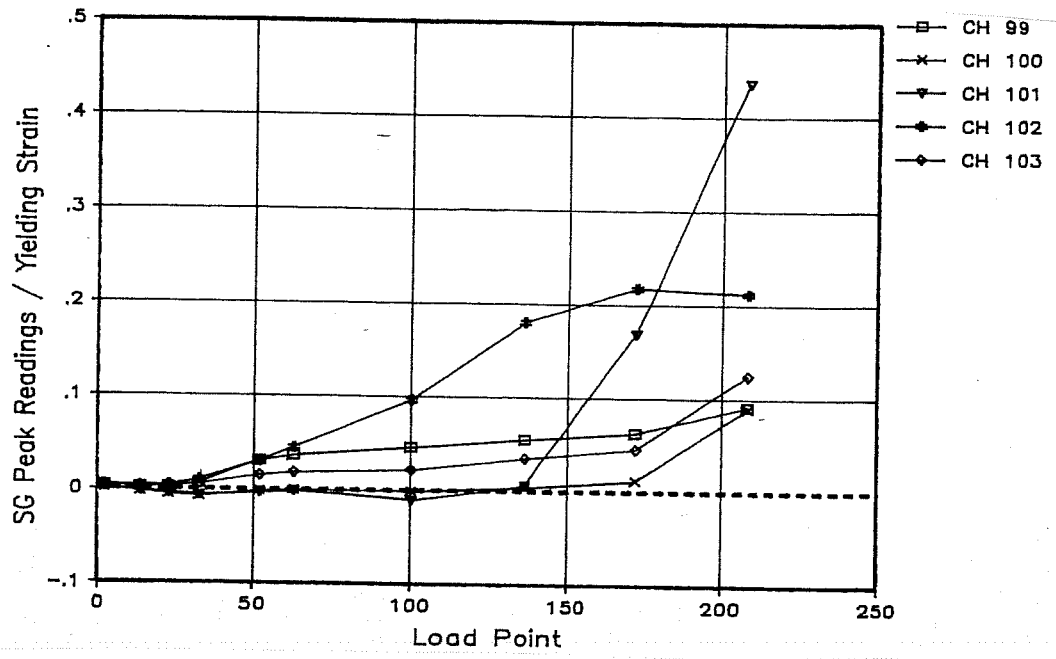

Figure 7.41a Sp. 2b: Strain in Transverse Steel for First Story South Wall - North Loading

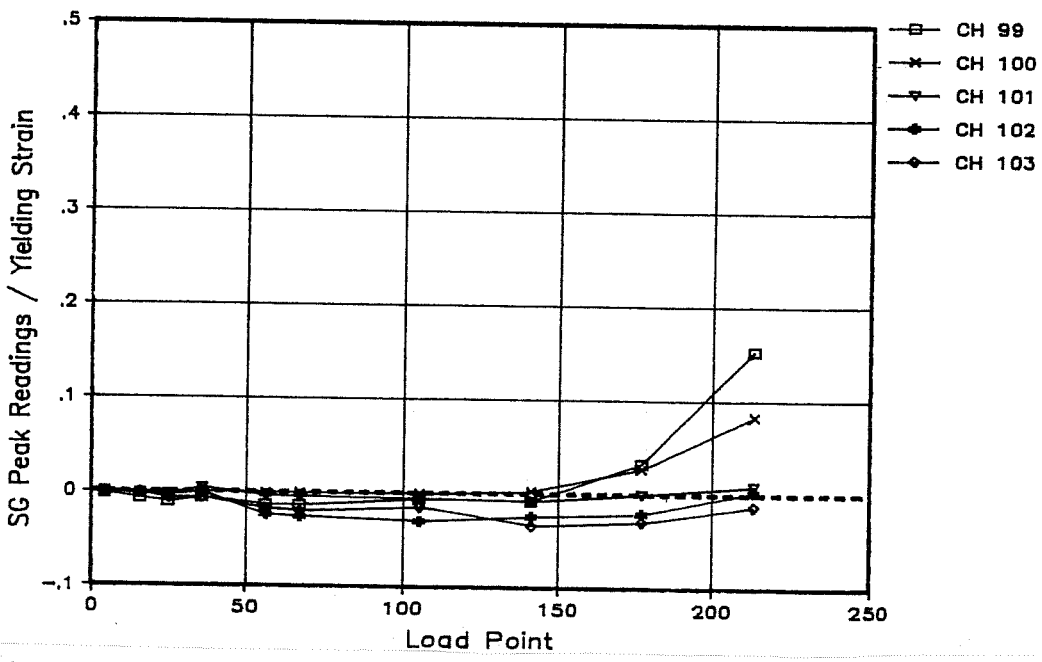

Figure 7.41b Sp. 2b: Strain in Transverse Steel for First Story South Wall - South Loading

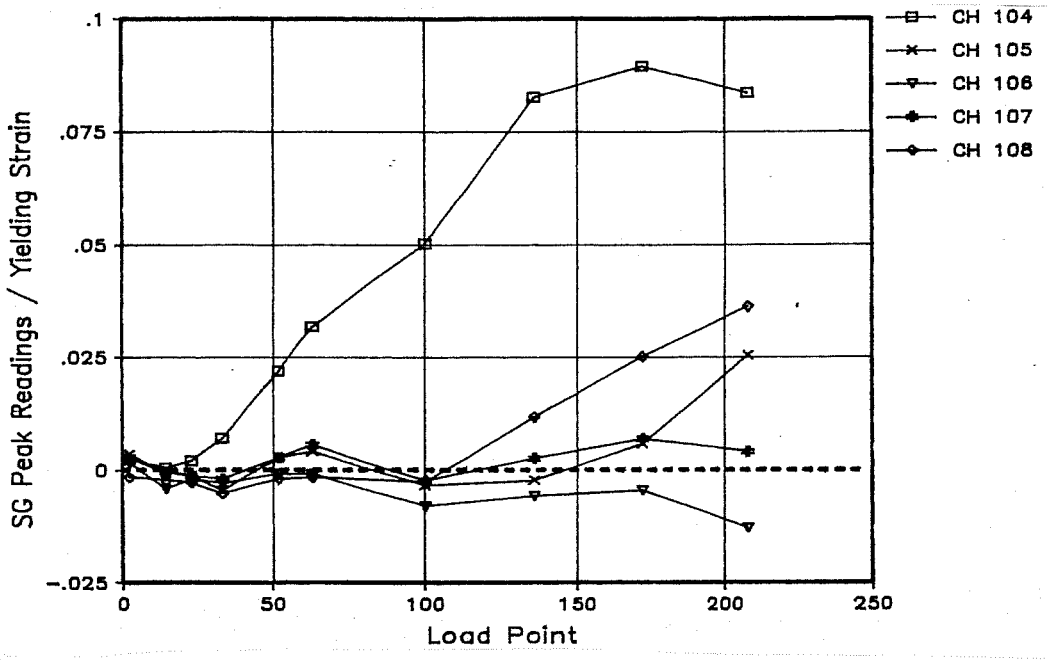

Figure 7.42a Sp. 2b: Strain in Transverse Steel for Second Story South Wall - North Loading

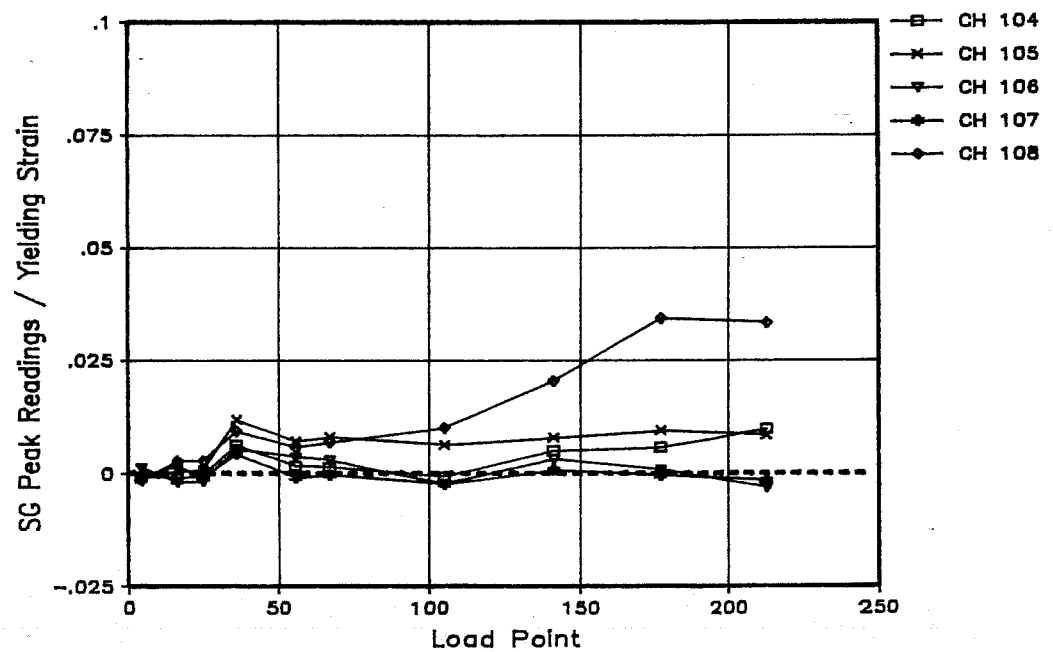

Figure 7.42b Sp. 2b: Strain in Transverse Steel for Second Story South Wall - South Loading

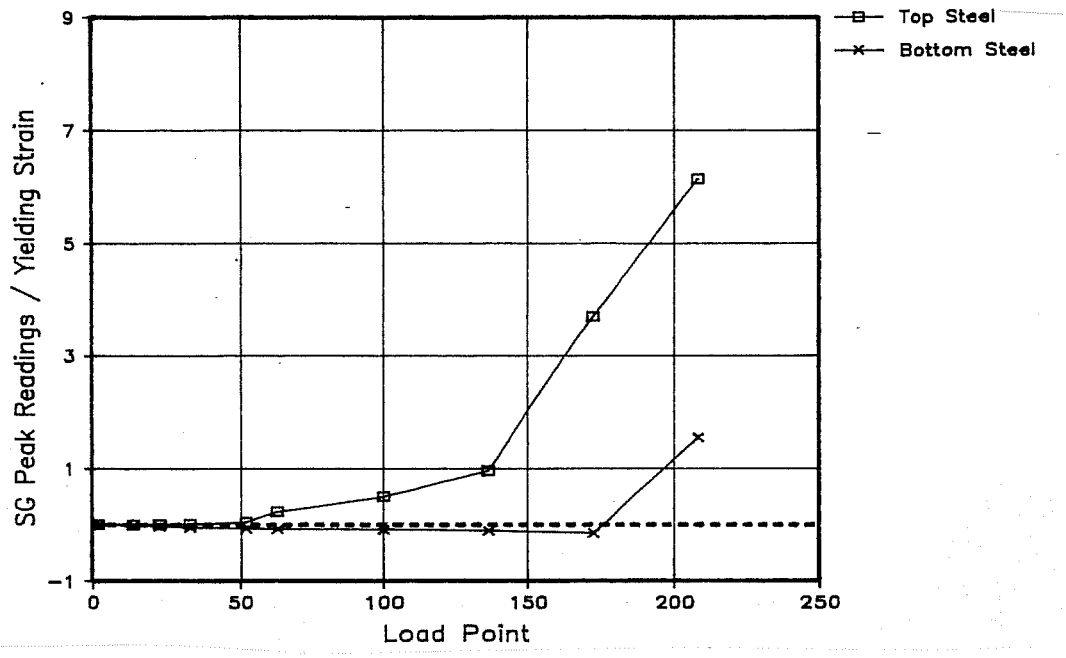

Figure 7.43a Sp. 2b: Strain in Longitudinal Reinforcement for Second Floor Slab - North Loading

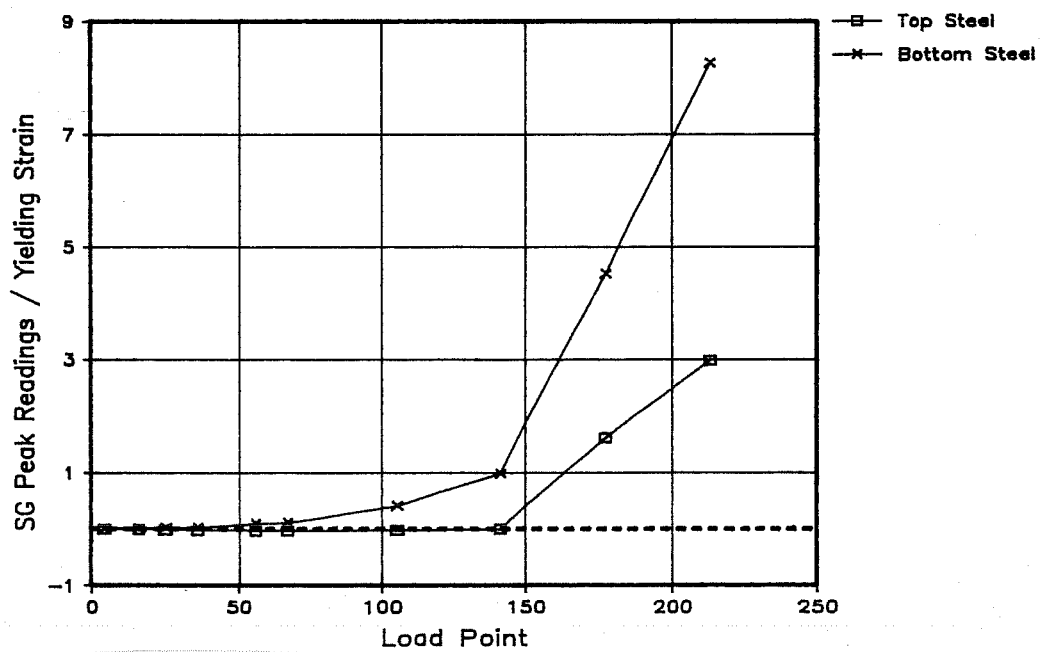

Figure 7.43b Sp. 2b: Strain in Longitudinal Reinforcement for Second Floor Slab - South Loading

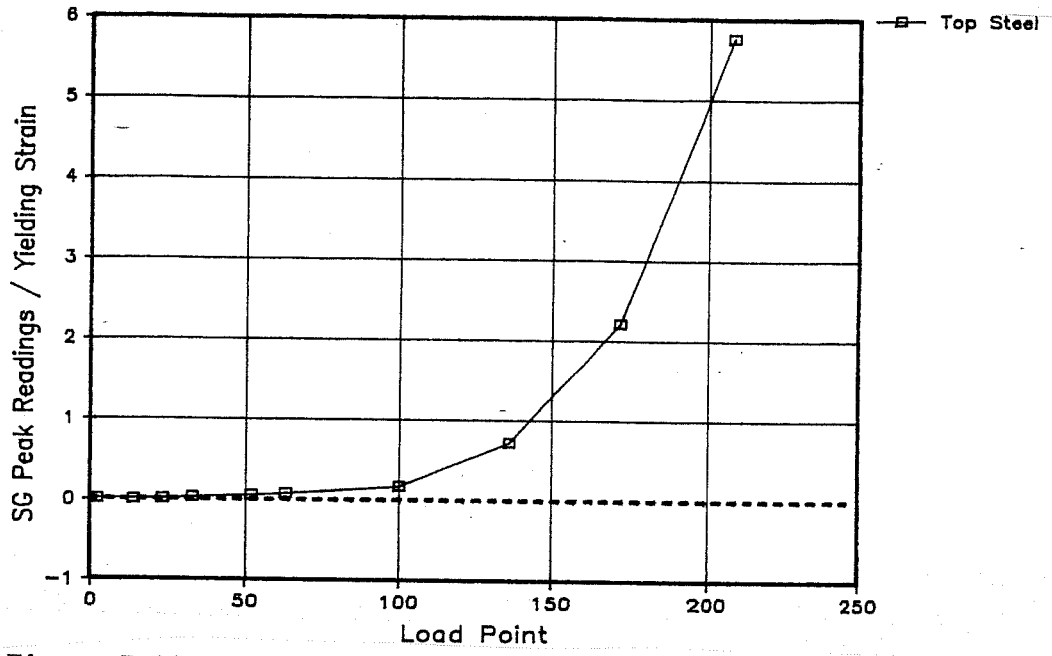

Figure 7.44a Sp. 2b: Strain in Longitudinal Reinforcement for Roof Slab - North Loading

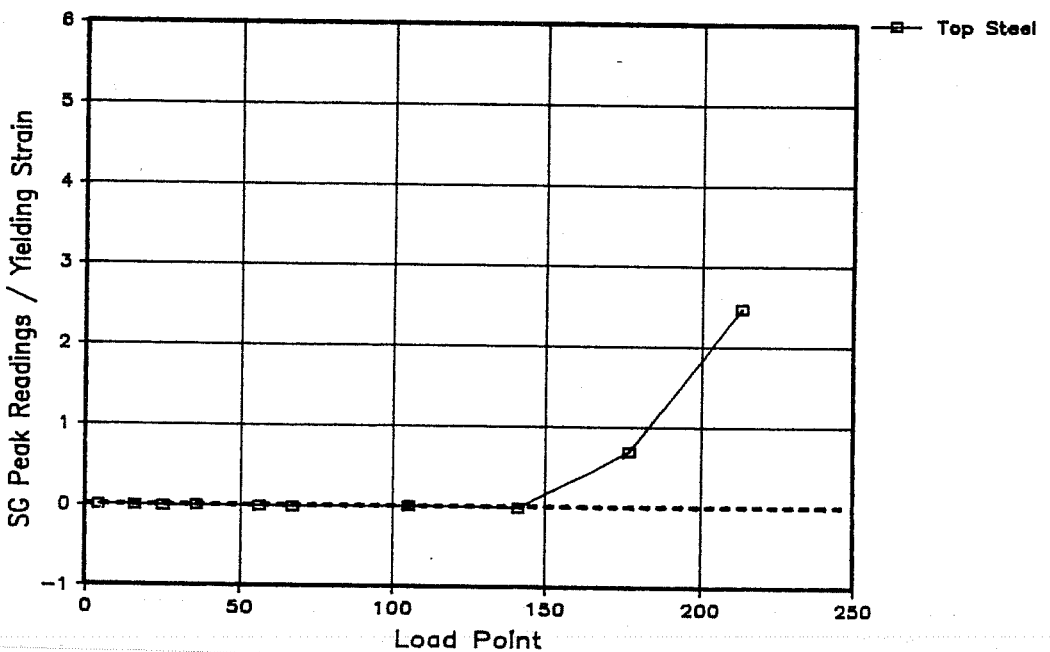

Figure 7.44b Sp. 2b: Strain in Longitudinal Reinforcement for Roof Slab - South Loading

Table 7.3 Observed Behavior of Specimen 2b
(March 30 - April 3, 1989) Northward Loading.

Load Pt	Specimen Behavior	Base Shear		Top Displacement	
		kips	kN	inches	mm
52	Flexural cracking of 2nd story tension wall; yield of 1st story tension wall	34.9	155.2	0.112	2.8
63	Flexural cracking of 2nd story compression wall; yield of 1st story compression wall; cracking of 2nd floor slab top face	43.9	195.3	0.202	5.1
85	Yield of 2nd story north wall joint opening	67.9	302.0	0.59	15.0
100	Cracking of roof slab top face	59.1	262.9	0.40	10.2
135	Diagonal shear cracking of both 1st story walls; yield of 2nd story south wall joint opening; cracking of 2nd story slab bottom face	65.5	291.3	0.56	14.2
171	Yield of 2nd story tension wall base	80.8	359.4	1.25	31.8
172	Cracking of roof slab bottom face; yield of 1st story south wall joint opening; Longitudinal shear cracking of roof slab top face	88.0	391.4	1.69	42.9
207	Cracking of compression toe of both walls; face shell spall at toe of compression wall; Longitudinal shear cracking of 2nd floor slab top face	86.6	385.2	2.55	64.8
208	Maximum load and top displacement; Longitudinal shear cracking of bottom face of both slabs	88.1	391.9	3.46	87.9
217	Fracture of extreme tension bar of compression wall	46.0	204.6	2.51	63.8
219	Loss of compression toe	-55.4 (South)	-246.4	-2.34 (South)	-59.4
220	Extreme compression bar of compression wall buckles	6.9	30.7	0.00	0.0

Table 7.4 Observed Behavior of Specimen 2b
(March 30 - April 3, 1989) Southward Loading.

Load Pt	Specimen Behavior	Base Shear		Top Displacement	
		kips	kN	inches	mm
16	Flexural cracking of tension wall and compression wall	10.3	45.8	0.017	0.4
36	After load jump; Yield of longitudinal steel of 1st story tension and compression wall	53.8	239.3	0.40	10.2
56	Flexural cracking of 2nd story walls; cracking of both slabs' top faces; diagonal shear cracking of tension wall	42.3	188.2	0.27	6.9
85	After load jump; yield of 2nd story north wall joint opening	67.9	302.0	0.59	15.0
105	Longitudinal shear cracking of 2nd floor slab bottom face	46.1	205.1	0.41	10.4
140	Cracking of 2nd story slab bottom face	60.3	268.2	0.62	15.7
176	Longitudinal shear cracking of roof slab bottom face	69.1	307.4	1.18	30.0
177	Yield of 1st story north wall joint opening	74.8	332.7	1.57	39.9
212	Yield of 2nd Story tension wall; cracking of roof slab bottom face	72.4	322.0	2.32	58.9
213	Maximum load and top displacement; vertical cracking of compression wall toe	78.3	348.3	3.10	78.4

the bottom three courses, and extended halfway across the wall. At Load Point 27, the base shear was 20.3 kips at a top displacement of 0.067 inches to the north. Flexural cracking occurred on the lower half of the first- story south wall's southern edge.

The next load series was at about 30 kips base shear. At Load Point 33, the load was northward at a base shear of 30.6 kips and a top displacement of 0.11 inches. The north wall developed flexural cracks on the north edge at the top of the first-story. The flexural cracking is due to the double curvature of the walls. The south wall suffered flexural

yielding had occurred, based on the yield strain of the longitudinal reinforcement. The first-story north wall yielded at the base at a base shear of about 30.7 kips and a top displacement of 0.21 inches. The first-story south wall yielded at the base at a base shear of 44.1 kips and a top displacement of 0.278 inches.

After the system was corrected, the specimen was loaded to the south at approximately the same load cycle level to examine for cracks. The base shear was 30.7 kips and the top displacement was 0.21 inches at Load Point 39. The first-story north wall exhibited more flexural cracking along the tension side. A flexural crack extended along half the wall length at the longitudinal reinforcement splice. Flexural cracking occurred along the wall and slab joint at the opening at the top of the north wall. The first-story south wall had more flexural cracking towards the mid-height of the wall. Due to double curvature, flexural cracks formed at the top of the south edge of the first-story.

The next load series was at about 40 kips base shear. At Load Point 52, the base shear was 39.3 kips at a top displacement of 0.16 inches toward the north. Due to double curvature, the first-story of the north wall had more flexural cracking along the north edge. The second-story of the north wall cracked one course below the roof slab at the wall opening. The first-story south wall longitudinal steel yielded at the base at the south edge as shown in Figure 7.32(a). This was not known until after testing, when corrections were made to strain gauge Channel 81 for the loading problems incurred at Load Point 36 (Appendix C). The first-story south wall continued to crack near the wall opening by the second-floor slab and wall connection. In the second-story south wall, a flexural crack about 10 inches long formed along the base. Loading to the south, the base shear was 42.3 kips and the top displacement was 0.27 inches at Load Point 56. The first diagonal shear crack formed on the first-story north wall at the second course. The second-story base of both walls cracked along the north edge. The slabs in both stories cracked on the top side. The second- story slab cracked at the south edge of the opening across the entire slab width. The crack was several inches away from the wall edge. The roof slab cracked along the south side of the opening. The crack pattern is shown in Figure 7.49.

The First Major Event was to be defined as yield of the longitudinal steel at the base of the tension wall. Due to the problem encountered after Load Point 36 while loading to the south, the longitudinal steel had already yielded for this loading direction as shown in Figure 7.31(b). Therefore, the First Major Event was defined as coinciding with a base shear of 44 kips. The event occurred at Load Point 63, whose base shear was 43.9 kips, and whose top displacement was 0.20 inches. The longitudinal reinforcement yielded at the base of the south side of the first-story north wall. A flexural crack formed at the base of the second-story north wall. Due to double curvature, extensive flexural cracking continued above mid-height

along the north side of the first-story south wall. A flexural crack extended along about two-thirds of the base of the second-story south wall. The top face of the second-floor slab cracked across the entire width on the northern edge of the wall opening.

Loading to the south at a base shear of about 100% of the First Major Event base shear, the base shear was 47.4 kips and the top displacement was 0.30 inches (Load Point 67). Flexural cracking occurred at mid-height of the first- story north wall. The first diagonal shear crack formed on the first-story south wall.

Since the walls had yielded in flexure, the loading system was switched from load control to displacement control. Testing under displacement control began at Load Point 81, using the top displacement of 0.20 inches as the First Major Event displacement.

While loading southward for the first time under displacement control at the First Major Event displacement, a sudden increase in load occurred at Load Point 85. The system was immediately shut down. The system was thoroughly examined and no problem could be detected. After rechecking the system under low pressure, the testing was continued with no further system malfunctions occurring.

At Load Point 85, the total applied load and the top displacement were calculated from the plotter as 67.9 kips and 0.59 inches, respectively. As shown in Figure 7.37(b), yielding occurred at the wall and slab joint at the wall opening of the second-story north wall. This applied load was large enough to have cracked the slabs, but the slabs exhibited no new cracking. Again, inertial effects are believed to have made the base shear considerably less than the applied load. At the next load point towards the south, the walls exhibited no further cracking.

While cycling further at displacements corresponding to the First Major Event, flexural cracks formed near the mid-height of the first-story north wall. A crack formed in a head joint of the first-story south wall. More flexural cracking occurred in the second-story south wall, and more flexural cracking occurred due to double curvature of the walls.

The next load series was at a top displacement of about 200% of the First Major Event displacement. At Load Point 100, the base shear was 59.1 kips and the top displacement was 0.40 inches towards the north. As shown in Figure 7.38(a), longitudinal reinforcement yielded at the roof slab and the south wall opening. The crack at the opening extended halfway along the wall length. The flexural crack, along the longitudinal reinforcement splice of the first-story north wall, extended across more than half the wall length. Loading to the south, the base shear was 46.1 kips and the top displacement was 0.40 inches at Load Point 105. A second diagonal shear crack formed on the first-story north wall. Flexural cracking continued on both first-story walls. After cycling at the 200% FME load series, flexural

cracking began along the second-story walls along their southern edges when the walls were loaded to the north.

The next load series was at a top displacement of about 400% of the First Major Event displacement. When loading up to 400% FME, a reading was taken at 300% FME and the walls were examined for cracking.

At about 300% of the First Major Event displacement, the base shear was 65.5 kips at a top displacement of 0.56 inches at Load Point 135. The load was to the north. The first diagonal shear crack appeared in the first-story of both walls for the north load direction. Figures 7.39(a) and 7.42(b) show that the transverse reinforcement remained elastic throughout the test. The second-floor slab's bottom face cracked at the south wall opening edge. The crack extended almost completely across the slab width. The top face of the roof slab cracked along the width of the slab at the north wall opening edge.

At Load Point 136, the top displacement was increased to approximately 400% of the First Major Event displacement. The base shear was 75.1 kips and the top displacement was 0.82 inches to the north. More diagonal shear cracking occurred across the first-story north wall. The first-story south wall cracked completely across, at one course below the second-floor slab. A diagonal crack formed at the top of the first-story south wall near the south edge running to the north edge about four courses from the top. More flexural cracking occurred along the south edge of the second stories of both walls. The top face of the second-story slab cracked across the slab width about 8 inches into the wall from the north wall opening edge. The top face of the roof slab cracked all the way across the slab width towards the center of the wall opening from the northern edge.

At Load Point 140, the specimen was loaded to the south at a top displacement of about 300% of the First Major Event displacement. The base shear was 60.3 kips, and the top displacement was 0.62 inches. The bottom face of the second-floor slab cracked on the north side of the wall opening. The crack was across half the western side of the slab. More flexural cracking occurred on the top face of the second-story slab.

At a top displacement of about 400% of the First Major Event displacement, the base shear was 70.4 kips, and the top displacement was 0.80 inches at Load Point 141. The load was to the south. More diagonal shear cracking formed along the first-story north wall. Flexural cracking continued on both slabs.

The next load series was up to a top displacement of about 800% of the First Major Event displacement. Readings were taken and cracks were marked at an intermediate point of about 600% FME displacement.

At Load Point 171, the base shear was 80.8 kips, and the top displacement was 1.25 inches. The loading was to the north at a top displacement of about 600% of the First Major Event displacement. Longitudinal reinforcement yielded at the base of the south side of the second-story south wall (shown in Figure 7.36(a)). Cracking on the bottom face of the roof slab formed at the south end floor plates. The localized cracking was due to transfer of load from the floor plates to the slab. The second-floor slab exhibited more cracking on the top and bottom face. The cracks tended to project at an angle from the edge of the wall opening at the center of the slab towards the middle of the wall opening at the slab edge.

At a top displacement of about 800% of the First Major Event displacement, the base shear was 88 kips, and the top displacement was 1.69 inches to the north at Load Point 172. As shown in Figure 7.34(a), longitudinal reinforcement yielded near the intersection between the first-story of the south wall and first floor slab at the wall opening. The second-story south wall and roof slab joint separated about 1/4 inch at the wall opening. More cracking occurred on the top and bottom faces of both floor slabs. The slabs formed a definite S-shape, and remained elastic. On the top face of the roof slab, a longitudinal shear crack formed along the intersection of the east edge of the south wall and the slab. The crack ran from the south end to the center of the wall. Diagonal shear cracking continued in the first-story of the north wall. The cracks ran from about five courses up on the south wall edge towards the compression toe at the north edge. The flexural crack was opening at the longitudinal reinforcement splice of the first-story south wall. Crushing began at the compression toe of the first-story south wall. The base of both walls were uplifting about 1/4 inch.

At Load Point 176, the loading was to the south at a top displacement of about 600% of the First Major Event displacement. The base shear was 69.1 kips, and the top displacement was 1.18 inches. On the roof slab's bottom face, a longitudinal shear crack formed along the opening at the intersection of the wall's west edge and the slab. The crack ran about 5 inches from the north end of the wall opening towards the center. Localized cracking formed from the floor plate to the wall edge along the top faces of both slab floors. Another flexural crack formed on the roof slab's top face. The wall base was sliding up to about 3/4 inch as shown in Figures 7.29 and 7.30.

The top displacement was increased to about 800% of the First Major Event displacement at Load Point 177. The base shear was 74.8 kips, and the top displacement was 1.57 inches to the south. Longitudinal reinforcement yielded at the first-story north wall and slab opening joint. Diagonal shear cracking continued in the first-story south wall at an angle towards the compression toe. Both slabs exhibited a definite S-shape for the south loading direction. On the bottom face of the second-floor slab, a longitudinal shear crack

formed along the opening at the intersection of the west edge of the wall and the slab. The crack ran from the north end to across two-thirds of the center of the wall opening. The longitudinal shear crack, which formed on the bottom face of the roof slab at Load Point 176, extended to the center of the wall opening.

After cycling at about 800% of the First Major Event displacement, no new cracking or yielding occurred. The next load series was up to a top displacement of about 1600% of the First Major Event displacement. Readings were taken at about 1200% FME displacement, and the walls were examined for new cracking.

At Load Point 207, the top displacement was approximately 1200% of the First Major Event displacement. The base shear was at 86.6 kips, and the top displacement was 2.55 inches to the north. Cracking began at the compression toe of both first-story walls. Also, the face shell spalled off at the compression toe of the first-story north wall. Diagonal cracking became more extensive at the first-story north wall. More diagonal cracking occurred in the first-story south wall. Another longitudinal shear crack formed across the opening on the bottom face of the second-floor slab. On both slabs, cracks extended and new flexural cracks formed. The second-story south wall and slab connection at the opening had a 3/8 inch crack.

At a top displacement of about 1600% of the First Major Event displacement, the base shear was 88.1 kips, and the top displacement was 3.46 inches. This was the maximum load and displacement for the north load direction. The first-story north wall's compression toe continued to separate from the wall. The base of the north wall at the south edge lifted 3/4 inches off the base. The base of the south wall at the south edge was lifting 1 inch from the base. More diagonal shear cracks occurred in the first-story north wall. Cracking continued in both slabs.

At Load Point 212, the loading was to the south at a top displacement of about 1200% of the First Major Event displacement. Longitudinal reinforcement yielded, due to flexure, at the base of the north side of the second-story north wall, as shown in Figure 7.35(b). The first flexural crack formed for the south load direction on the bottom face of the roof slab. Also, localized cracking occurred around the northwest loading plate.

At a top displacement of approximately 1600% of the First Major Event displacement, the base shear was 78.3 kips, and the top displacement was 3.10 inches to the south at Load Point 213. This was the maximum load and displacement for the south loading direction. Vertical cracking and crushing occurred at the compression toe of the first-story south wall.

While cycling down from the 1600% FME displacement, the compression toes were lost from both first-story walls for the north load direction. The north wall compression toe completely separated and fell away from the wall at Load Point 219, while loading to the south at a top displacement of about 1200% FME displacement. At Load Point 217 while loading to the north at a top displacement of about 1200% FME displacement, the extreme tension longitudinal bar fractured in the first-story north wall. After losing the compression toe of the north wall, the first-story longitudinal bar buckled at Load Point 220, at zero displacement. Lateral displacement of the walls' bases became notable while cycling. At Load Point 215, the maximum lateral displacement of the north wall was 1/2 inch, and of the south wall, 3/4 inch. By Load Point 217, the lateral displacement of the north wall was 3/4 inch and of the south wall was 1-1/8 inches.

When the test ended, the final out-of-plane displacement was 7/8 inches for the north wall and 1-3/8 inches for the south wall. The final in-plane displacement is shown in Figures 7.29 and 7.30. The north wall had a final in- plane displacement of 0.13 inches to the south, and the south wall had a final in-plane displacement of 0.19 inches to the north.

8. DISCUSSION OF TEST RESULTS

8.1 General

In this chapter, test results are examined in terms of the load-deflection response of the specimens, and in terms of the load-deformation response of their structural elements (walls and coupling slabs). Structural response is described in terms of the following:

1) the load-displacement histories of Specimens 2a and 2b;

2) the deformations, strains, and construction details of the walls;

3) the coupling behavior and construction details of the slabs; and

4) the failure modes of each specimen.

8.2 Discussion of Load-Displacement History

8.2.1 General. The load-displacement history of Specimens 2a and 2b will be examined in terms of hysteresis loops, load-displacement envelopes, and the comparison between those load-displacement envelopes and the analytically predicted envelopes.

Some figures used in this and subsequent sections compare different loading cycles within the same load series. Within each load series, the peaks are defined as shown in Fig. 8.1: "first peak," which is the first time the peak load is reached in a particular load series; "second peak," which is the second time the peak value is attained; "last peak," which refers to the last cycle in the load series at the peak value; and "next peak," which is the peak value of the last load series, loading up to a higher value in the next load series.

8.2.2 Discussion of Hysteresis Loops. The hysteresis loops for the entire tests are shown in Figures 7.5 and 7.26 for Specimens 2a and 2b respectively. In Figures 8.2 to 8.3, the first peak cycles of each load series are displayed for Specimen 2a and 2b respectively.

As shown in Figures 8.2 and 8.3, the hysteresis loops remain very stable throughout both tests. For Specimen 2a, fracture of the longitudinal reinforcement at the north end of the first story of the north wall and the subsequent loss of strength, are shown in Figure 8.2 by the decrease of base shear in the largest loop while loading to the south. Both specimens' hysteretic behavior was basically flexural, which concurs with the observed failure modes, discussed in Subsections 7.2.1 and 7.3.1 for Specimens 2a and 2b respectively.

The plots for the last complete load series in each test are reproduced in Figures 8.4 and 8.5 for Specimens 2a and 2b respectively. The plots give details of the hysteresis loops

which are not apparent from the discrete readings of the data acquisition system. Pinching can be seen in the hysteresis loops for both specimens. This pinching is due to sliding of the coupled wall at the base of the first story. Plots of earlier load series, before substantial base sliding, exhibit little pinching. For Specimen 2a, the last complete load series was at a peak roof displacement of about 1.70 inches (4800% of the First Major Event). During this load series, the maximum slip at the base of the first story walls was 0.10 inches to the north and 0.28 inches to the south, for the north and south load directions respectively. For Specimen 2b, the last complete load series was at a peak roof displacement of about 1.6 inches. The maximum slip at the base of the first story walls during this load series was 0.28 inches to the north and 0.40 inches to the south, for the north and south loading directions respectively. As shown in Figure 8.4 and 8.5 for Specimens 2a and 2b, slip at the base of the first story walls correlates well with the point at which the stiffness begins to increase after pinching of the loops. Pinching can also be due to shear. However as discussed in Subsection 8.4.4, shear was not a critical factor for either specimen.

Energy dissipation seems satisfactory at the first peak cycle throughout testing of both specimens (Figures 8.2 and 8.3). Tables 8.1 and 8.2 show the energy dissipation for the last complete load series of Specimens 2a and 2b as calculated from Figures 8.4 and 8.5 using a planimeter. This was expressed in terms of energy dissipation normalized by peak lateral displacement. An elasto- plastic specimen would have a nearly constant value of this ratio. Decreases in this ratio indicate departures from elasto-plastic behavior due either to pinching or strength deterioration. For Specimen 2a, the reduction in (Energy/Peak Displacement) between first and last peak was 31% for the north direction, and 33% for the south direction. For Specimen 2b, the reduction in (Energy/Peak Displacement) between first and last peak was 48% for both load directions. The first peak energy dissipation for Specimens 2a and 2b were similar as shown in Tables 8.1 and 8.2. However, the energy dissipation ability of Specimen 2a was better than for Specimen 2b after cycling to the last peak in the load series.

8.2.3 Discussion of Load-Displacement Envelopes. Figures 7.6 and 7.28 show envelopes of base shear at first peak versus the roof displacement for Specimens 2a and 2b. As shown in those figures, both specimens' envelopes exhibit linear and nonlinear regions.

Specimen 2a started to become nonlinear at about 250% of the First Major Event for both north and south load directions, corresponding with yielding of compression walls, and cracking and yielding of both slabs. For the north direction, base shear was 58.5 kips at a roof displacement of 0.16 inches, and for the south direction, base shear was 54.5 kips at a roof displacement of 0.14 inches.

Specimen 2b's north and south envelopes started to become nonlinear at different load series due to loading problems encountered during testing. For the north envelope at

Table 8.1 Energy Dissipation at Last Complete Load Series, Specimen 2a.

Loading Direction	Peak	Energy (k-in)	Peak Disp. (in)	Energy/Peak Disp (k-in/in)
North	First Peak (LP 357)	6.04	1.70	3.56
	Last Peak (LP 388)	4.19	1.71	2.45
South	First Peak (LP 361)	5.76	1.61	3.58
	Last Peak (LP 390)	3.87	1.61	2.41

Table 8.2 Energy Dissipation at Last Complete Load Series, Specimen 2b.

Loading Direction	Peak	Energy (k-in)	Peak Disp. (in)	Energy/Peak Disp (k-in/in)
North	First Peak (LP 172)	6.46	1.69	3.82
	Last Peak (LP 202)	3.34	1.69	1.98
South	First Peak (LP 177)	5.68	1.57	3.62
	Last Peak (LP 204)	2.93	1.56	1.88

load point 63, base shear was 43.9 kips at a roof displacement of 0.202 inches, corresponding to yielding of the compression wall and cracking of the top face of the second-story slab. For the south envelope at Load Point 36 (after the load spike), the base shear was 53.8 kips at a roof displacement of 0.40 inches, which corresponds to flexural yield of compression and tension walls.

For both Specimens 2a and 2b, the curves shown in Figures 7.6 and 7.28 changed from linear to nonlinear at about the same time that the compression wall yielded.

Figures 8.6 and 8.7 show strength degradation for Specimens 2a and 2b respectively. The figures show envelopes of the first peak, last peak, and next peak for the entire tests. As shown in Figures 8.6 and 8.7, strength reductions coincided with the appearance of nonlinearity in the envelopes. For Specimen 2a, strength reduction between first peak and next peak for the maximum base shear was 12% for the north load direction and 23% for the south load direction. For Specimen 2b, strength reduction between first and next peak for the last complete load series (800% FME) was 24% for both load directions. Both specimens maintained satisfactory strength while cycling at each load series.

8.2.4 Comparison of Load-Displacement Envelopes with Predicted Envelopes. Figures 8.8 and 8.9 compare the predicted envelopes (Figures 6.3 and 6.4) with base shear at first peak value versus roof displacement envelopes for the north and south load direction, for Specimens 2a and 2b respectively.

The predicted envelopes are based on monotonic loading, while both specimens were tested cyclically. As shown in both Figures 8.8 and 8.9, the north and south envelopes model the predicted envelope fairly well. The difference between the predicted envelope and the north envelope can be accounted for by the fact that predicted analysis did not include slip at the base of the first-story walls (which actually occurred during the tests).

As observed for both specimens, base shear for the south envelope is always less than for the north envelope at the same roof displacement. This difference in base shear is due to the loading sequence. For each load cycle, specimens are first loaded towards the north, and the resulting loss in stiffness of the walls when loading to the north causes a reduced strength for the same displacement towards the south. Therefore, comparisons between the predicted and observed envelopes will be based on the observed envelope for northward loading.

For Specimen 2a's north envelope, the maximum base shear was 98% of the predicted value, and the maximum displacement was 140%. For Specimen 2b's north envelope, the maximum base shear was 97% of the predicted value and the maximum displacement

was 81%. Therefore, both specimens' cyclic response envelopes corresponded reasonably well with predicted monotonic loading behavior.

8.2.5 Comparison of Maximum Lateral Load Capacity of Coupled Walls with Uncoupled Walls. The maximum lateral load capacity of the shear walls without coupling slabs is calculated using simple plastic analysis (Equation 5 of Subsection 6.3.1). The flexural capacities of the wall base sections are obtained from the RCCOLA computer program [22] used in Subsection 6.3.2. Since there is no axial force due to the coupling system, the moments at the walls' bases are equal. This results in an overturning moment capacity of 7,052.4 kip-in for the shear walls without a coupling system. The resulting lateral load capacity is 46.4 kips.

For Specimen 2a, the maximum lateral load reached was 88.1 kips, which is a 90% increase over the capacity of the uncoupled shear walls. For Specimen 2b, the maximum lateral load reached was 95.9 kips which is a 107% increase over the capacity of the uncoupled shear walls. Since lateral load capacity for the coupled walls (Specimens 2a and 2b) is greater than for the uncoupled shear walls, the specimens' coupling slabs transferred shear and moments between the walls resulting in the greater lateral load and flexural capacity (Eqn. 5, Subsection 6.3.1).

8.3 Discussion of Specimen Stiffness

Figures 8.10 and 8.11 show tangent stiffness and first peak value backbone stiffness envelopes for Specimens 2a and 2b. The tangent stiffness is calculated point to point, while the backbone stiffness is calculated from the origin to the point at which the stiffness is required. Figures 8.12 and 8.13 illustrate stiffness degradation for backbone stiffness envelopes from beginning to end of the load series for Specimens 2a and 2b respectively.

As shown in Figures 8.10 and 8.11, the difference between backbone stiffness envelopes for the north and south direction is greatest at the beginning of the test, when the specimens are stiffest. Both north and south backbone stiffness envelopes follow about the same path after the point corresponding to when base shear at the first peak value versus roof displacement envelopes became nonlinear (Fig. 7.6 and 7.28).

For Specimens 2a and 2b, stiffness degradation within each load series was not critical, as shown in Figures 8.12 and 8.13. Degradation of stiffness was always greater for the south load direction than for the north load direction. As previously explained in Subsection 8.2.4, this difference is due to the loading sequence.

For Specimen 2a, the largest degradation of stiffness between first and last peak was 39% for the south load direction, and 14% for the north load direction. This occurred at

400% of the First Major Event load series (0.14 inches roof displacement), when both slabs had cracked and yielded and both compression walls had yielded in each load direction.

For Specimen 2b, degradation of stiffness between first and last peak was greatest during the 100% FME load series (0.20 inches) when a loading problem (Subsection 7.3.8) occurred at Load Point 85. Degradation of stiffness was 38% for the south load direction, and 15% for the north load direction.

8.4 Discussion of Wall Behavior

8.4.1 General. Response of wall elements for the specimens will be examined in terms of wall deformations, longitudinal reinforcement strain, transverse reinforcement strain, and construction details.

8.4.2 Discussion of Wall Deformations. Deformations considered to contribute to the total lateral displacement of the walls include: flexural deformation, shear deformation, and slip at the base of the first story walls. Calculations of flexural and shear deformations are discussed in Appendix D. Slip at the bases of the walls was obtained directly from test results (Figs. 7.7 - 7.8 for Specimen 2a, and Figs. 7.29 - 7.30 for Specimen 2b). Figures 8.14 to 8.17 and 8.18 to 8.21, for Specimens 2a and 2b respectively, show the contribution of each type of deformation to each specimen's total lateral displacement. Because contributing deformations are calculated independently of each other, an error term is introduced to account for any difference between total measured lateral displacement and the summation of the other displacements corresponding to each contributing deformation.

As shown in those figures, the flexural deformation contribution dominates the total lateral wall displacement for Specimens 2a and 2b. Shear and base slip contribute relatively little displacement. For Specimen 2b, when loading to the south, slip at the base of the first story walls contributes more to the total displacement. This larger contribution of deformation is due to the load jumps to the south, which increased the base sliding in that direction.

For each specimen, the percentage contributions of each type of deformation to the total lateral displacement are calculated at the maximum roof lateral displacement, and are shown in Table 8.3 and 8.4 for Specimens 2a and 2b respectively. For both walls of Specimen 2a, the flexural deformation contribution (103%) is greater than the total displacement for the north load direction. This is accounted for by the wall base slip contribution in the opposite direction. For Specimen 2b, the base slip contribution is 23.2% for the north wall and 19.2% for the south wall for the south load direction.

Table 8.3 Deformation Contributions to Maximum Lateral Roof Displacement, Specimen 2a.

Loading Direction	Wall	Total Lateral Disp. [in]	Displacement Contributions [% of Total Disp.]			
			Flex. Def.	Shear Def.	Wall Base Slip	Error
North	North	2.26	103.0	5.8	-5.0	-3.8
	South	2.26	103.0	4.9	-15.2	7.3
South	North	2.14	74.1	4.2	10.4	11.3
	South	2.14	73.6	7.4	23.3	-4.3

Table 8.4 Deformation Contributions to Maximum Lateral Roof Displacement Specimen 2b.

Loading Direction	Wall	Total Lateral Disp. [in]	Displacement Contributions [% of Total Disp.]			
			Flex. Def.	Shear Def.	Wall Base Slip	Error
North	North	3.58	88.7	6.0	8.5	-3.2
	South	3.34	86.8	6.0	9.7	-2.5
South	North	3.04	71.8	12.4	23.2	-7.4
	South	3.16	64.5	7.0	19.2	9.3

8.4.3 Discussion of Behavior of Wall Longitudinal Reinforcement Strain. Longitudinal strains at the base of the first story walls for Specimens 2a and 2b are shown in Figures 7.9 to 7.10, and 7.31 to 7.32 respectively.

Specimen 2a

Because the base of the first story north wall only had the outside two strain gauges, the strain profiles cannot be obtained. Figure 7.10 shows the strain profiles for the base of the first story south wall. The strain profiles remain approximately linear until yielding.

The strain profiles for the north and south walls when these act in tension are shown in Figures 7.9b and 7.10a. When they act in compression, the corresponding profiles are shown in Figures 7.9a and 7.10b. Strain profiles for the tension wall are similar for both north and south walls. The neutral axis is located near the opening edge of each wall until yielding, after which time the wall does not have a definite neutral axis depth. From visual observations at the end of each test, the tension walls uplifted across their entire length. Strain profiles of the compression wall do not behave quite the same for the north and south walls. The north wall has a definite neutral axis location near the outside wall edge (Fig. 7.9a). The compressive strain in the compression toe gradually increases almost until the end of testing. For the south wall, the compression toe appears to be very close to the outside edge of the wall, approximately at the strain gauge location, almost until the end of the test.

Specimen 2b

The loading sequence used for Specimen 2b (Subsection 5.3.2), and the loading problems incurred during testing (Subsection 7.3.1) did not allow many data readings before yielding of the walls; therefore, conclusions on neutral axis location cannot be made.

Figures 7.31 and 7.32 shows the strain profiles for the base of the first story walls. Strain profiles remain approximately linear before yielding.

8.4.4 Discussion of Behavior of Wall Transverse Reinforcement Strain. As shown in Figures 7.11 to 7.14 and 7.39 to 7.42 for Specimens 2a and 2b respectively, transverse steel did not come close to yielding during testing, and visual observations during the tests also showed that diagonal shear cracks formed but did not increase in width. Therefore, shear was not a critical factor, either for Specimen 2a or 2b.

8.4.5 Discussion of Behavior of Wall Construction Details. The construction details of primary concern for Specimen 2a and 2b were the quality of grouting of the walls, the behavior of the longitudinal reinforcement splices, and the behavior of the transverse reinforcement hooks.

The primary concern with the grouting was that no voids be present in the walls. The walls of Specimen 2a were tested for voids as described in Section 4.4, and questionable areas were checked after testing [16]. When concrete masonry units were chipped away to expose the grout, no voids were found. For Specimen 2b, the grout was not tested for

voids, but visual observations of the cutouts at the base of the walls showed that grout had completely filled the base units. For Specimens 2a and 2b, the grouting procedures followed in Subsection 4.4.2 provided satisfactory results.

Behavior of longitudinal reinforcement splices was another area of concern. A 20-inch (40d) splice was used at the base of the first and second-story walls for both Specimen 2a and 2b (Figure 3.6). Although base sliding of up to about 0.5 inches occurred for Specimen 2a, and up to about 0.75 inches for Specimen 2b, splices did not appear to deteriorate during the tests. When the specimens were demolished after testing, no visual evidence of bond deterioration was observed.

Regarding the transverse reinforcement hook, the two primary concerns are that the hook remain bonded with the grout and that it be able to constrain the longitudinal reinforcement. The transverse reinforcement 180 degree hook detail (Subsection 3.2.2) performed satisfactorily for both functions. Visual observations were made after the compression toe failures occurred, exposing the hook. For both Specimens 2a and 2b, the grout around the transverse and longitudinal reinforcement connection remained intact at the load levels attained in the tests. Also, transverse reinforcement effectively constrained longitudinal reinforcement. When the longitudinal reinforcement buckled at the compression toes, buckling was restricted between the base and first transverse reinforcement hook above the base.

8.6 Discussion of Slab Behavior

8.6.1 Discussion of Slab Coupling Behavior.

Specimen 2a

Specimen 2a had a cast-in-place concrete slab. Throughout the test, the slab and wall remained monolithic, and the slab-wall joint showed no signs of deterioration. As shown in Figures 7.18 to 7.21, slab cracks formed in a regular, flexural pattern across the full width of both slabs near the slab-wall intersection at the openings. As shown in Figures 7.18 and 7.19, the full widths of both slabs were effective in transferring shear and moment between the walls. As evident from the observed yielding of the longitudinal reinforcement across the full width of both slabs (Figs. 7.15 and 7.16), plastic hinges formed in each slab at both sides of the opening. The slabs performed satisfactorily and as intended.

For Specimen 2a, it can be shown that the coupling system was effective in transferring shear and moments and did not allow the walls to act as independent cantilever walls by comparing the maximum lateral load capacity of the coupled wall with the maximum lateral load capacity of uncoupled walls (discussed in Subsection 8.2.5). The maximum lateral load

capacity for the coupled wall is 90% greater than the maximum lateral load capacity for the walls if they were uncoupled. Therefore, transfer of shears and moments was occurring which resulted in the greater lateral load capacity of the coupled wall system over the uncoupled walls.

Using the behavioral model of eccentric shear transfer in ACI 318-83 [15], eccentric shear stresses at the slab-wall interface were checked for Specimen 2a, and calculations are shown in Appendix F. It was conservatively assumed that all shears and moments would be transferred from the coupling slabs by eccentric shear stresses to the walls. Based on an effective slab depth of 6.5 inches, the resulting eccentric shear stress is 136 psi, less than the ACI code's concrete shear strength of 140 psi. Therefore, as was observed during testing, the coupling slab transferred shears and moments to the walls without deterioration at the slab-wall interface.

Specimen 2b

The slabs of Specimen 2b were composed of precast concrete planks running parallel to the walls, covered by a concrete topping. As shown in Figures 7.46 to 7.49, cracking did not follow any regular pattern, for various reasons: 1) flexural cracking, while present, was limited to a couple of cracks across the full width of the slab at the wall openings; 2) local cracking was produced by load transfer from the testing apparatus to the second-floor and roof slabs; 3) shear cracks formed at portions of the intersection of the planks with the walls; 4) punching shear cracks developed at the slab-wall intersection near the openings; and 5) deterioration of the horizontal joint between slab and walls occurred at the top of wall openings in both stories.

The ability of the slab to transfer shear and moment between walls was reduced, due to two principal factors: shear cracking at portions of the slab- wall intersections; and deterioration of the horizontal joint at the coupled wall openings between second-floor and roof slabs and walls. These factors caused reduced continuity between the walls and the slabs, allowing the slabs to rotate less than the walls at each story level. Smaller rotations of the slabs result in lower slab moments, which in turn reduce the amount of shear transferred by the slabs between the walls. The total base overturning moment (as discussed in Subsection 2.2.2) is dependent on the moments at the base of each wall (M_1 and M_2), and on the product of the shear transfer between the walls, multiplied by the distance between the plastic centroids of the walls (L*T). As discussed in Subsection 2.2.2, the reduced effectiveness of the coupling system in transferring shear reduces the L*T term, and the walls act more like independent cantilevers. Evidence of this effect was observed during testing of Specimen 2b, double curvature flexural cracking was observed in the early stages of the test, but as the load cycles increased during the test single curvature flexural cracking governed.

Although the effectiveness of the coupling system deteriorated, the coupling slab did not allow the walls to act as independent cantilever walls. This is verified by comparing the maximum lateral load capacity of the coupled wall with the maximum lateral load capacity of uncoupled walls (discussed in Subsection 8.2.5). The maximum lateral load capacity for the coupled wall is 107% greater than the maximum lateral load capacity for the walls if they were uncoupled. Therefore, transfer of shears and moments was still occurring which resulted in the greater lateral load capacity of the coupled wall system over the uncoupled wall system.

Deterioration of the coupling system due to the aforementioned factors did not allow the flexural capacity of the slab to be reached due to the smaller rotations of the slabs. In addition, the flexural cracks that developed in the planks were totally closed at the end of testing, which indicates that the planks remained essentially elastic throughout the test. Also, the reduction of shear transfer between the walls reduced the stiffness of the coupled wall, causing the coupling system to be more flexible.

To evaluate the reduction of shear transfer from slabs to walls, the eccentric shear stress transfer for Specimen 2b was calculated (Appendix E). To account for the possible worst and best case, a minimum effective depth of 2 inches and a maximum effective depth of 8 inches were used, since the actual effective depth is between these two values. As before it was conservatively assumed that the total nominal moment capacity of the coupling slabs would be transferred to the walls by eccentric shear stresses. Assuming an effective depth of 2 inches, the eccentric shear stress is 564 psi, which is much greater than the concrete shear strength resistance (140 psi). Assuming a total effective depth of 8 inches, the eccentric shear stress is equal to the concrete shear strength resistance. Since a cold joint is present between the precast planks and the embedded beam, the actual effective depth is less than 8 inches and presumably closer to 2 inches. Therefore, eccentric shear stress calculations indicate possible problems in shear transfer from the slabs to the walls, which was the observed case for Specimen 2b.

The eccentric shear stress transfer for Specimen 2b is a limiting case. In the prototype building, restraint against the longitudinal shear cracking and subsequent movement of the planks is provided by the adjoining floor system; while for Specimen 2b, restraint is not provided to inhibit plank movement away from the coupled walls.

Using simple plastic analysis as discussed in Chapter 6, an "effective coupling length" can be derived for Specimen 2b. The "effective coupling length" is that coupling beam length which, when substituted into Equation (4) in Subsection 6.3.1, using the nominal coupling beam capacity, gives the observed base shear capacity. At the maximum base shear,

the "effective coupling length" (88.1 kips to the north) was calculated to be approximately 86.5 inches which is 1.54 times greater than the assumed coupling length of 56 inches.

8.6.2 Discussion of Behavior of Slab Construction Details. Since Specimens 2a and 2b have different floor systems, their slab construction details differ.

Specimen 2a

Specimen 2a's floors are reinforced cast-in-place slabs (Subsection 3.2.3). Transverse and longitudinal reinforcement performed properly for Specimen 2a (Subsection 3.2.3) allowing the second-floor and roof slabs to behave monolithically.

The cast-in-place concrete slabs used a reinforcing detail which in effect created an embedded beam centered over the walls and spanning the full length of Specimen 2a (Subsection 3.2.3). This reinforcing beam detail was used to ensure sufficient slab coupling. Visual observations showed that both the second-floor and roof slabs cracked and yielded across their entire widths. This suggests that the beam reinforcement detail of Specimen 2a was unnecessary.

Specimen 2b

Specimen 2b's floor system was composed of two precast, prestressed planks with an embedded beam reinforcement detail between planks, and a reinforced 2- inch topping slab (Subsection 3.2.3).

As discussed in Subsection 8.6.1, the welded wire reinforcement in the 2-inch topping was not sufficient for transverse continuity of the plank floor system. Complete transverse restraint of the floor to achieve monolithic behavior is not possible. Therefore, the beam detail is needed.

8.7 Discussion of Failure Modes

The lateral strength of Specimens 2a and 2b was limited by flexural failure of the coupled walls. The observed failure modes, of crushing of the compression toes and fracturing of the longitudinal reinforcement, are consistent with a flexural failure. Figures 8.12 to 8.19 confirm that flexure was critical, since flexural deformation was the chief contributor to the total lateral displacement of both specimens throughout the tests.

Inelastic deformation capacity of both specimens was limited by the in- plane and out-of-plane displacements of the bases of the first story walls.

9. SUMMARY, CONCLUSIONS AND RECOMMENDATIONS

9.1 Summary

As part of Task 3.1(c) of the TCCMAR program, 2 full-scale reinforced masonry specimens, each two stories high, were constructed and tested. The specimens were fully grouted hollow concrete masonry. The two specimens involved coupled shear walls without lintels, and with different floor systems. Specimen 2a had cast-in-place slabs, while Specimen 2b had precast plank floors. In the prototype building on which Specimen 2a was based, the floor slabs spanned perpendicular to the coupled shear walls; in the prototype building of Specimen 2b, the floor slabs spanned parallel to the coupled shear walls.

Both specimens were tested under quasi-static, reversed cyclic lateral loads applied in the plane of the walls at the second-floor and roof level. Specimen 2a was also loaded vertically by constant loads representing gravity loads on the coupling slabs' tributary areas.

The lateral load capacities of Specimens 2a and 2b were governed by formation of a flexural mechanism. Shearing cracks formed near the bases of both walls of the specimens, but they did not widen. In both specimens, pinching was present due to sliding at the base of the walls, but did not lead to a sliding shear failure. The maximum base shear reached for Specimen 2a was 95.9 kips (north direction) and for Specimen 2b was 88.1 kips (north direction). Inelastic deformation capacity of both specimens was limited by buckling of the longitudinal bars at the wall bases and by the subsequent lateral (out-of-plane) slip of the bases of both wall bases with respect to the base beam. Specimen 2a had a maximum drift of 1.09% to the north and 1.06% to the south, and Specimen 2b had a maximum drift of 1.70% to the north and 1.52% to the south.

For Specimen 2a, the coupling slab remained monolithic with the walls during the entire test. For Specimen 2b, the horizontal joint between the walls and the slab planks deteriorated at the top of the openings, and longitudinal shear cracking occurred at portions of the intersection of the planks and the walls. These effects reduced the effectiveness of the coupling system. Specimen 2b also exhibited local slab cracking at points of load transfer from the lateral loading test set-up to the floor slabs; however, this did not cause local slab failure.

Specimens 2a and 2b both showed satisfactory strength, stiffness, and energy dissipation up to story drifts in excess of 1% for Specimen 2a, and in excess of 1.5% for Specimen 2b.

9.2 Conclusions

1) The test setup performed satisfactorily.

2) Both Specimen 2a and 2b showed satisfactory cyclic shear resistance.

3) Both Specimen 2a and 2b exhibited flexural failures, as designed.

4) Specimens 2a and 2b both performed satisfactorily compared with analytical predictions. For Specimen 2b, the analytical collapse model did not correctly model the observed deterioration in the connection between the precast plank floor and the coupled walls.

5) Specimen 2a showed satisfactory floor-wall joint behavior. Specimen 2b's floor-wall horizontal joint deteriorated during the test, but did not fail. In Specimen 2b, the continuity between the slabs and walls was reduced due to longitudinal shear cracking at portions of the intersection of the planks and the walls.

6) The coupling system of Specimen 2a performed effectively. The coupling system of Specimen 2b did not behave as intended (plastic hinge formation at wall openings), due to the deterioration of the horizontal slab-wall joint at the top of the wall openings, and to longitudinal shear cracking at portions of the intersection of the planks and the walls. These factors reduced the effectiveness of the coupling system, decreasing moments in the planks, thus not allowing them to yield. Although Specimen 2b's coupling system did not provide as much coupling as intended, it performed satisfactorily.

7) The eccentric shear transfer model of ACI 318-83 can be used to predict possible deterioration of the slab-wall connections.

9.3 Recommendations

1) For future tests, the loading points at which the test set-up connects to the floor slabs should have additional reinforcement.

2) For future tests, additional data readings should be taken during peak cycles of each load series of the modified sequential phased loading diagram.

3) A method should be developed to limit in-plane and out-of-plane sliding at the base of coupled walls (shear keys, roughening of the bed joint at the base of the walls, or some type of rigid connection at the base of the coupled walls).

4) When eccentric shear stress calculations indicate possible problems, additional local reinforcement should be placed at wall-floor joints to improve the continuity of future specimens, particularly those with precast plank floor systems.

5) To take into account the flexibility of the precast plank floor system (as in Specimen 2b), capacity prediction models need to consider a larger effective length of the coupling beams, thereby reducing the maximum shears and moments developed in the coupling system.

9.4 Recommendations for Future Research

1) The sliding shear capacity of coupled masonry walls should be investigated further.

2) Methods should be developed to limit in-plane and out-of-plane sliding at the base of coupled masonry walls.

3) Methods should be developed for estimating the effective coupling length for precast, prestressed plank floor systems in cases in which deterioration of the wall-slab joint is anticipated.

APPENDIX A
DESIGN OF TYPE 2 SPECIMENS [14]

Design Criteria

Materials:

6" x 8" x 16" Concrete Masonry Units (hollow-core); fully grouted cells

Type S Mortar

Grade 60 reinforcement

Assume:

f'_m = 2000 psi

wall density = 120 psf

Wall Dimensions: (obtained from Prototype Building)

Tributary Width = 20 ft

Wall Length = 16.67 ft

Wall Height = 8 ft 8 in per story

Total Wall Height (H) = 17 ft 4 in for two stories

Gravity Load:

Dead Load = 80 psf for floors

20 psf for partitions (1985 UBC Section 2304(d) [13]

5 psf for floor finish

8 psf for HVAC

Live Load:

Live Load = 50 psf

Live Load Reduction (1985 UBC Section 2306) [13]

LL Reduction = 0.08 x (L x W - 150)

where:

L = 16.67 ft

W = 20 ft

LL Redution = 14.67% and Live Load = 42.67 psf

Calculate Axial Load (Using service level vertical loads):

P_{total} = (DL + LL) x 20 ft x 16.67 ft x 2 stories

P_{total} = 103.8 kips

f_{axial} = P_{total} / (Wall Length x CMU width)

f_{axial} = 92.2 psi

Calculate Lateral Load: (Using Zone 4 seimic design provisions of the 1985 UBC [13])

V_{base} = ZIKCSW

where:

W = DL x (20 ft x 16.67 ft) x

2 stories + wall weight; and

wall weight = 12.0 psf

Z = 1.0; I = 1.0; K = 1.33;

CS = 0.14

V_{base} = 16.26 kips

Lateral Load Design

Assume: compression wall takes 2/3 of shear

V_{base} = 16.26 kips

Calculate Moment at Base of Compression Wall:

M_{base} = 2/3 x $\left[(V_{base}$ /2 x H/2) + (V_{base} /2 x H)$\right]$

where: H = 17 ft 4 in

M_{base} = 1692 kip-in

M $\approx$ A_s x f_y x (L) x 0.9; $A_s = M_{base}$ / (0.9 x L x f_y)

where:

L = 6.67 ft x 12 in/ft (length of one wall of coupled walls)

f_y = 60 ksi

A_s = 0.40 in^2

Try: #4 longitudinal reinforcement at 16 inches

Results in 1 rebar per CMU and 5 rebars per wall

A_s = 1.0 in^2; ρ = 1 / (L x 5.63 in) = 0.00223

where: 5.63 in. is wall depth

Estimate Flexural Capacity: (Develop interaction diagram)

Calculate Pure Compression:

$P = A_g$ x (0.85 x f'_m) x 2 walls

where:

A_g = 6.67 ft x 12 in/ft x 5.63 in;

f'_m = 2 kips

P = 766 kips

Calculate Balance Point:

Find c: $c/d = 0.003/(0.003 + \epsilon_y)$

where:

d = 0.8 x 6.67 ft (length of one wall) x 12 in/ft; d = 64 in

ϵ_y = 0.00208

c = 37.88 in

Find Axial Load (P) and Moment (M) at Balance Point:

P = C - T (ignoring steel: tensile and compressive areas similar)

P $\approx$ 0.85 x f'_c x b x β_1 x c

where: $f'_c = f'_m$; β_1 = 0.85; c = 37.88 in; b = 5.63 in

P = 308 kips

M $\approx$ P x [L/2 - (β_1 x c/2)]

where: L = 6.67 ft x 12 in/ft (length of one wall)

M = 7362 kip-in (This value will be slightly low)

Calculate Pure Flexure:

Assume 2.5 tension longitudinal rebars yielded per wall

M = w x b x d^2 x f'_m x (1 - 0.59 x w)

where:

w = ρ x f_y/f'_m

ρ = 2.5 x 0.2 in^2 / (6.67 in x 12 in/ft x 5.63 in)

w = 0.03

b = 5.63 in

A_s / 8 in = 0.0007 x (5.63 in x 12) = 0.05

Use #3 transverse reinforcement every other course

APPENDIX B
CORRECTIONS FOR SLIP BETWEEN WALLS AND BASE BEAM [24]

Introduction:

During the testing of Specimen 2a some problems were encountered involving the slip potentiometers and the brackets supporting them. Specifically, one of the potentiometers did not extend at one point during the test. Also, the reaction brackets were glued to the base beam using epoxy which did not cure properly, was too soft as a result, and therefore experienced some creep during the test.

Because of those problems, the original linear potentiometer readings for slip between the walls and the base beam are not directly usable from Load Point (LP) 1 to LP 335. Beyond that point, all problems were corrected, and the results are directly usable.

By the end of the test, base slip was an important part of the response of Specimen 2a. Base slip in that part of the test was recorded correctly. Direct observations and photographs taken during the test confirm that prior to LP 335, base slip was negligible (about 1/16 inch or less). Therefore, the problems with the linear potentiometers did not hurt the slip data in the important part of the test. In that sense, it might have been sufficient to simply ignore the erroneous slip data recorded before LP 335.

However, in an effort to recover all the slip data, two different approaches were adopted to correct the small slip measurements recorded prior to LP 335. Both approaches lead to very similar results, which are consistent with each other, consistent with visual observations during the test, and internally consistent within themselves. The corrected slip measurements do not change any conclusions regarding the test results. For documentation purposes, both correction procedures are presented here.

Uncorrected Slip Potentiometer Readings (Figures B.1 - B.5)

North Wall (Channel 52)

LP 1 - 17: Readings did not change.

LP 18 - 303: When the wall was loaded in the North direction, readings did not change. When the wall was loaded in the South direction, readings were obtained (this direction corresponded to extension of the potentiometer).

LP 303 - 330: The potentiometer reached its maximum extension, and readings remained constant.

LP 330 - 334: The potentiometer inexplicably extended and retracted its total travel (it was probably bumped). The problem was detected, and the potentiometer was replaced. Inadvertently, it was not re-zeroed on the data acquisition system.

LP 335 - 354: The new potentiometer worked correctly, but it hadn't been re-zeroed. The potentiometer was re-zeroed at LP 354.

LP 354 - 406: The potentiometer worked correctly, and was correctly zeroed. However, when edge bar fractured at the north edge of the North wall, the potentiometer jumped from its reaction plate and extended completely. Its readings therefore remained constant from LP 396 to LP 406, when the problem was detected and fixed.

LP 406 - End: The potentiometer was re-zeroed. It worked correctly until the end of the test.

South Wall (Channel 21)

LP 1 - 190: Potentiometer readings showed only small monotonic increases, at points corresponding to overnight periods. This shows that the potentiometer was not retracting at all, and was slowly extending overnight due to creep of the epoxy holding a support bracket.

LP 191 - 212: Readings changed only in the South direction when the specimen was loaded in that direction. When the specimen was loaded in the North direction, potentiometer readings remained constant.

LP 213 - 229: Readings remained constant at the value corresponding to LP 212.

LP 330 - 333: The potentiometer extended completely. The problem was detected. The potentiometer was removed, the support system was fixed and a different potentiometer was inserted.

LP 334 - 354: The potentiometer worked correctly, but it hadn't been re-zeroed. It was re-zeroed at LP 354.

LP 354 - End: The potentiometer worked correctly. It showed a permanent South displacement of the wall at the end of the test.

Discussion of Uncorrected Slip Potentiometer Readings

During the initial part of the test, the linear potentiometers measuring slip between the walls and the base beam appeared to change in reading only when the wall slip tended to extend them. When the wall slip would have tended to retract them, the potentiometers did not record such a change. This problem is believed due to the characteristics of the system. The tip of each slip potentiometer was fixed to the interior face of one of the webs of a piece of angle. The second web of the angle was fixed to the wall base using a structural epoxy adhesive. As noticed later, however, the epoxy wasn't well mixed, and didn't harden sufficiently. The potentiometer springs, however, were stiff.

When the wall slipped in such a direction as to retract the potentiometer, the potentiometer tip pushed against the angle, it must have rotated the angle about its toe, without a change in length of the potentiometer itself. Potentiometer retraction did not occur, and was not registered. When the wall slipped so as to extend the potentiometer, however, the stiffness of the potentiometer spring kept the tip of the potentiometer against the angle. Potentiometer extension did occur and was registered.

The potentiometer at the South wall seems to have been totally locked between LP 212 and LP 330.

The readings from both potentiometers followed almost the same path from LP 183 to LP 212.

Simple Corrections to Slip Potentiometer Readings

As noted above, the slip potentiometers functioned correctly from LP 334 to the end of the test, during the period when most of the base slip occurred. To recover the correct slip potentiometer readings for the initial part of the test, two different procedures were used. Both gave essentially the same results. The first procedure, the simpler of the two, was based on the following chain of logic:

1) At the end of the test, each slip potentiometer reading should agree with the physically measured slip between the respective wall and the base beam.

2) The South wall slip potentiometer reading at the end of the test was corrected so that its reading equalled the measured slip. All South wall slip readings between LP 334 and the end of the test were corrected by the same value.

This simple process applies only to values between LP 334 and the end of the test. The results are shown in Fig. B.6.

Complex Corrections to North Wall Readings (Channel 52)

Because the cause of error in the initial part of the slip readings was known, it was possible to correct those initial readings, step by step, for each type of error. The results of all corrections are shown in Figs. B.7 to B.11. Six different types of correction were successively applied to the original data. Each type of correction is explained below, and the effects of each are discussed in the corresponding figures.

1) *Correction for Accumulated Uni-Directional Readings (LP 18 - LP 303):* During this range, it was assumed that there was no permanent slip between the wall bases and the base beam. This assumption was verified by the symmetry exhibited by the hysteretic load-displacement loops in this range. The slip should have returned to zero at each cycle, rather than increasing monotonically.

   Readings were corrected by subtracting the previous peak from each raw reading. In effect, it was assumed that the slip should have returned to zero after each negative peak. The results are shown in the curves below the horizontal axis in Fig. B.12.

   In reality, the North Wall slip readings should have exhibited positive as well as negative peaks. That point was addressed in Correction 4 below. First, some other problems were corrected.

2) *Corrections for Zero Level after Replacing Potentiometer (LP 335 - LP 354, and LP 354 - LP 395):* Since the potentiometer was not re-zeroed after having been replaced, slip readings were corrected for zero level: the slip reading at LP 335 was subtracted from all subsequent readings. In doing so, it was assumed there was no permanent slip at LP 335 and the same zero level was maintained after re-zeroing at LP 354. The slip curves before and after this correction are shown in Fig. B.13.

3) *Corrections after Jump of Potentiometer (LP 396):* The potentiometer jumped off its support plate at LP 396. This jump occurred when the edge bar of the South wall was fractured. It was re-zeroed at LP 406.

   It was first assumed that at LP 406, a permanent slip existed, equal in value to the wall displacement at zero lateral load. The slip reading at LP 406 was corrected to this value, and the same correction was applied to all subsequent load points.

   It was then assumed that the slip of the North Wall would follow the same trends as the slip of the South Wall. This assumption was based on the trend showed before and after these points. The slip curves before and after these corrections are shown in Fig. B.14.

4) *Correction for Uni-Directional Displacements (LP 18 - LP 303):* Because of the symmetry of the load-displacement loops in that phase of the test, and because of the lack of any apparent permanent displacement, peak slip values were assumed the same in the positive (north) direction as in the negative (south) direction.

   As shown in Fig. B.15, the peak slip value for each cycle in the positive direction was assumed equal to the peak slip value from the corresponding following peak in the negative direction. If the following peak had a different maximum displacement, the slip at the appropriate displacement was used.

5) *Corrections in Zone Where No Readings Were Available (LP 303 - LP 333):* Peak slip values were obtained from previous cycles having the same wall displacement amplitudes. Slip curves before and after these corrections are shown in Fig. B.16.

6) *Corrections in Zone of Large Peaks (LP 207 - LP 357):* Plots of the slip peaks showed that the general trend was distorted in the zone between LP 207 and LP 357 for northward loading, and between LP 211 and LP 323 for southward loading. In that same zone, slip values were observed to increase with respect to the flexural and total displacements. Slip values in this zone had been estimated based on readings obtained at other load points.

   To resolve these abnormalities, peak slip readings were assumed to increase linearly with load points. The corresponding corrected values are shown in Figs. B.17 and B.18.

Complex Corrections to South Wall Readings (Channel 21)

Because the cause of error in the initial part of the slip readings was known, it was possible to correct those initial readings, step by step, for each type of error. The results of all corrections are shown in Figs. B.7 to B.11. It should be noted that these results are almost identical to those obtained independently by the simple process outlined above. Thus, the corrected readings can be used with considerable confidence. Five different types of correction were successively applied to the original data. Each type of correction is explained below, and the effects of each are discussed in the corresponding figures.

1) *Correction for Accumulated Uni-Directional Readings (LP 191 - LP 212):* As above, it was assumed (based on the appearance of the load-displacement curves) that there was no permanent slip.

   Readings were corrected by subtracting the previous peak from each raw reading. In effect, it was assumed that the slip should have returned to zero after each

negative peak. The results are shown in the curves below the horizontal axis in Fig. B.19.

In reality, the South Wall slip readings should have exhibited positive as well as negative peaks. That point was addressed in Correction 3 below. First, another problem was corrected.

2) *Corrections for Zero Level after Replacing Potentiometer (LP 335 - LP 354, and LP 354 - LP 422):* Since the potentiometer was not re-zeroed after having been replaced, slip readings were corrected for zero level: the slip reading at LP 335 was subtracted from all subsequent readings. In doing so, it was assumed there was no permanent slip at LP 335 and the same zero level was maintained after re-zeroing at LP 354. The slip curves before and after this correction are shown in Fig. B.20.

3) *Correction for Uni-Directional Displacements (LP 191 - LP 212):* Because of the symmetry of the load-displacement loops in that phase of the test, and because of the lack of any apparent permanent displacement, peak slip values were assumed the same in the positive (north) direction as in the negative (south) direction.

   As shown in Fig. B.21, the peak slip value for each cycle in the positive direction was assumed equal to the peak slip value from the corresponding following peak in the negative direction. If the following peak had a different maximum displacement, the slip at the appropriate displacement was used.

4) *Corrections in Zone Where No Readings Were Available (LP 212 - LP 333):* It was assumed that the slip of the South Wall would follow the same trends as the slip of the North Wall. This assumption was based on the trend showed before and after these points.

5) *Corrections in Zone of Large Peaks (LP 207 - LP 357):* Plots of the slip peaks showed that the general trends was distorted in the zone between LP 207 and LP 357 for northward loading, and between LP 211 and LP 323 for southward loading. In that same zone, slip values were observed to increase with respect to the flexural and total displacements. Slip values in this zone had been estimated based on readings obtained at other load points.

   As with the North wall, these abnormalities were resolved by assuming that peak slip readings increased linearly with load points. The corresponding corrected values are shown in Figs. B.22 and B.23.

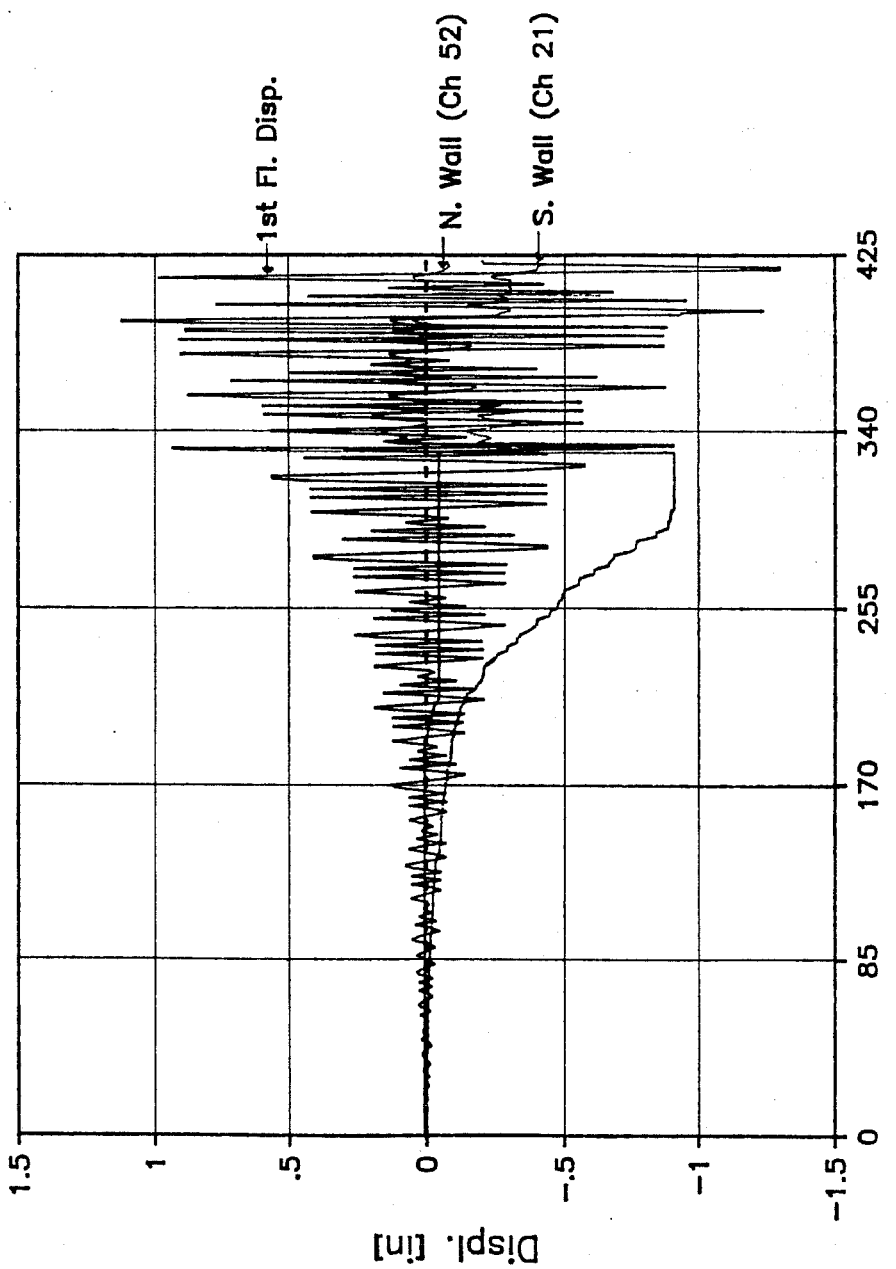

Figure B.1 Sp. 2a: Uncorrected Slip Potentiometer Readings

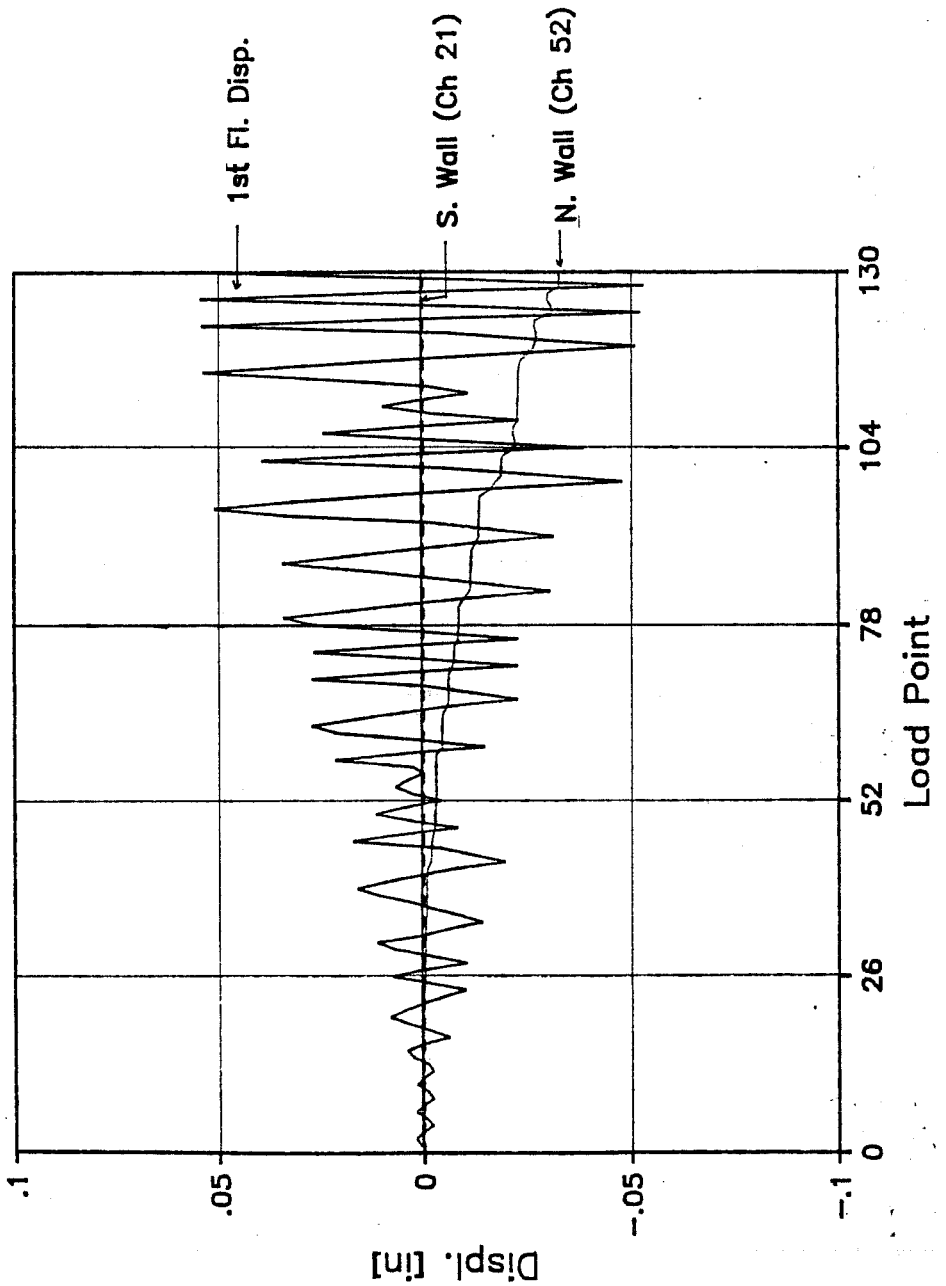

Figure B.2 Sp. 2a: Uncorrected Slip Potentiometer Readings

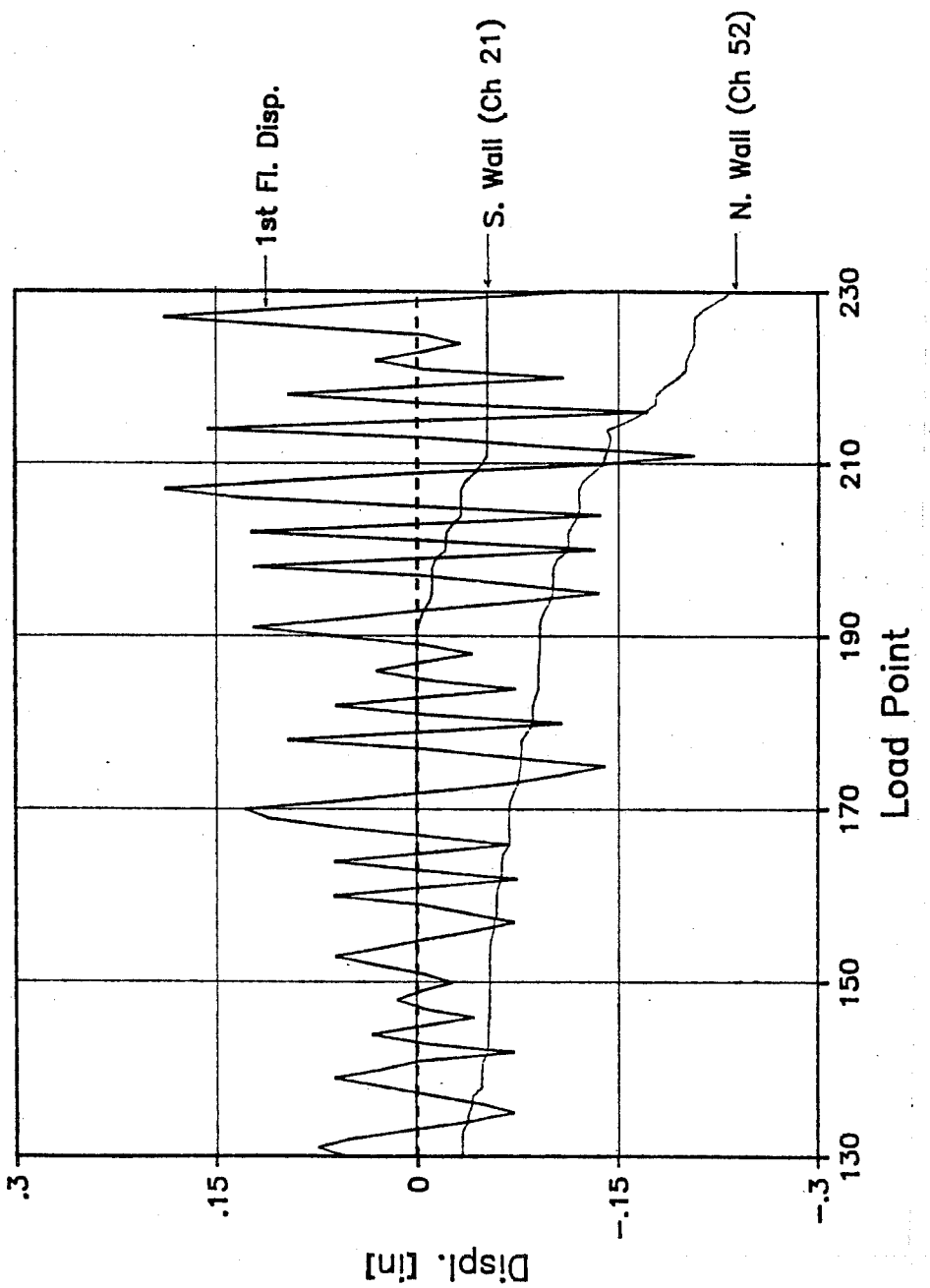

Figure B.3 Sp. 2a: Uncorrected Slip Potentiometer Readings

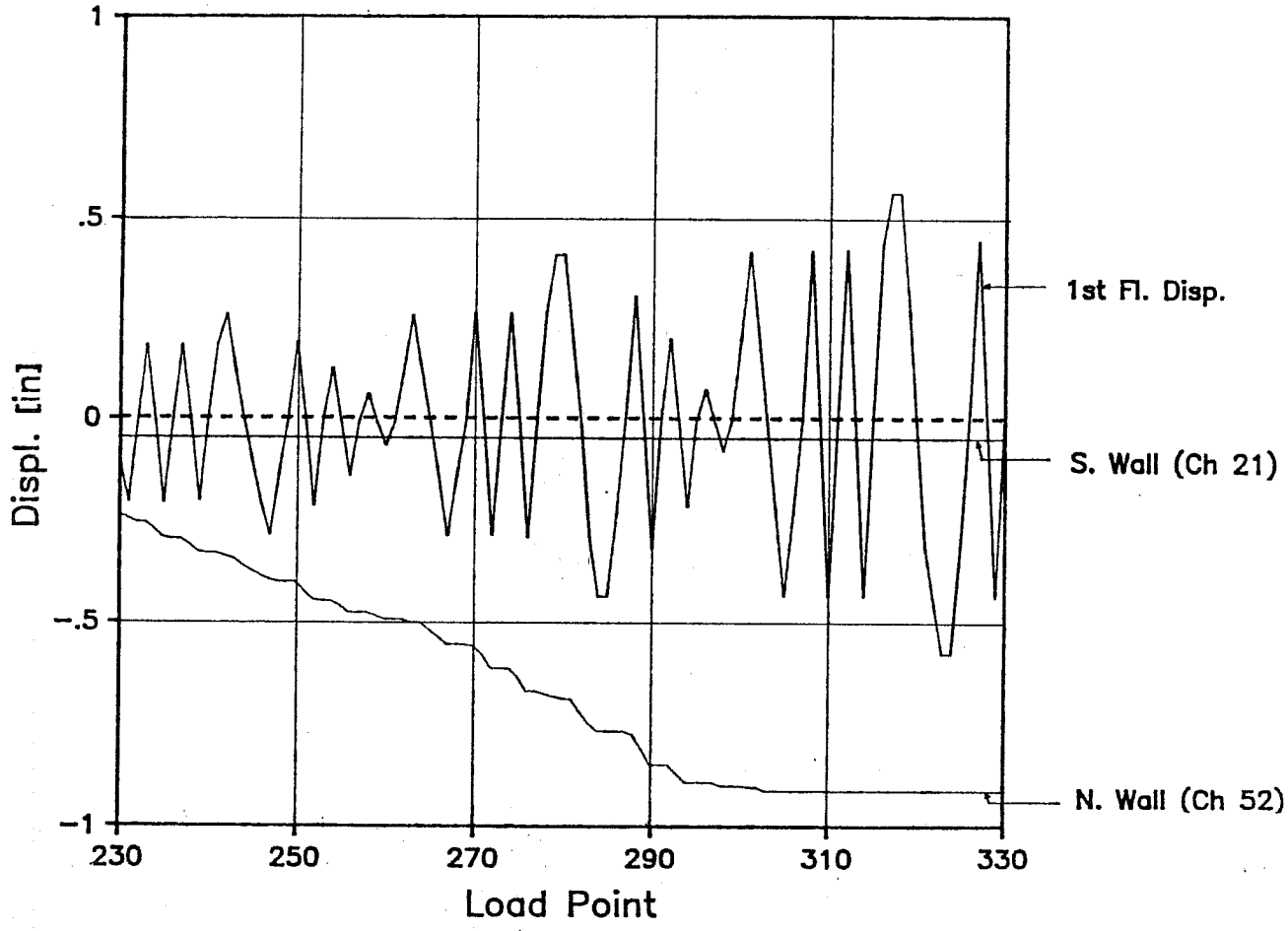

Figure B.4 Sp. 2a: Uncorrected Slip Potentiometer Readings

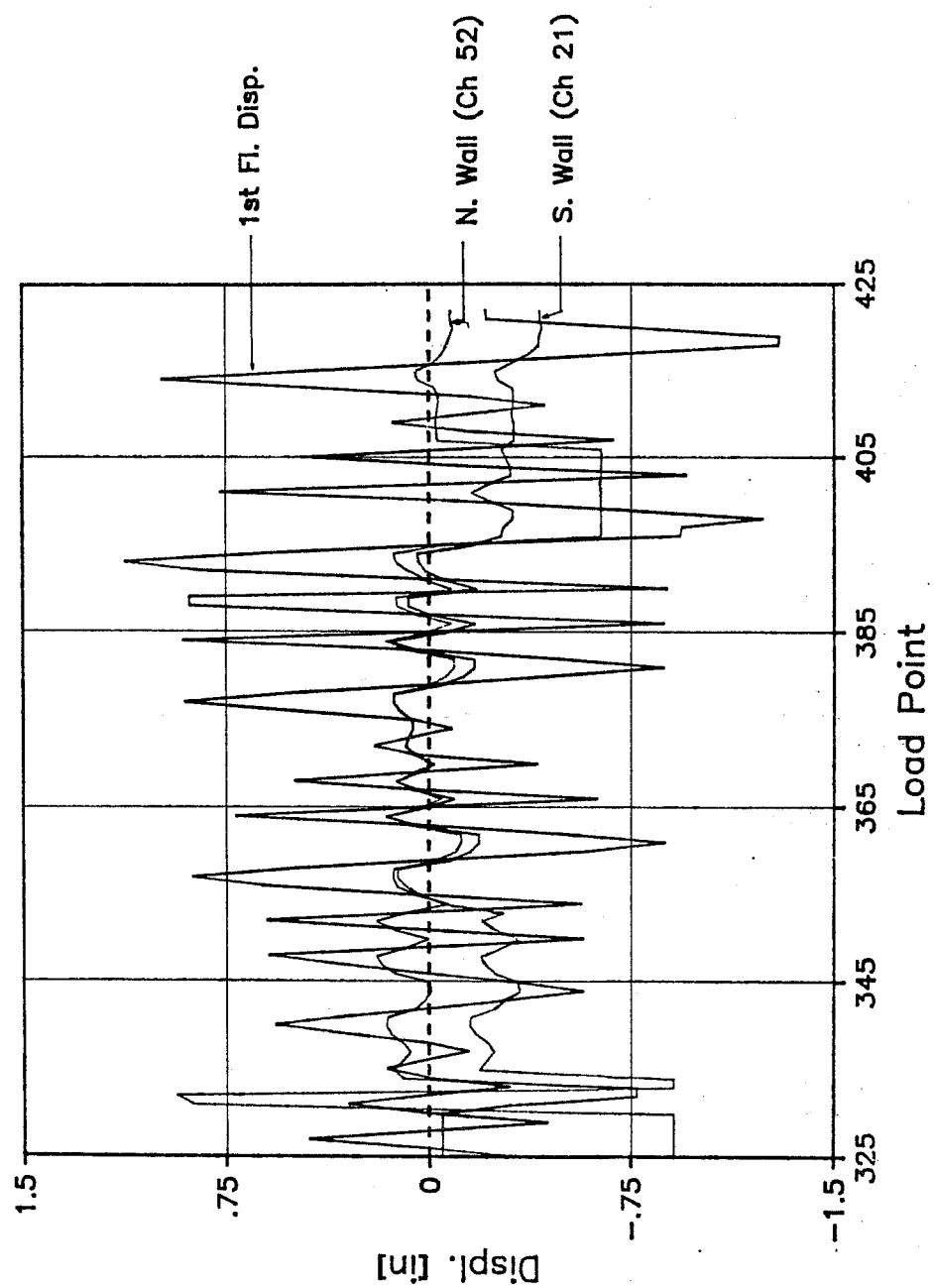

Figure B.5 Sp. 2a: Uncorrected Slip Potentiometer Readings

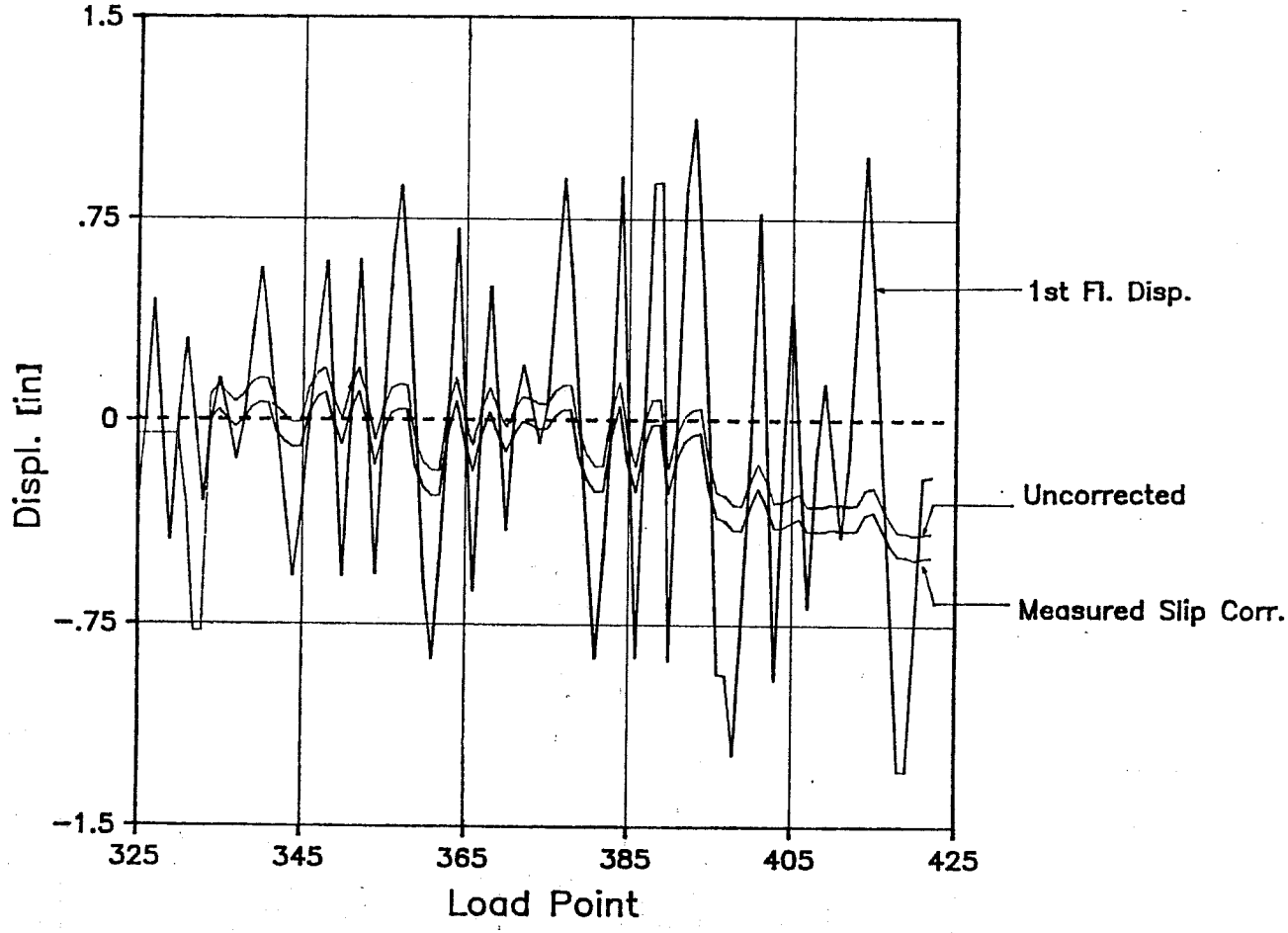

Figure B.6 Sp. 2a: South Wall Slip Potentiometer Reading - Simple Corrections

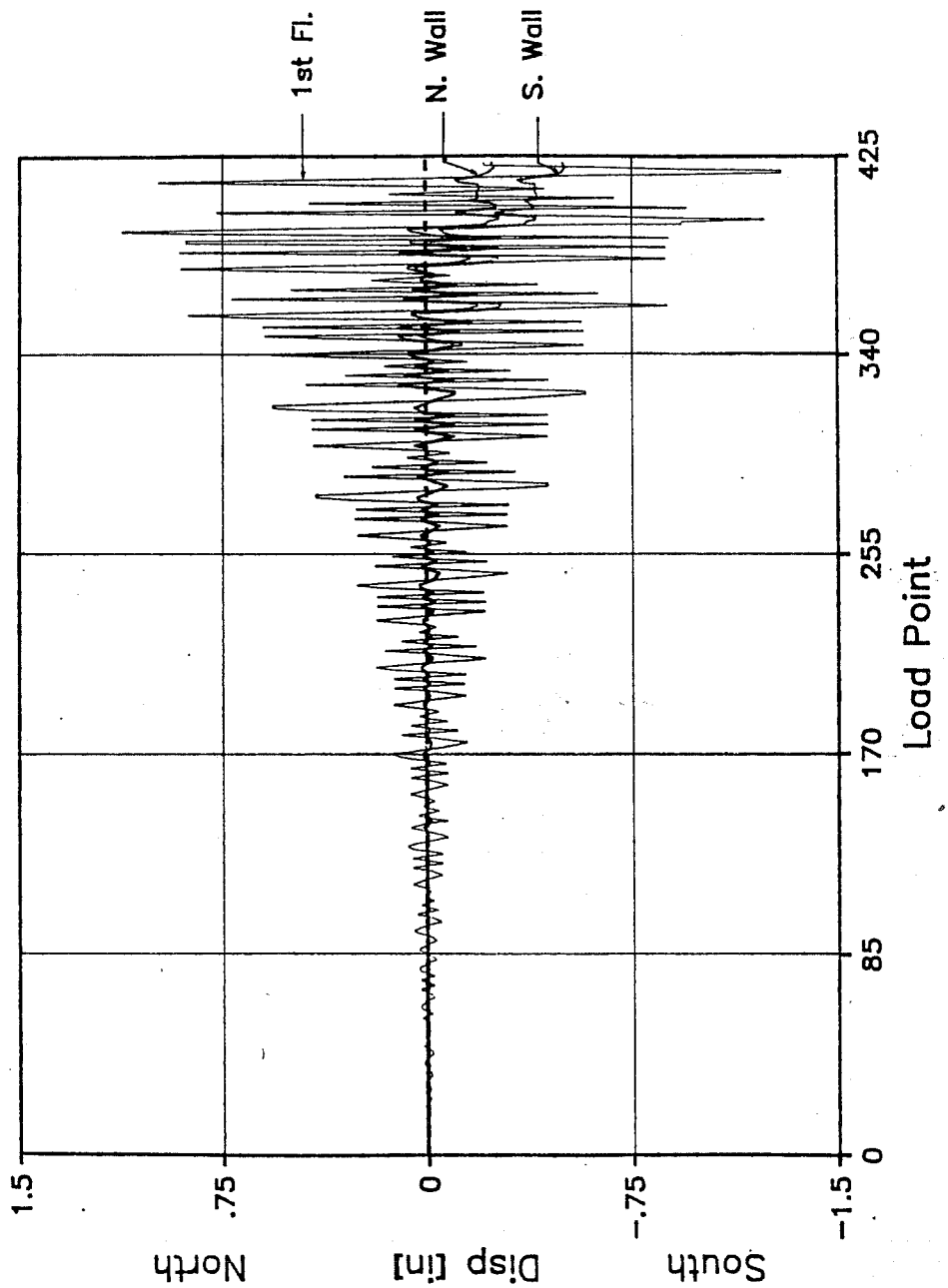

Figure B.7 Sp. 2a: Wall Slip After Complex Corrections

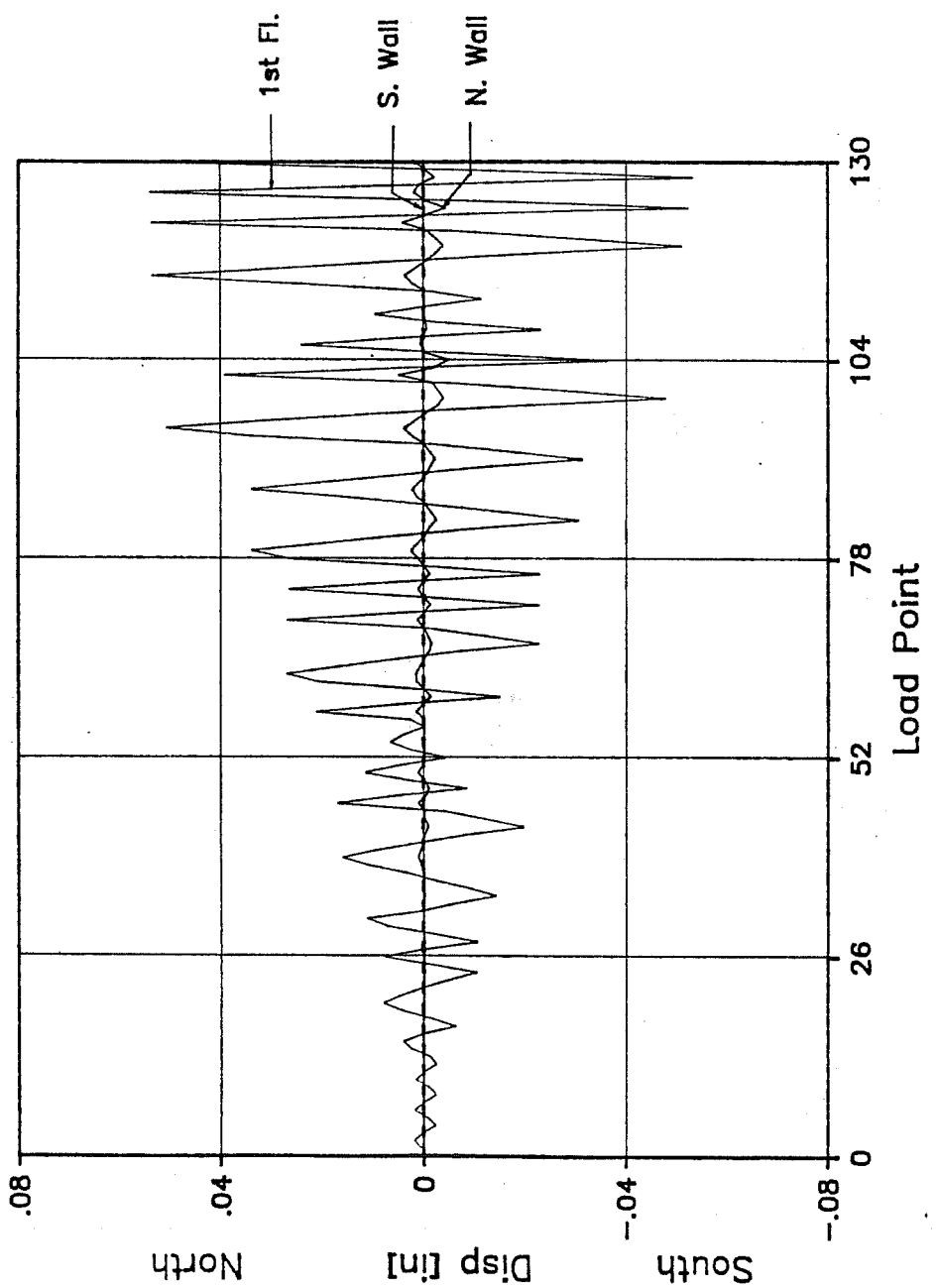

Figure B.8 Sp. 2a: Wall Slip After Complex Corrections

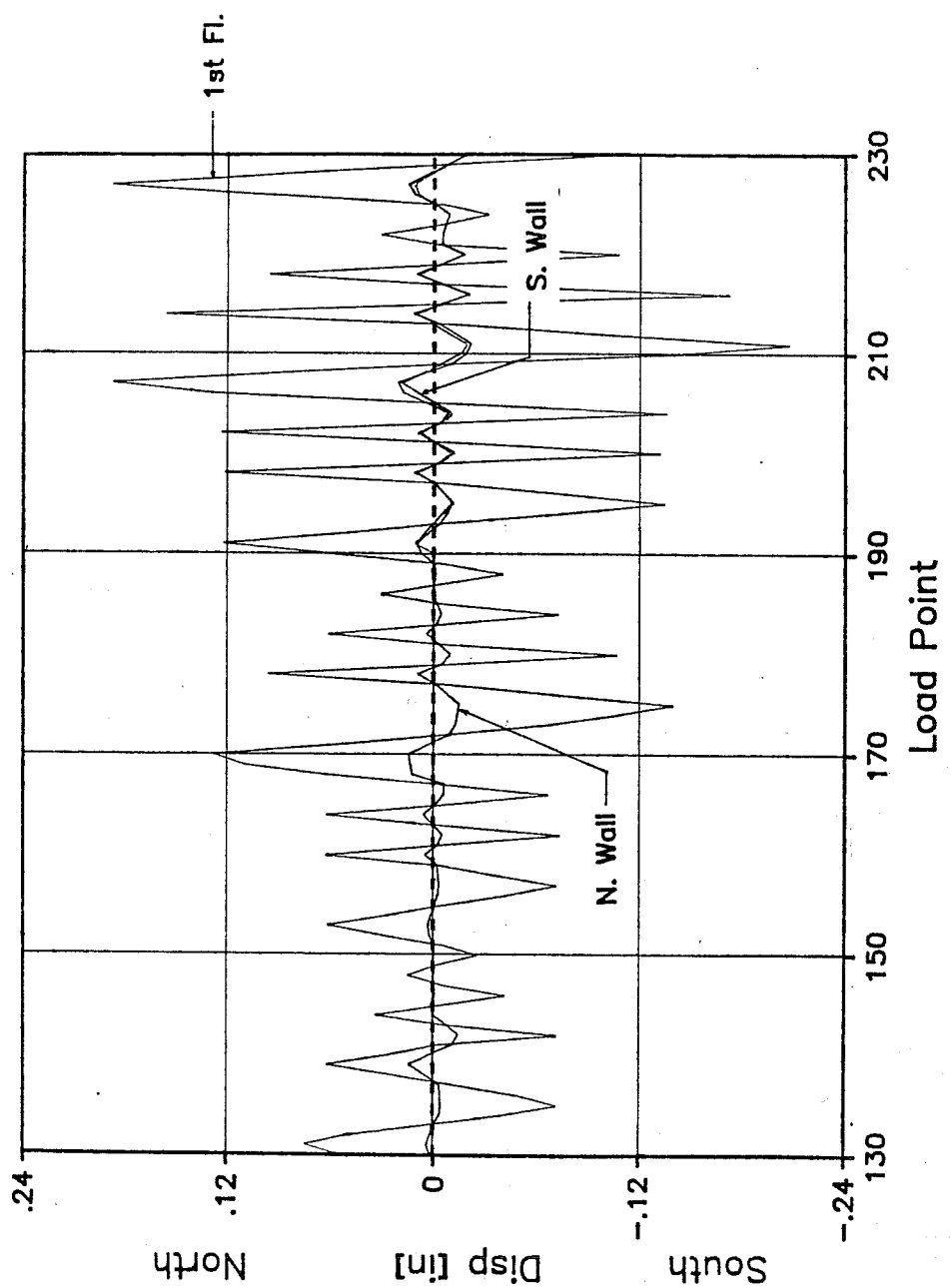

Figure B.9 Sp. 2a: Wall Slip After Complex Corrections

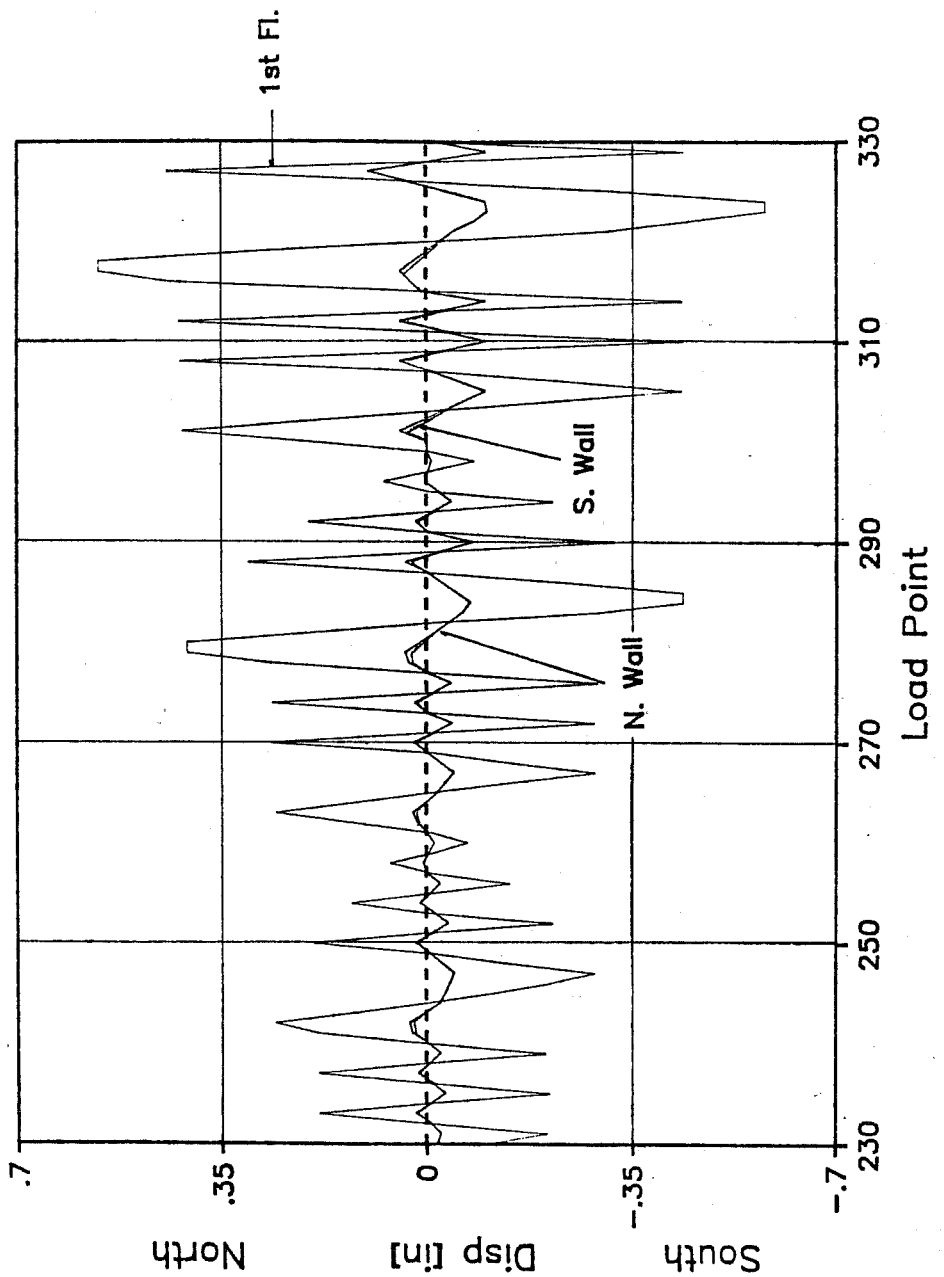

Figure B.10 Sp. 2a: Wall Slip After Complex Corrections

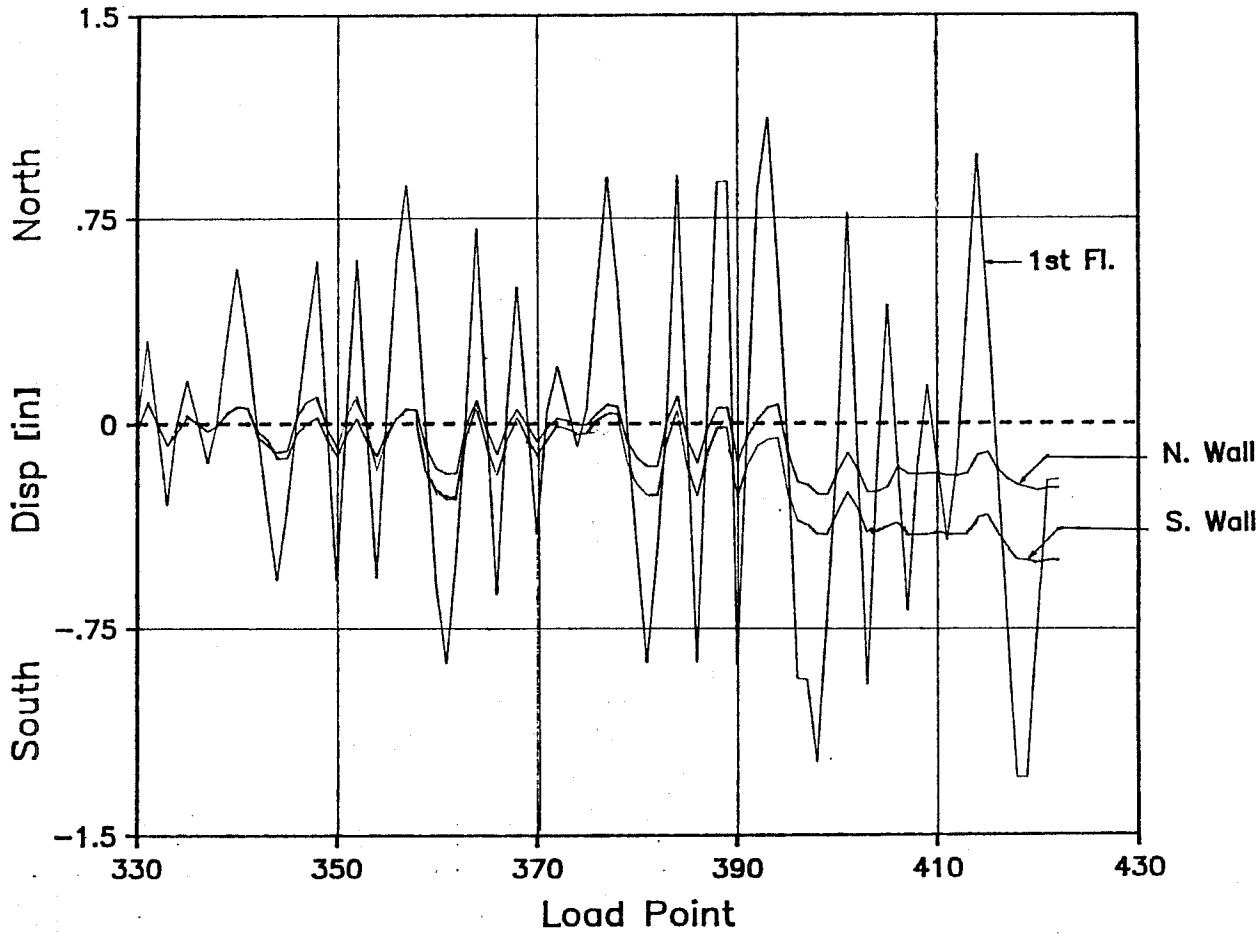

Figure B.11 Sp. 2a: Wall Slip After Complex Corrections

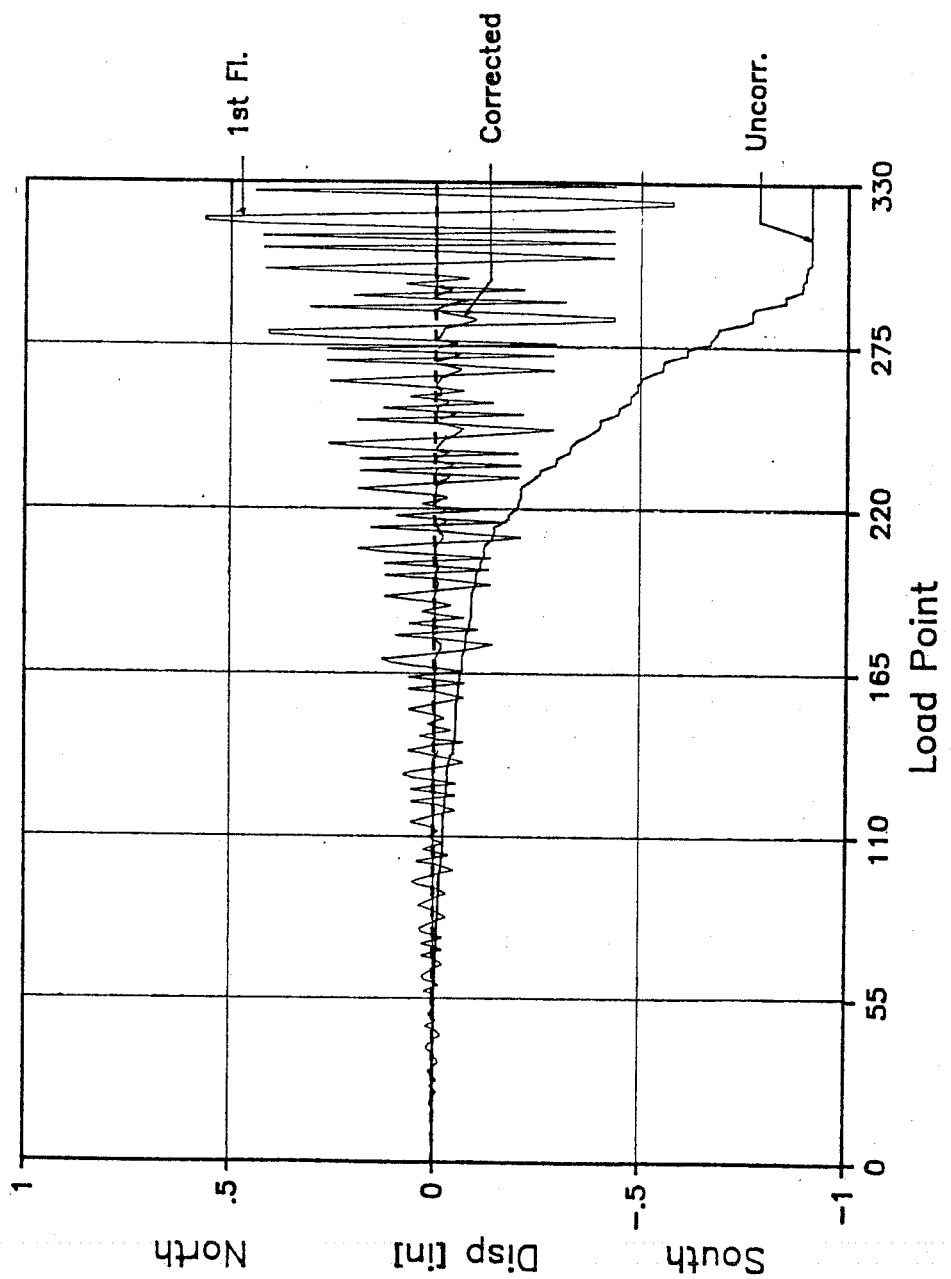

Figure B.12 Sp. 2a: North Wall Slip After Accumulated Uni-Directional Reading Correction (1)

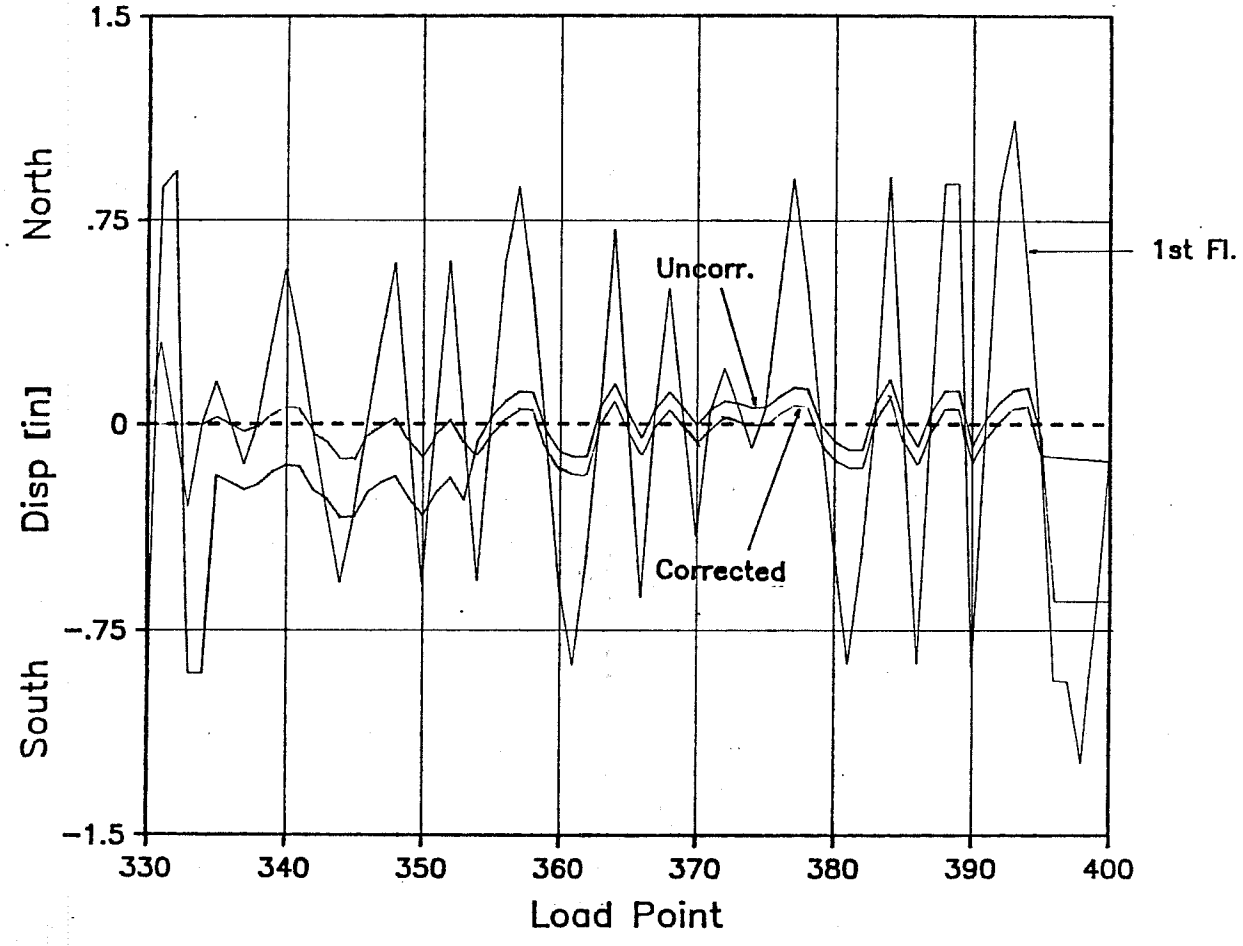

Figure B.13 Sp. 2a: North Wall Slip After Zero Level Correction (2)

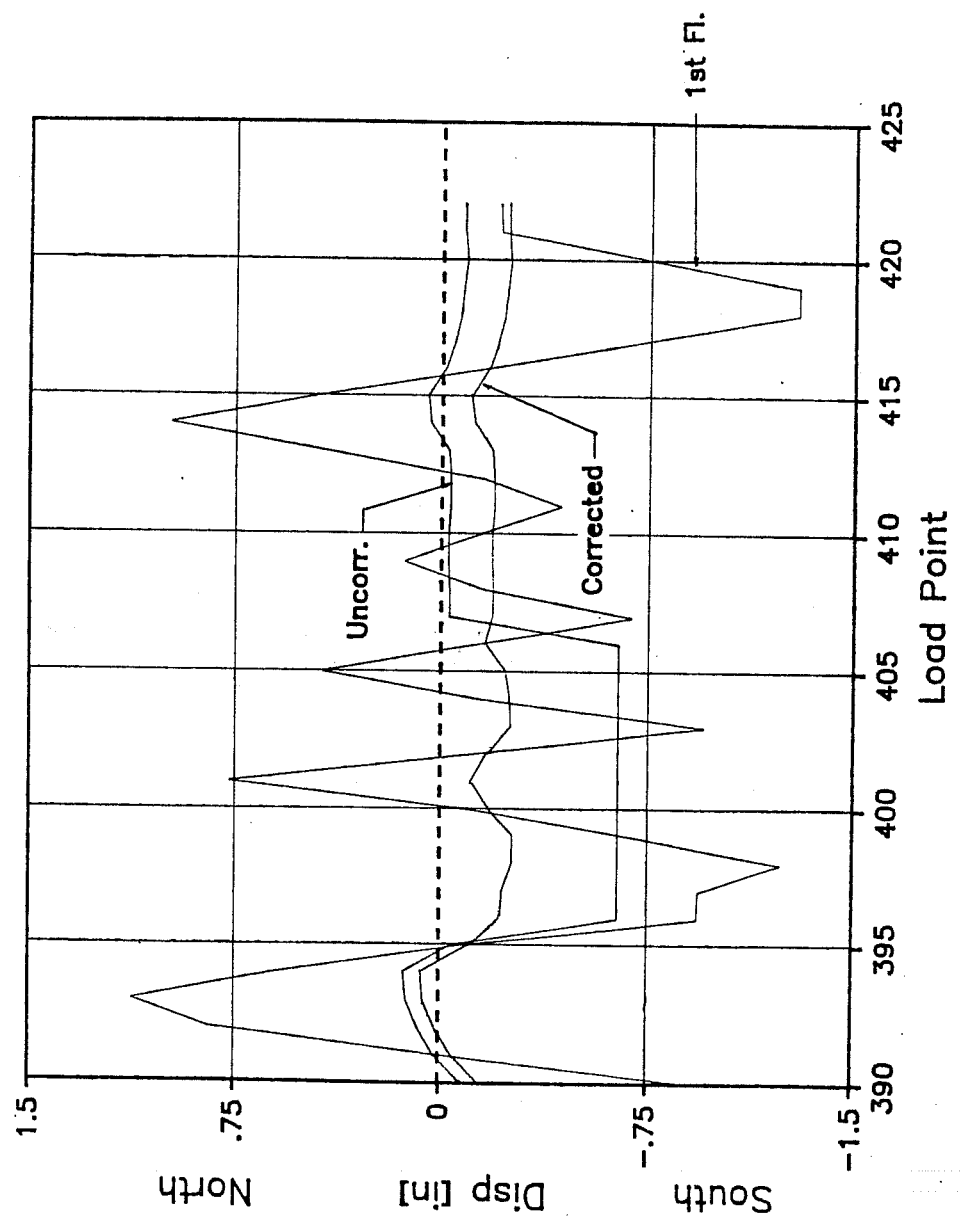

Figure B.14 Sp. 2a: North Wall Slip After Corrections for Jump of Potentiometer (3)

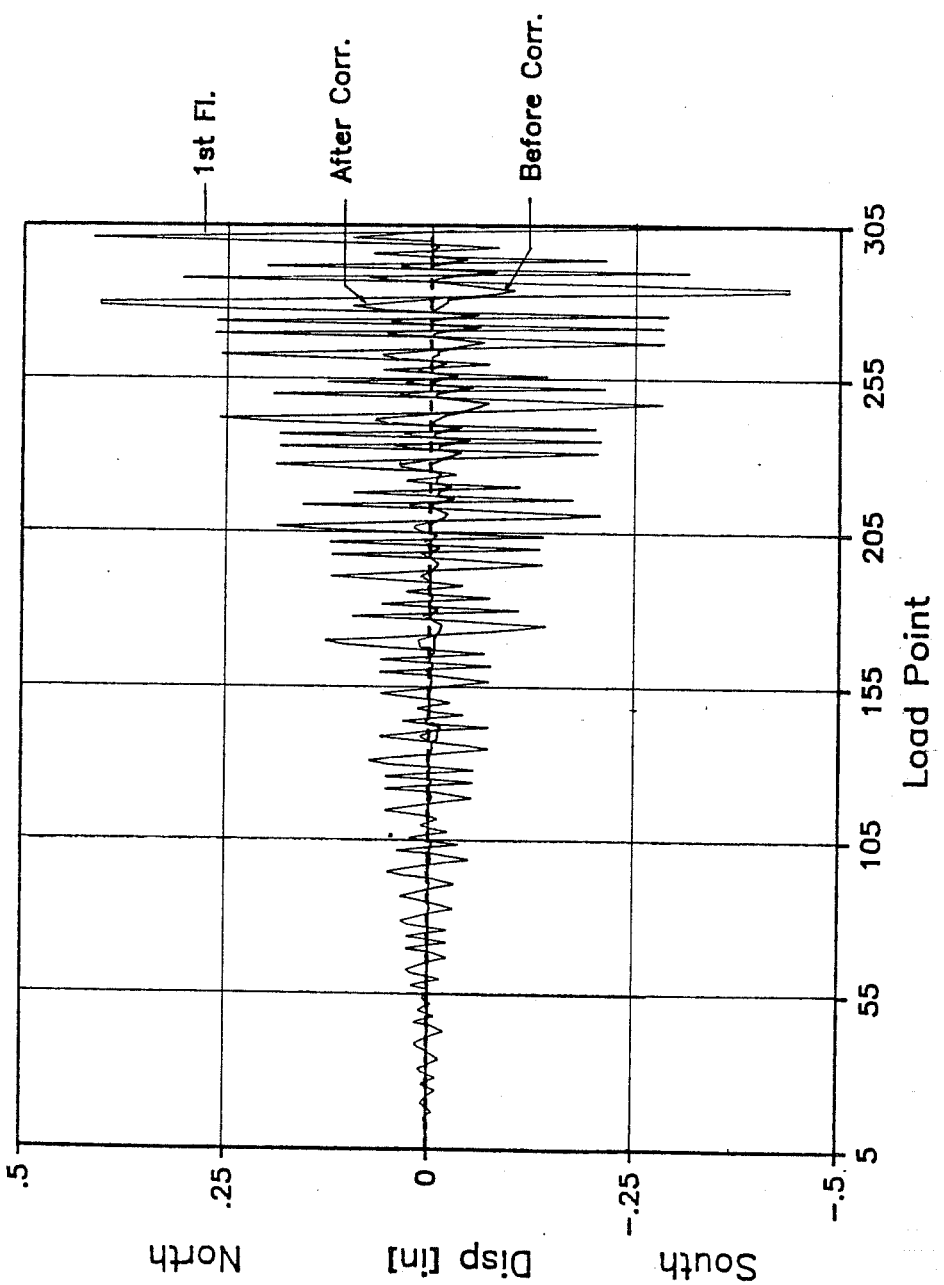

Figure B.15 Sp.2a: North Wall Slip After Correction for Uni-Directional Readings (4)

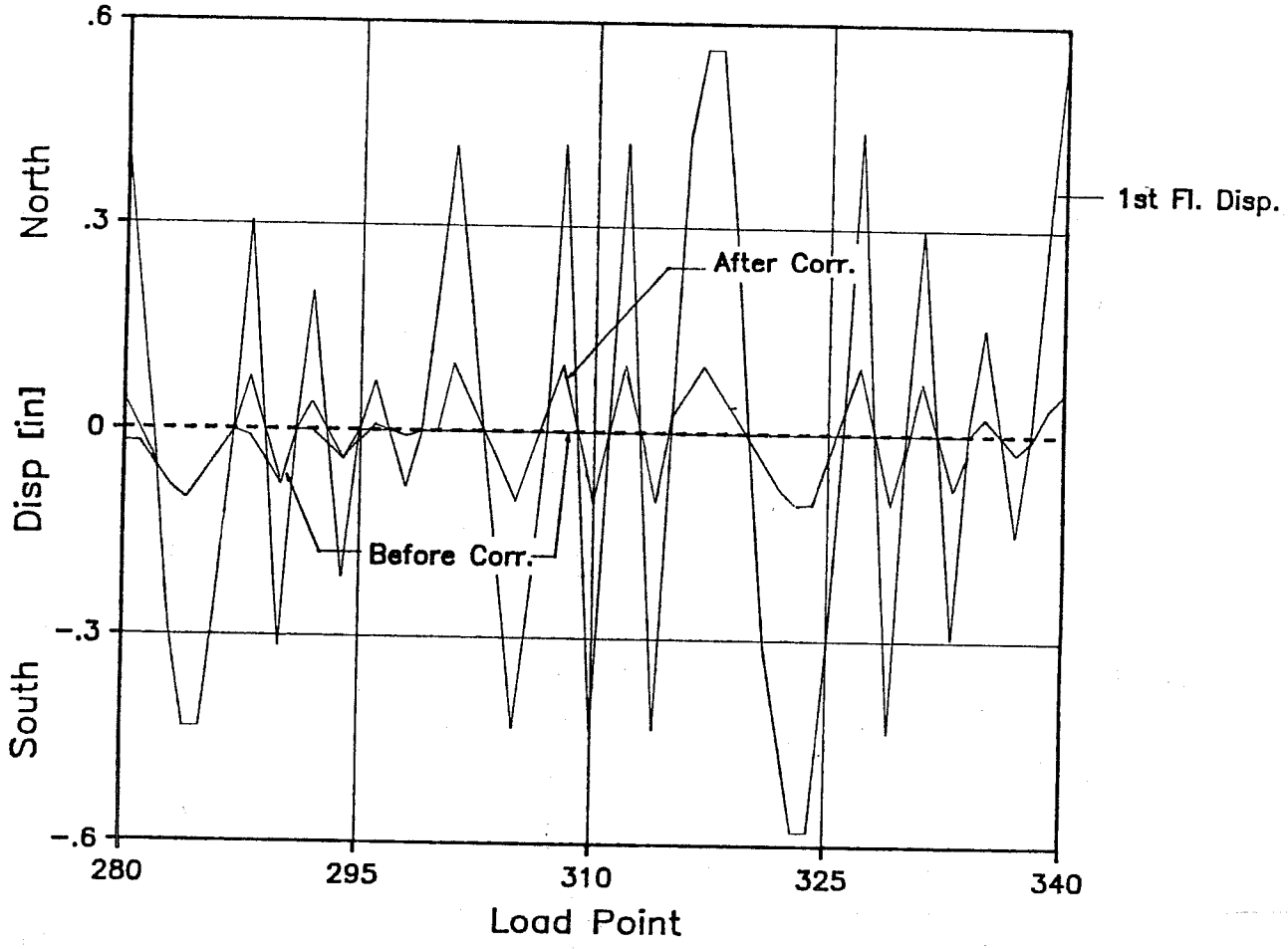

Figure B.16 Sp. 2a: North Wall Slip Correction in Zone of No Available Readings (5)

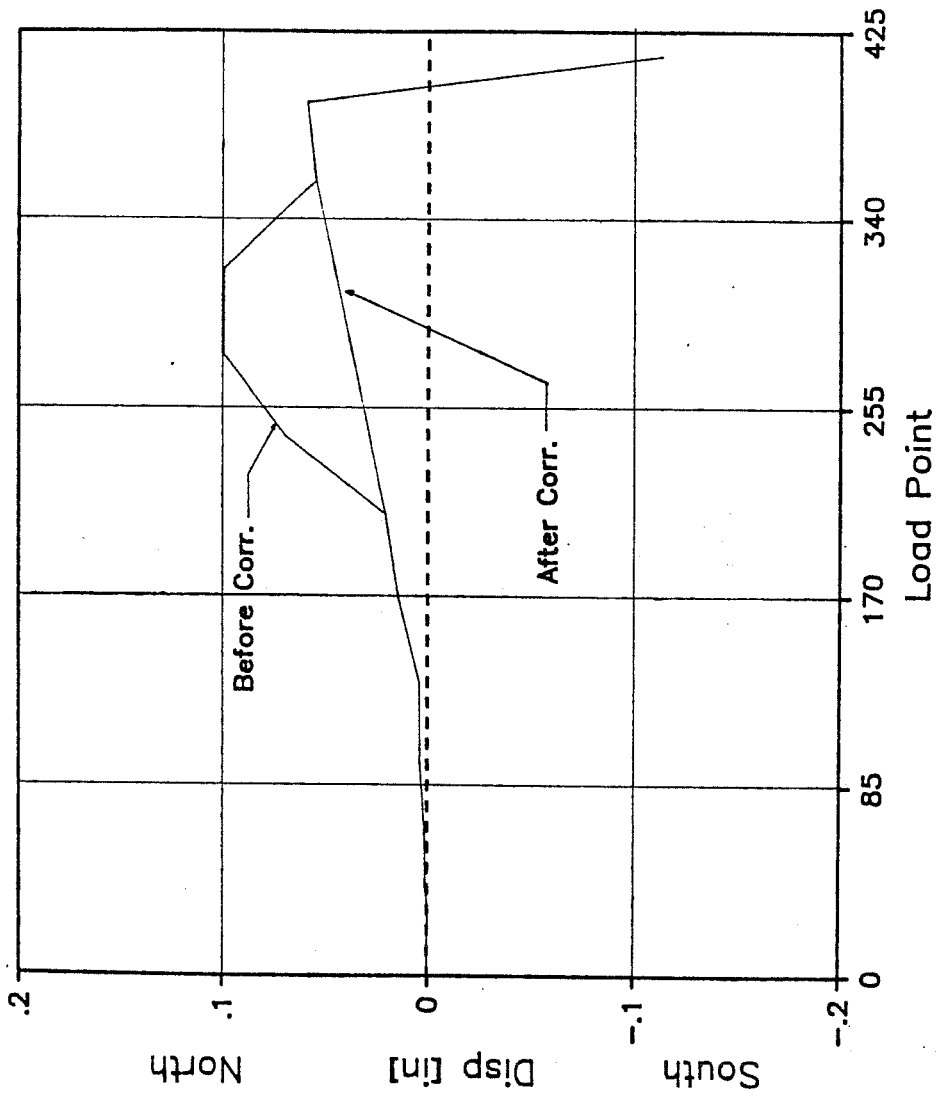

Figure B.17 Sp. 2a: North Wall Peak Slip Correction in Zone of Large Peaks (5) - North Load Direction

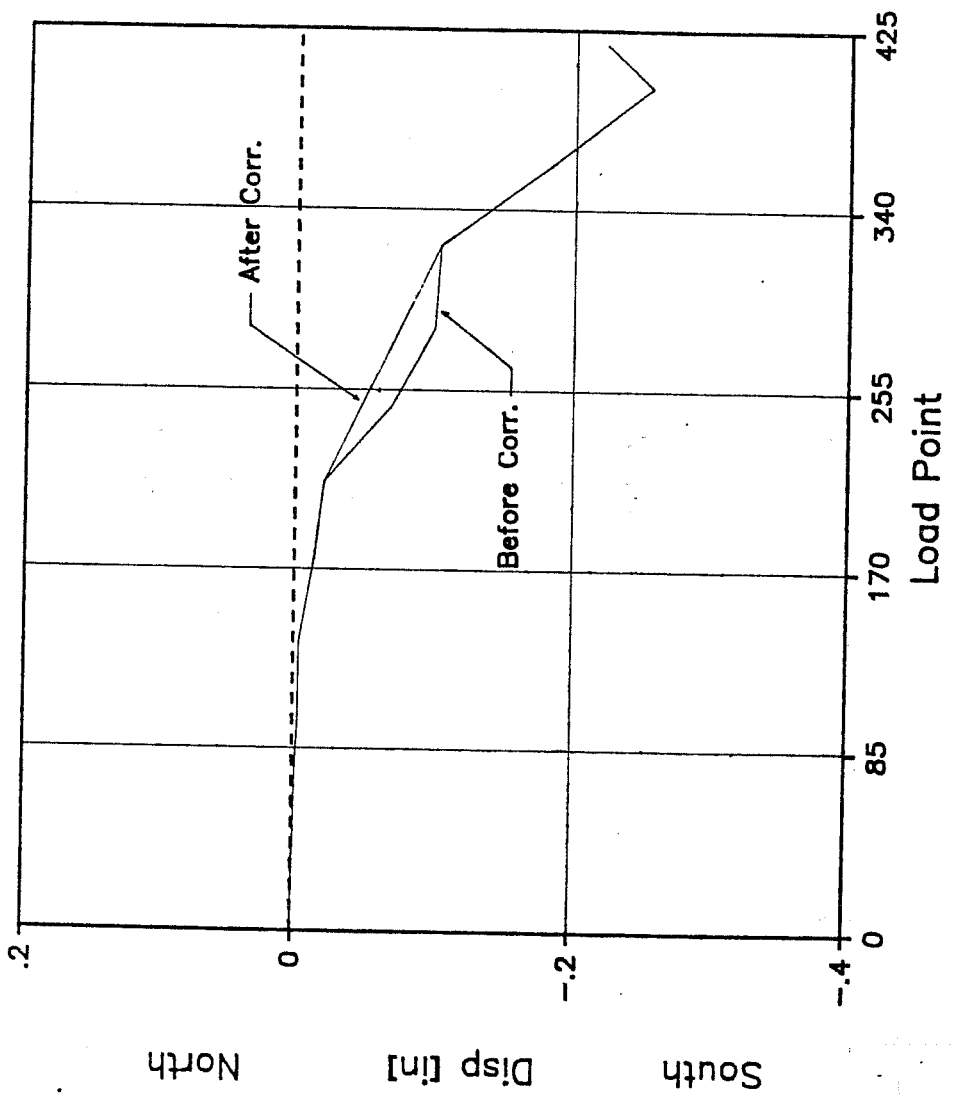

Figure B.18 Sp. 2a: North Wall Peak Slip Correction in Zone of Large Peaks (5) - South Load Direction

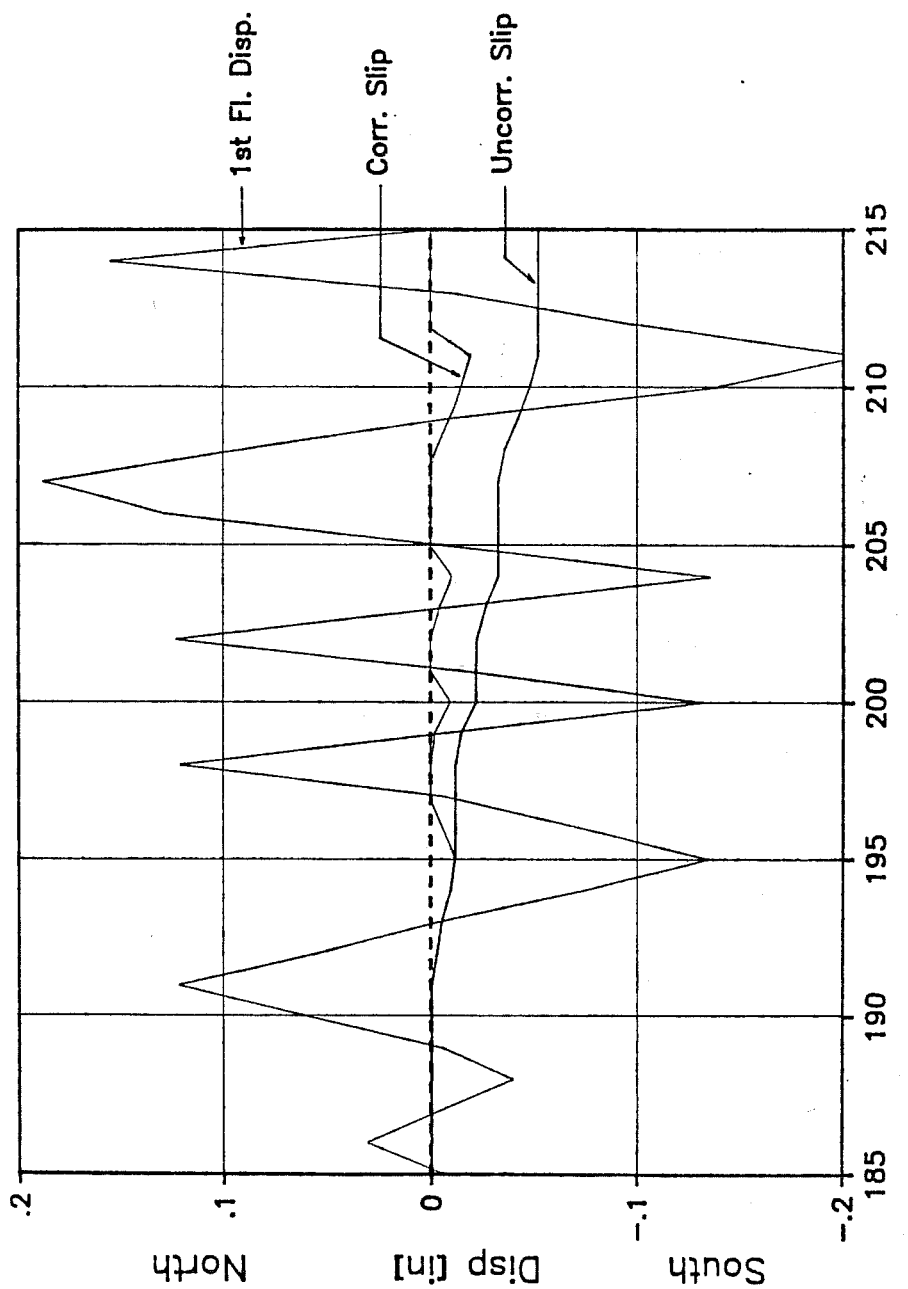

Figure B.19 Sp. 2a: South Wall Slip After Accumulated Uni-Directional Reading Correction (1)

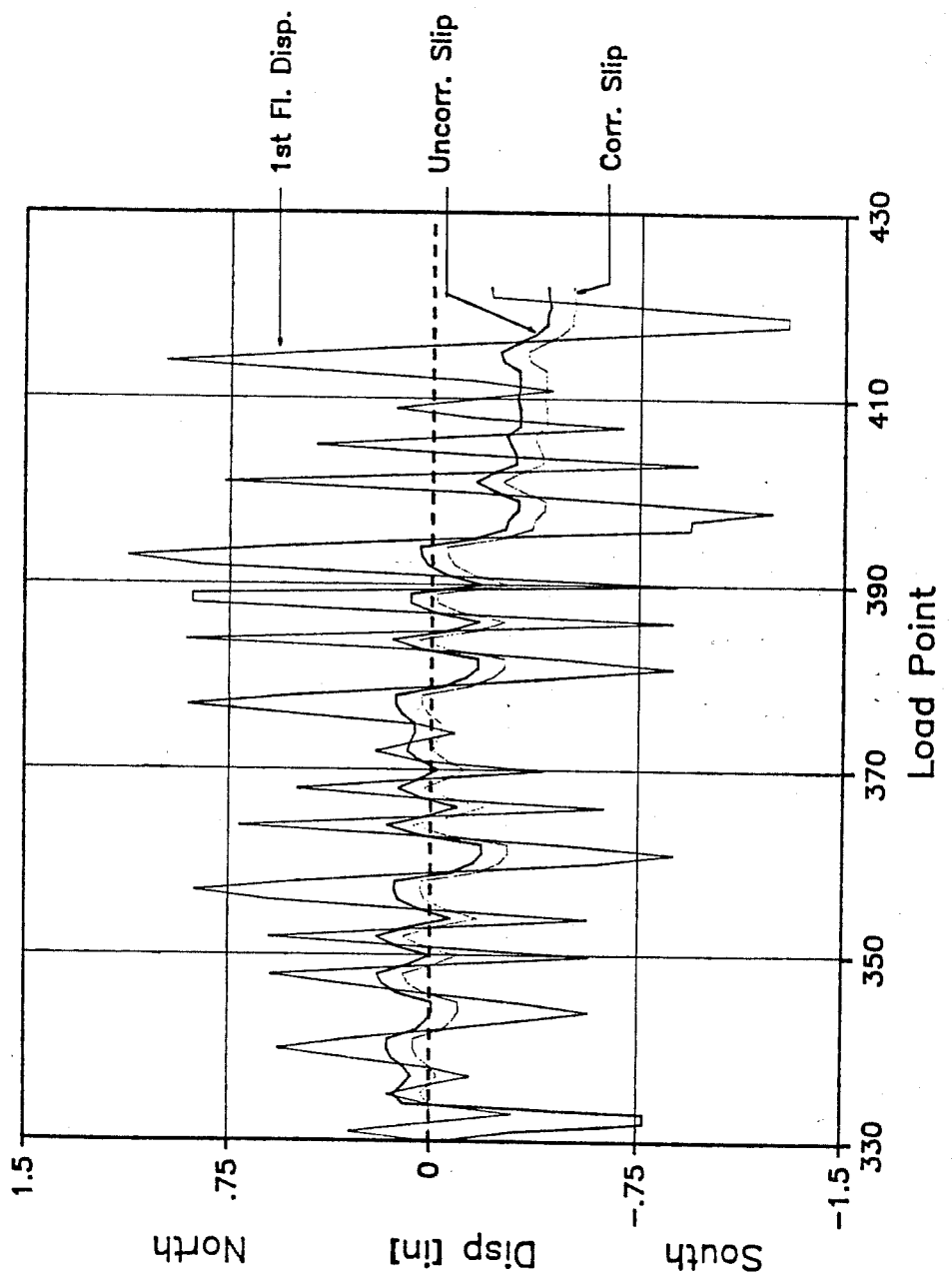

Figure B.20 Sp. 2a: South Wall Slip After Zero Level Correction (2)

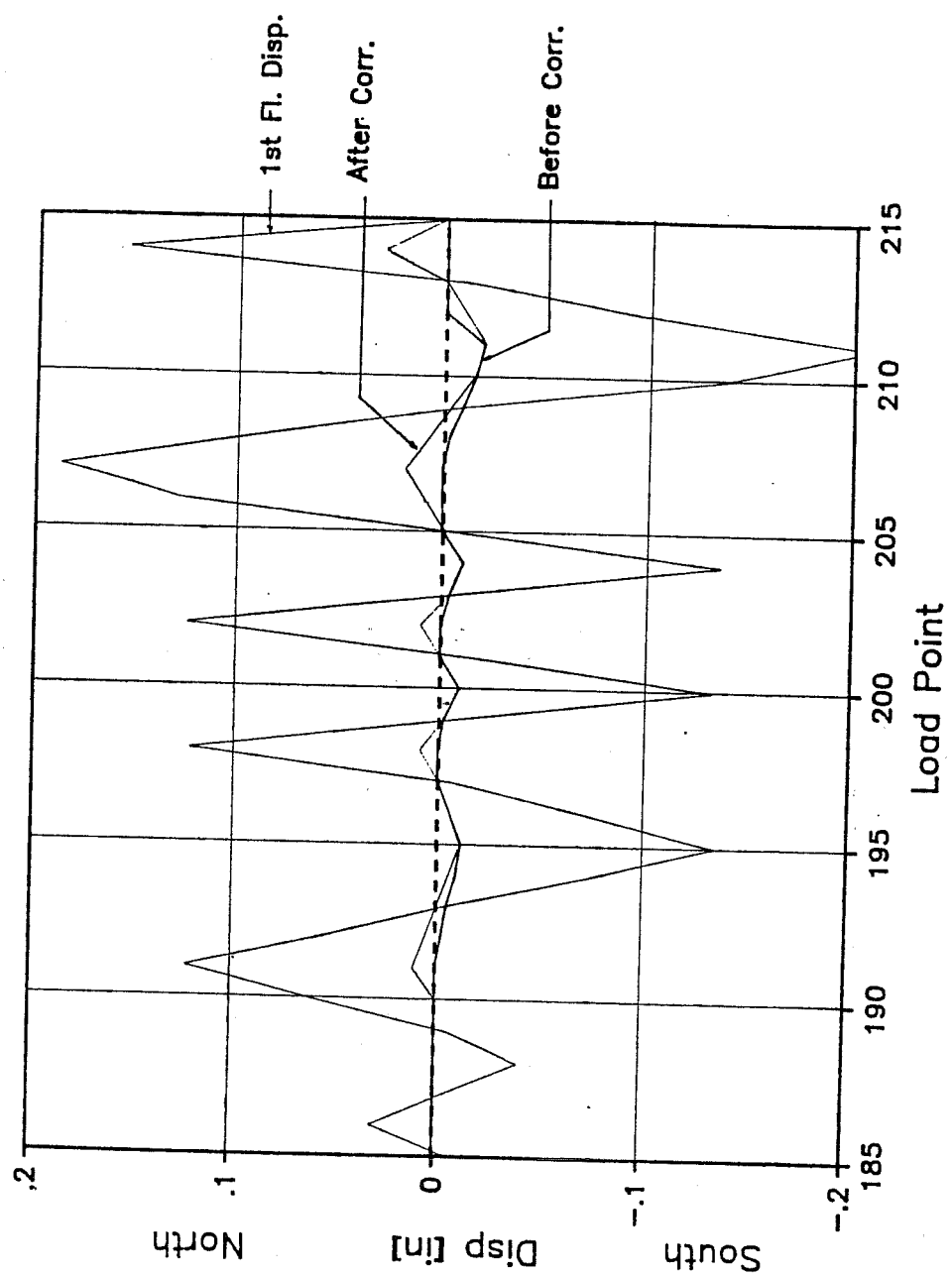

Figure B.21 Sp. 2a: South Wall Slip After Correction for Uni-Directional Readings (3)

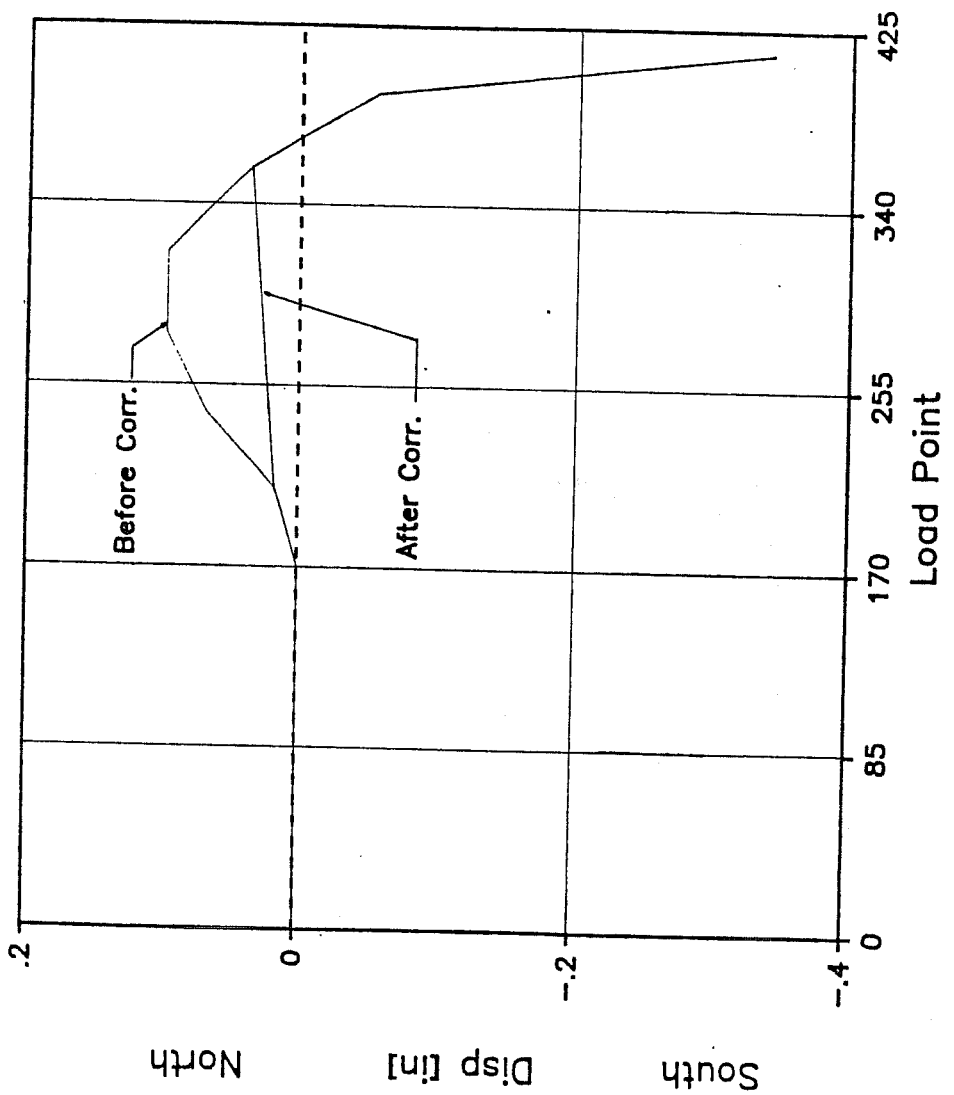

Figure B.22 Sp. 2a: South Wall Peak Slip Correction in Zone of Large Peaks (5) - North Load Direction

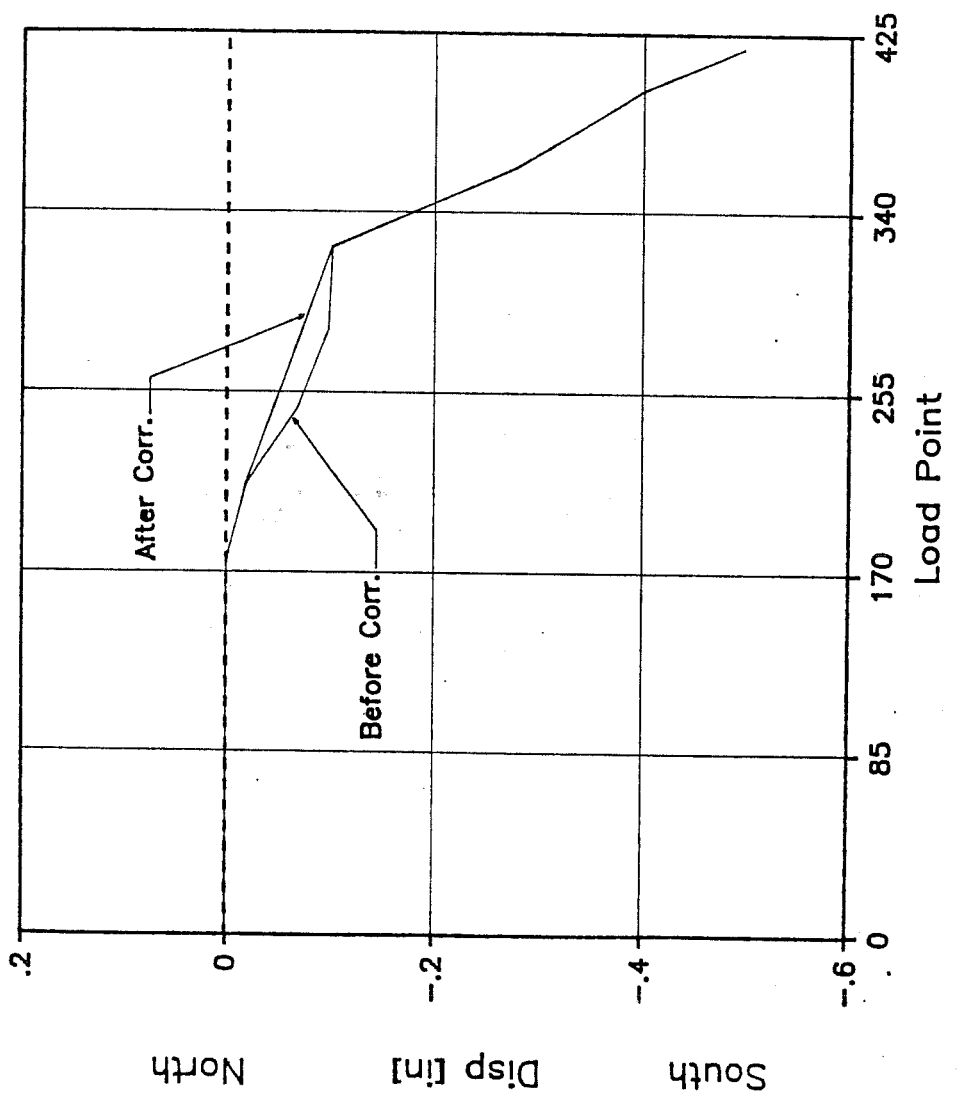

Figure B.23 Sp. 2a: South Wall Peak Slip Corrections in Zone of Large Peaks (5) - South Load Direction

APPENDIX C
CORRECTIONS OF CHANNEL 81 AND 87 STRAIN GAUGE READINGS FOR SPECIMEN 2b

Introduction:

During the testing of Specimen 2b, loading problems at Load Point 36 caused the zero base line to be shifted for Strain Gauge Channels 81 and 87. Channel 81 and 87 are located on the extreme south longitudinal reinforcement bar in the south wall (Fig. 5.9). The load spike to the south placed this bar in compression as shown in Figures C.1 and C.2. At the spike, the strain reading for Channel 81 (located at the base of the south wall) was 0.00272, very close to the typical ultimate strain of masonry (0.003). This suggests that the coupled wall was close to its flexural capacity. No evidence to support the readings was found: crushing of the compression toe was not observed; flexural cracking at the base was minimal; and the coupled walls were not close to its maximum flexural capacity (Load Point 36: Base Shear = 30.7 kips, Maximum Base Shear = 78.3 kips to the south). Based on these facts, corrections to the zero base line were made for Strain Gauge Channels 81 and 87.

Corrections of Channels 81 and 87:

Channel 81 (Figure C.1)

Corrections from Load Jump after Load Point 36 to Load Point 40: Load Point 37 was read at a base shear of approximately zero. The strain was changed to correspond with the approximate strain of zero base shear before the jump ($\epsilon \approx 26.29 \times 10^{-6}$). For the load jump after Load Point 36 and Load Points 38 to 40, the strain gauge readings were modified by subtracting from their strain gauge reading the original strain reading at Load Point 37 and then adding the new zero value ($\epsilon \approx 26.29 \times 10^{-6}$) for Load Point 37.

Corrections from Load Point 41 to End of Testing: Load Point 43 was taken at a base shear of about zero. The strain was changed to correspond with the approximate strain for zero base shear before the jump ($\epsilon \approx 26.29 \times 10^{-6}$). For Load Points 41, 42 and 44 to the end of testing, The strain gauge readings were modified by subtracting from their strain gauge reading the original strain gauge reading at Load Point 43 and then adding the new zero value ($\epsilon \approx 26.29 \times 10^{-6}$) for Load Point 43.

Channel 87 (Figure C.2)

The values for the Load Points were modified in the same manner as for Channel 81 except that a strain of -130.9 x 10^{-6} for the zero base shear was used.

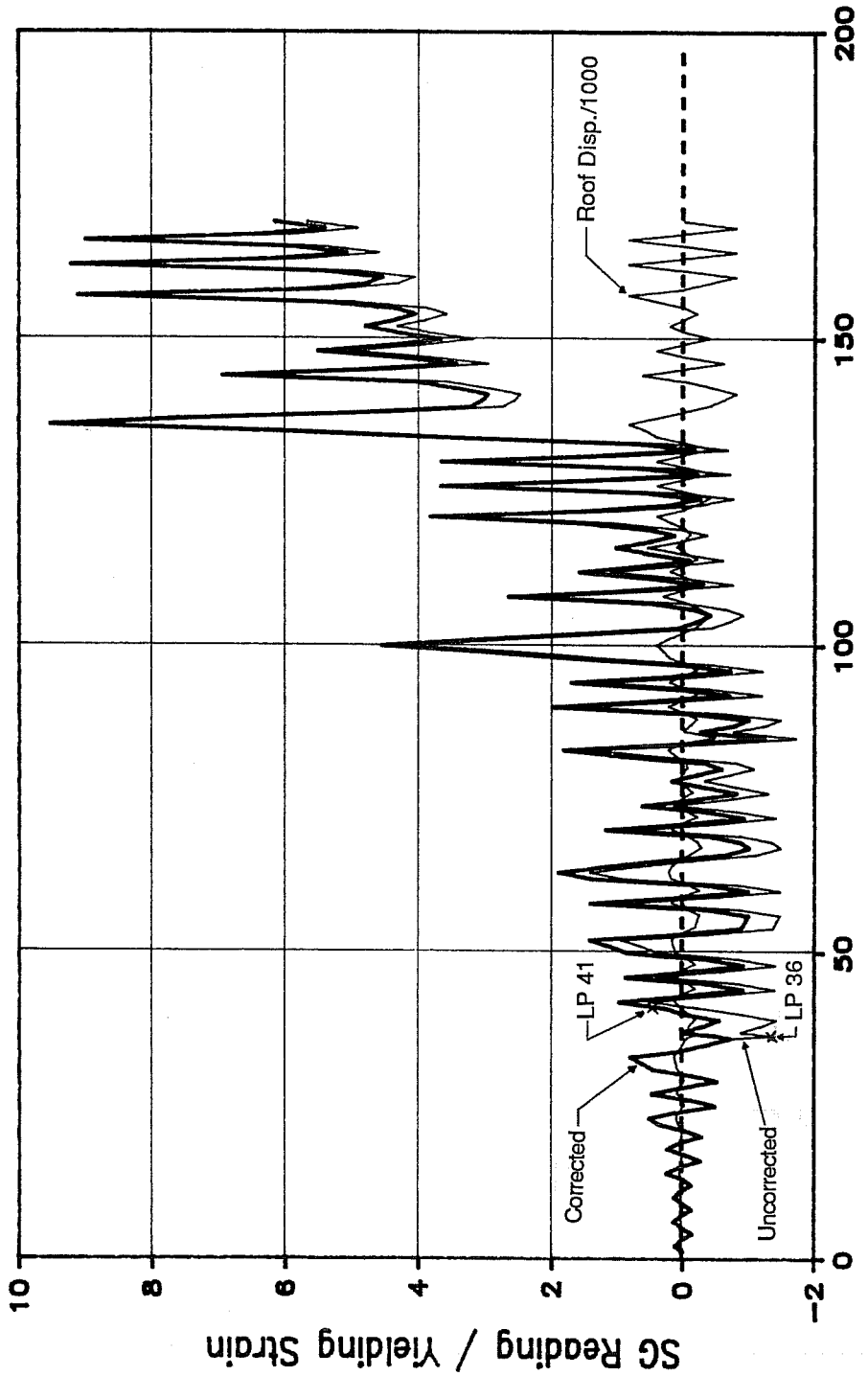

Figure C.1 Sp. 2b: Corrections to Channel 81 Strain Gauge Readings

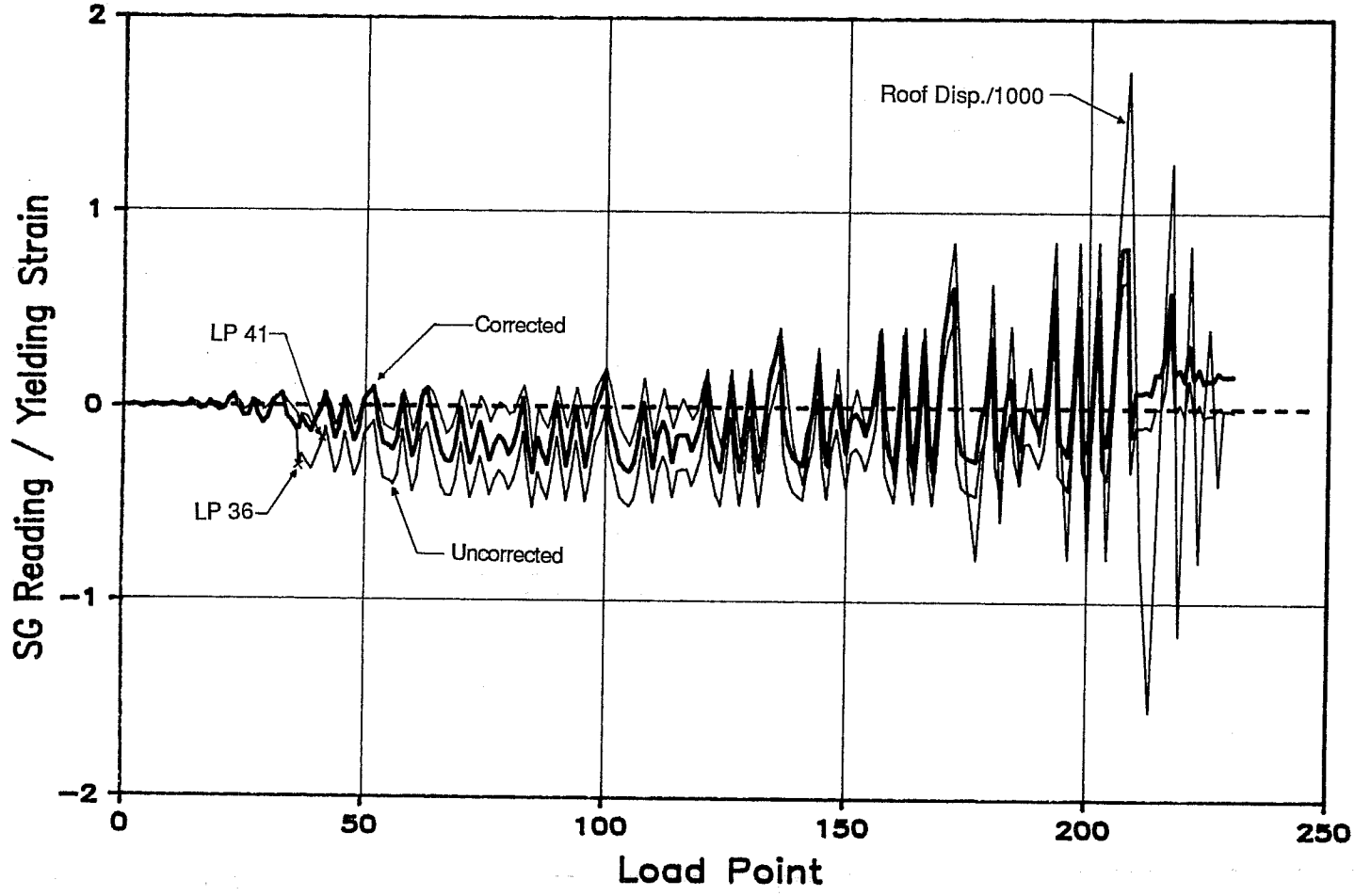

Figure C.2 Sp. 2b: Corrections to Channel 87 Strain Gauge Readings

APPENDIX D
WALL DEFORMATIONS

Introduction

Walls of Specimens 2a and 2b were provided with the instrumentation necessary to measure lateral displacements at each story, and to measure and/or compute all the components of these displacements. The methods used to compute each component of the total lateral displacement are described in this appendix.

Total Lateral Displacement

Each wall was instrumented with linear potentiometers at the floor levels to measure directly the total lateral displacements (Figs. 5.4 and 5.8).

Since all the displacement components were measured or computed independently, it was possible to assess the accuracy of the results by calculating the difference between the measured total displacement and the summation of all the components.

Flexural Displacements

Each wall story was instrumented with four pairs of linear potentiometers intended to measure rotation of the walls' cross sections. Potentiometers were placed at vertical lines close to the edges of the walls. Since flexural deformations were expected to be concentrated close to the bases of the walls, three of these pairs were evenly distributed in the lower half of the first story walls, with the last pair covering the upper half of the wall. In the second story walls, the four pairs were evenly distributed along the wall height (Figs. 5.4 and 5.8).

Rotations of the cross sections were computed as the difference between cumulative displacements at both edges of the section, divided by the horizontal distance between the gauges.

Flexural displacements were computed assuming a linear variation of rotation between gauges. This assumption implies a constant curvature between wall cross sections defined by the position of the pairs of gauges. Since an important part of flexural deformation is due to the concentrated rotation at the bases of the walls, rotation measured with the bottom pair of gauges was assumed to be distributed over a height of one inch only. Flexural displacements were calculated integrating this distribution of rotations.

Shear Displacements

Each wall story was instrumented with two linear potentiometers intended to measure angular deformations of that story. Potentiometers were placed at diagonal lines as shown in Figures 5.4 and 5.8.

Angular deformation γ, calculated as the function of diagonal deformations, is given by:

$$\gamma = (\Delta_1 - \Delta_2)d/2\ell h$$

Where:

Δ_1, Δ_2 : Deformation of diagonals
d : Length of gauge (diagonal)
ℓ : Horizontal length of gauge
h : Vertical length of gauge

Assuming diagonal deformations are due only to shear effect, shear displacement u_s is given by:

$$u_s = \gamma H$$

Where:

H : Total wall height

Since flexural deformation contributes to deformation of the diagonals in the case of non-uniform curvature, it was necessary to correct the above expression for shear displacement to take flexural effects into account. The method proposed by Hiraishi [26] was used:

$$u_s = \gamma H - \left[u_b + (v_r - v_l)h/2\ell\right] H/h$$

Where:

u_b : Flexural lateral displacement of the zone covered by diagonal gauges
v_r, v_l : Vertical displacements measured at the top right and left ends respectively of the zone covered by diagonal gauges

In the case of the first story walls, since the diagonal gauges did not cover wall base deformations, flexural and vertical displacements measured with the bottom gauges covering this area were not considered in the correction term.

In the case of the second story walls, shear displacements before correction resulted smaller than the correction term. For this reason, no correction was made in this case.

Slip Displacements

Slip displacements were obtained directly using potentiometers at each wall-base beam joint and wall-slab joint (Figs. 5.4 and 5.8).

APPENDIX E
ECCENTRIC SHEAR STRESS CALCULATIONS FOR SPECIMENS 2a AND 2b

Introduction:

The eccentric shear stress model for slab-column connections [15] is used to calculate the eccentric shear transfer for Specimens 2a and 2b. These calculations are used to indicate possible problems with the transfer of shear and moment from the coupling slab to the wall.

Eccentric Shear Stress Calculations:

Formula Definitions: (as applicable to Specimens 2a and 2b)

$$v_c = (V_u \;/\; A_{cs}) \pm (\gamma_v * M_s * c_v \;/\; J_c) \qquad \text{[Eqn. (5) Ref. 25]}$$

where:

v_c = factored concrete shear stress

V_n = $M_n \;/\; \ell_{coupling\ slab}$

A_{cs} = area of critical section (area of slab-wall interface using assumed effective depth)

γ_v = percentage of unbalanced moment to be transferred by eccentric shear (assumed as 1.0 for this case)

M_s = M_n (nominal slab flexural capacity)

c_v = distance from geometric centroid of the slab critical section to the point where the shear stress is calculated

J_c = polar moment of inertia of the slab critical section about its geometric centroid

Eccentric Shear Capacity of Specimen 2a

Assume: Effective depth (d) equal to depth from top of slab to bottom reinforcement (6.5 inches).

Wall width (x) = 5.625 inches

Wall length (ℓ_w) = 72 inches

Calculate c_v:

$c_v = \ell w^2$ * d / A_{cs} which reduces to: $(\ell_w)^2$ / (2*ℓ_w + x)

where:

ℓ_w = 72 in. (length of wall)

d = 6.5 in.

A_{cs} = 1197 in^2

c_v = 34.65 in.

Calculate J_c:

J_c = [2(d * ℓ_w^3) / 12] + [2(ℓ_w * d^3) / 12] + (x * d * c_v^2) + 2[ℓ_w * d * ($\frac{1}{2}$ ℓ_w - c_v)^2 (same formula for both Specimens)

J_c = 463,775.03 in.

Calculate v_c:

where:

M_n = M_{s1} + M_{s2}; (M_{s1} = M_{s2} = 760.1 kip-in; Subsection 6.3.2)

M_n = 1520.2 kip-in

V_n = 1520.2 kip-in / 56 in;

Calculate concrete shear stress (using Eqn. 5):

v_c = 136 psi

Calculate shear strength resistance:

V_o = $(2 + 4/\beta_c) * \sqrt{f'_c}$

ϕ is not used since the actual concrete strength is known.

f'_c = 3660 psi (Table 3.7)

β_c = 72 in / 5.625 = 12.8

V_o = 140 psi

$v_c < V_o$ O.K.

Eccentric Shear Capacity of Specimen 2b

Assume: Effective depth (d) equal to a minimum depth of 2 inches and a maximum depth of 8 inches. Calculate eccentric shear capacity for both cases since actual case is somewhere between these two values.

$c_v =$ 34.65 in (same as for Specimen 2a; not dependent on d)

Calculate eccentric shear stress using minimum depth of 2 inches:

$A_{cs} =$ 299.25 in^2

$J_c =$ 138,543.88 in^4

Calculate v_c:

where:

$M_n =$ $M_{s1} + M_{s2}$; (M_{s1} = 1343 kip-in, M_{s2} = 478 kip-in; Subsection 6.3.2)

$M_n =$ 1821 kip-in

$V_n =$ 1821 kip-in / 56 in;

Calculate concrete shear stress (using Eqn. 5):

$v_c =$ 564 psi

Calculate shear strength resistance:

$V_o =$ $(2 + 4/\beta_c) * \sqrt{f'_c}$

ϕ is not used since the actual concrete strength known.

$f'_c =$ 3670 psi

$\beta_c =$ 72 in / 5.625 = 12.8

$V_o =$ 140 psi

$v_c > V_o$ Not Adequate

Calculate eccentric shear stress using maximum depth of 8 inches:

$A_{cs} =$ 1197 in^2

$J_c =$ 559,935.53 in^4

Calculate v_c:

where:

$$M_n = M_{s1} + M_{s2};\ (M_{s1} = 1343 \text{ kip-in}, M_{s2} = 478 \text{ kip-in; Subsection 6.3.2})$$

$$M_n = 1821 \text{ kip-in}$$

$$V_n = 1821 \text{ kip-in} / 56 \text{ in};$$

Calculate concrete shear stress (using Eqn. 5):

$$v_c = 140 \text{ psi}$$

Calculate shear strength resistance:

$$V_o = (2 + 4/\beta_c) * \sqrt{f'_c}$$

ϕ is not used since the actual concrete strength is known.

$$f'_c = 3670 \text{ psi}$$

$$\beta_c = 72 \text{ in} / 5.625 = 12.8$$

$$V_o = 140 \text{ psi}$$

$v_c \approx V_o$ O.K. for maximum assumption of d = 8 inches

APPENDIX F
DESCRIPTION OF DATA FILES FOR SPECIMENS' 2A AND 2B

Introduction:

Copies of the diskette can be obtained from Dr. Richard E. Klingner, professor of Civil Engineering at The University of Texas at Austin. Mailing address is: Ferguson Structural Engineering Laboratory, 10100 Burnet Road #24, Austin, Texas, 78758.

The diskette contains a WordPerfect 5.0 version of this document file (AppdxF), an ASCII version of the same file (AppdxF.ASC), and the data files themselves (Sp2a.CSV for Specimen 2a and Sp2b.CSV for Specimen 2b). The data files contain results obtained from the tests of Task 3.1(c)'s Specimen 2a in September 1988 and Specimen 2b in April 1989. These files are in CSV (Comma Separated Value) format, and are written in matrix form, with 38 columns and 422 rows for Specimen 2a and with 62 columns and 230 rows for Specimen 2b. Each row contains the values of different quantities obtained in one scan (LP, or Load Point). Values in each row are separated by commas. Some quantities are direct readings from the data acquisition system; others have been derived from one or more direct readings.

The first row contains the titles assigned to each column. Each title contains the column number and a brief description of the quantity. The rows correspond to the scans describing the test history.

Each column contains the values of one of the quantities measured during the test or computed after the test. Some locations in the matrix are blank (there is nothing between the commas). Such locations must be skipped; they cannot be filled in with zeros.

Description of Data Columns:

Specimen 2a Data File: Sp2a.CSV

(1) Load Point: Identifies the scan number.

(2) North Peak Load Point: Load point numbers corresponding to roof displacement peaks when the specimen was loaded in the north direction. Only some of the column positions are filled.

(3) South Peak Load Point: Load point numbers corresponding to roof displacement peaks when the specimen was loaded in the south direction. Only some of the column positions are filled.

(4) Base Shear: Total lateral load applied on the specimen in kips. During the load-controlled phase of the test (LP 1 to LP 137), the base shear was obtained as four times the reading of Channel 64 which corresponded to the reading from the load cell in one of the jacks at the top floor. During the displacement-controlled phase, (LP 137 to end of test), the base shear was calculated as twice the summation of readings of Channel 64 and Channel 65, corresponding to load cells in one of the jacks at the roof and at the 2nd floor respectively.

(5) Base Slip: Slip between the base beam and the laboratory floor, obtained directly from Channel 63.

(6) 2nd Floor Displacement: Lateral displacement (inches) of the center plane of the 2nd floor slab. This was obtained by correcting the readings from Channel 30, by the base beam slip (Column 5 above).

(7) Roof Displacement: Lateral displacement (inches) of the center plane of the roof slab. This was obtained by correcting the readings from Channel 31, by the base beam slip (Column 5 above).

(8) Slip of the north wall base with respect to the base beam (inches). This was obtained after extensive corrections to the readings from Channel 52 [24].

(9) Slip of the south wall base with respect to the base beam (inches). This was obtained after extensive corrections to the readings from Channel 21 [24].

(10) Lateral displacement (inches) of the north wall at the 2nd floor, due just to concentrated rotation at the wall base. Base rotation was computed from readings of displacement transducers on Channels 32 and 40. Corresponding lateral displacement was calculated by multiplying that base rotation by the height of the 2nd floor above the base.

(11) Lateral displacement (inches) of the north wall at the 2nd floor, due to concentrated rotation at the base of the wall (Column 10 above), plus the flexural displacement computed from readings of the displacement transducers on Channels 33 and 41, 34 and 42, and 35 and 43. Constant curvature was assumed within each gauge length.

(12) Lateral displacement (inches) at the top of the north wall, due just to concentrated rotation at the wall base. Base rotation was computed from readings of displacement transducers on Channels 32 and 40. Corresponding lateral displacement was calculated by multiplying that base rotation by the height of the top of the specimen above the base.

(13) Lateral displacement (inches) at the top of the north wall, due to concentrated rotation at the base of the wall (Column 12 above), plus the flexural displacement computed from readings of the displacement transducers on Channels 33 and 41, 34 and 42, 35 and 43, 36 and 44, 37 and 45, 38 and 46, and 39 and 47. Constant curvature was assumed within each gauge length.

(14) Lateral displacement (inches) of the south wall at the 2nd floor, due just to concentrated rotation at the wall base. Base rotation was computed from readings of displacement transducers on Channels 1 and 9. Corresponding lateral displacement was calculated by multiplying that base rotation by the height of the 2nd floor above the base.

(15) Lateral displacement (inches) of the south wall at the 2nd floor, due to concentrated rotation at the base of the wall (Column 14 above), plus the flexural displacement computed from readings of the displacement transducers on Channels 2 and 10, 3 and 11, and 4 and 12. Constant curvature was assumed within each gauge length.

(16) Lateral displacement (inches) at the top of the south wall, due just to concentrated rotation at the wall base. Base rotation was computed from readings of displacement transducers on Channels 1 and 9. Corresponding lateral displacement was calculated by multiplying that base rotation by the height of the top of the specimen above the base.

(17) Lateral displacement (inches) at the top of the south wall, due to concentrated rotation at the base of the wall (Column 16 above), plus the flexural displacement computed from readings of the displacement transducers on Channels 2 and 10, 3 and 11, 4 and 12, 5 and 13, 6 and 14, 7 and 15, and 8 and 16. Constant curvature was assumed within each gauge length.

(18) Lateral displacement (inches) at the 2nd floor and at the roof of the north wall, due to shearing deformations. Shearing deformations in the 1st story of the north wall were calculated from the readings of the displacement transducers on Channels 48 and 49 with corrections for flexural deformation (Appendix E) . Since readings obtained from 2nd-story displacement transducers on Channels 50 and 51 were below the sensitivity of the transducers, shearing deformations were assumed to be zero in the second story, and the displacement due to shearing deformations only is therefore the same for the roof, as for the 2nd floor.

(19) Lateral displacement (inches) at the 2nd floor and at the roof of the south wall, due to shearing deformations. Shearing deformations in the 1st story of the south wall were calculated from the readings of the displacement transducers on Channels

17 and 18 with corrections for flexural deformations (Appendix E). Since readings obtained from 2nd-story displacement transducers on Channels 19 and 20 were below the sensitivity of the transducers, shearing deformations were assumed to be zero in the second story, and the displacement due to shearing deformations only is therefore the same for the roof, as for the 2nd floor.

(20) Strain (μin./in.) in the longitudinal wall reinforcement at the south edge of the north wall base (Channel 106).

(21) Strain (μin./in.) in the longitudinal wall reinforcement at the north edge of the north wall base (Channel 107).

(22) Strain (μin./in.) in the longitudinal wall reinforcement at the south edge of the south wall base (Channel 81).

(23) Strain (μin./in.) in the longitudinal wall reinforcement at the center of the south wall base (Channel 82).

(24) Strain (μin./in.) in the longitudinal wall reinforcement at the north edge of the south wall base (Channel 83).

(25) Strain (μin./in.) in the south end of the bottom transverse reinforcement in the first story of the north wall (Channel 122).

(26) Strain in μin./in. at the north end of the bottom transverse reinforcement in the first story of the north wall (Channel 123).

(27) Strain (μin./in.) at the center of the transverse reinforcement at the mid-height of the first story of the north wall (Channel 124).

(28) Strain (μin./in.) at the south end of the bottom transverse reinforcement in the first story of the south wall (Channel 98).

(29) Strain (μin./in.) at the north end of the bottom transverse reinforcement in the first story of the south wall (Channel 99).

(30) Strain (μin./in.) at the center of the transverse reinforcement at the mid-height of the first story of the south wall (Channel 100).

(31) Strain (μin./in.) at the south end of the top transverse reinforcement in the first story of the south wall (Channel 101).

(32) Strain (μin./in.) at the north end of the top transverse reinforcement in the first story of the south wall (Channel 102).

(33) Strain (μin./in.) in the top longitudinal reinforcement of the coupling beam, at the top face of the 2nd floor slab, close to the south edge of the north wall (Channel 130).

(34) Strain (μin./in.) in longitudinal slab reinforcement at the top face of the 2nd floor slab, close to mid- width between wall and edge of slab (Channel 131).

(35) Strain (μin./in.) in other longitudinal slab reinforcement at the top face of the 2nd floor slab, close to the edge of the slab (Channel 132).

(36) Strain (μin./in.) in the top longitudinal reinforcement of the coupling beam, at the top face of the roof slab, close to the south edge of the north wall (Channel 136).

(37) Strain (μin./in.) in longitudinal slab reinforcement at the top face of the roof slab, close to mid-width between wall and edge of slab (Channel 137).

(38) Strain (μin./in.) in other longitudinal slab reinforcement at the top face of the roof slab, close to the edge of slab (Channel 138).

Specimen 2b Data File: Sp2b.CSV

(1) Load Point: Identifies the scan number.

(2) North Peak Load Point: Load point numbers corresponding to roof displacement peaks when the specimen was loaded in the north direction. Only some of the column positions are filled.

(3) South Peak Load Point: Load point numbers corresponding to roof displacement peaks when the specimen was loaded in the south direction. Only some of the column positions are filled.

(4) Base Shear: Total lateral load applied on the specimen in kips. During the load-controlled phase of the test (LP 1 to LP 81), the base shear was obtained as four times the reading of Channel 64 which corresponded to the reading from the load cell in one of the jacks at the top floor. During the displacement-controlled phase, (LP 81 to end of test), the base shear was calculated as twice the summation of readings of Channel 64 and Channel 66, corresponding to load cells in one of the jacks at the roof and at the 2nd floor respectively.

(5) Base Slip: Slip between the base beam and the laboratory floor, obtained directly from Channel 63.

(6) North Wall 2nd Floor Displacement: Lateral displacement (inches) of the center plane of the north edge of the 2nd floor slab, obtained directly from Channel 61.

(7) South Wall 2nd Floor Displacement: Lateral displacement (inches) of the center plane of the south edge of the 2nd floor slab, obtained directly from Channel 30.

(8) Average 2nd Floor Displacement: Average lateral displacement (inches) of Channels 30 and 61 (columns (5) and (6)) at the center plane of the 2nd floor slab.

(9) North Wall Roof Displacement: Lateral displacement (inches) of the center plane of the north edge of the roof slab, obtained directly from Channel 62.

(10) South Wall Roof Displacement: Lateral displacement (inches) of the center plane of the south edge of the roof slab, obtained directly from Channel 31.

(11) Average Roof Displacement: Lateral displacement (inches) of the center plane of the roof slab. Average lateral displacement (inches) of Channels 31 and 62 (columns (9) and (10)) at the center plane of the roof slab.

(12) Slip of the north wall base with respect to the base beam (inches), obtained directly from Channel 52.

(13) Slip of the south wall base with respect to the base beam (inches), obtained directly from Channel 21.

(14) Lateral displacement (inches) of the north wall at the 2nd floor, due just to concentrated rotation at the wall base. Base rotation was computed from readings of displacement transducers on Channels 32 and 40. Corresponding lateral displacement was calculated by multiplying that base rotation by the height of the 2nd floor above the base.

(15) Lateral displacement (inches) of the north wall at the 2nd floor, due to concentrated rotation at the base of the wall (Column 14 above), plus the flexural displacement computed from readings of the displacement transducers on Channels 33 and 41, 34 and 42, and 35 and 43. Constant curvature was assumed within each gauge length.

(16) Lateral displacement (inches) at the top of the north wall, due just to concentrated rotation at the wall base. Base rotation was computed from readings of displacement transducers on Channels 32 and 40. Corresponding lateral displacement was calculated by multiplying that base rotation by the height of the top of the specimen above the base.

(17) Lateral displacement (inches) at the top of the north wall, due to concentrated rotation at the base of the wall (Column 16 above), plus the flexural displacement computed from readings of the displacement transducers on Channels 33 and 41,

34 and 42, 35 and 43, 36 and 44, 37 and 45, 38 and 46, and 39 and 47. Constant curvature was assumed within each gauge length.

(18) Lateral displacement (inches) of the south wall at the 2nd floor, due just to concentrated rotation at the wall base. Base rotation was computed from readings of displacement transducers on Channels 1 and 9. Corresponding lateral displacement was calculated by multiplying that base rotation by the height of the 2nd floor above the base.

(19) Lateral displacement (inches) of the south wall at the 2nd floor, due to concentrated rotation at the base of the wall (Column 18 above), plus the flexural displacement computed from readings of the displacement transducers on Channels 2 and 10, 3 and 11, and 4 and 12. Constant curvature was assumed within each gauge length.

(20) Lateral displacement (inches) at the top of the south wall, due just to concentrated rotation at the wall base. Base rotation was computed from readings of displacement transducers on Channels 1 and 9. Corresponding lateral displacement was calculated by multiplying that base rotation by the height of the top of the specimen above the base.

(21) Lateral displacement (inches) at the top of the south wall, due to concentrated rotation at the base of the wall (Column 20 above), plus the flexural displacement computed from readings of the displacement transducers on Channels 2 and 10, 3 and 11, 4 and 12, 5 and 13, 6 and 14, 7 and 15, and 8 and 16. Constant curvature was assumed within each gauge length.

(22) Lateral displacement (inches) at the 2nd floor of the north wall, due to shearing deformations. Shearing deformations in the 1st story of the north wall were calculated from the readings of the displacement transducers on Channels 48 and 49, with corrections for flexural deformations (Appendix E).

(23) Lateral displacement (inches) at the roof of the north wall, due to shearing deformations. Shearing deformations in the 2nd story wall were added to the 1st story shearing deformations (Column (22) above).

(24) Lateral displacement (inches) at the 2nd floor of the south wall, due to shearing deformations. Shearing deformations in the 1st story of the south wall were calculated from the readings of the displacement transducers on Channels 17 and 18, with corrections for flexural deformations (Appendix E).

(25) Lateral displacement (inches) at the roof of the south wall, due to shearing deformations. Shearing deformations in the 2nd story of the south wall were added to 1st story south wall shearing deformations (Column (24) above).

(26) Strain (μin./in.) in the longitudinal wall reinforcement at the south edge of the north wall base (Channel 109).

(27) Strain (μin./in.) in the longitudinal wall reinforcement at the center of the north wall base (Channel 110).

(28) Strain (μin./in.) in the longitudinal wall reinforcement at the north edge of the north wall base (Channel 111).

(29) Strain (μin./in.) in the longitudinal wall reinforcement at the south edge of the south wall base (Channel 81). Corrections were made to Channel 81 readings due to load problems.

(30) Strain (μin./in.) in the longitudinal wall reinforcement at the center of the south wall base (Channel 82).

(31) Strain (μin./in.) in the longitudinal wall reinforcement at the north edge of the south wall base (Channel 83).

(32) Strain (μin./in.) in the longitudinal wall reinforcement at the south edge of the top of the first story north wall (Channel 115).

(33) Strain (μin./in.) in the longitudinal wall reinforcement at the center of the top of the first story north wall (Channel 116).

(34) Strain (μin./in.) in the longitudinal wall reinforcement at the north edge of the top of the first story north wall (Channel 117).

(35) Strain (μin./in.) in the longitudinal wall reinforcement at the south edge of the top of the first story south wall (Channel 87).

(36) Strain (μin./in.) in the longitudinal wall reinforcement at the center of the top of the first story south wall (Channel 88).

(37) Strain (μin./in.) in the longitudinal wall reinforcement at the north edge of the top of the first story south wall (Channel 89).

(38) Strain (μin./in.) in the longitudinal wall reinforcement at the south edge of the base of the second story north wall (Channel 118).

(39) Strain (μin./in.) in the longitudinal wall reinforcement at the center of the base of the second story north wall (Channel 119).

(40) Strain (μin./in.) in the longitudinal wall reinforcement at the north edge of the base of the second story north wall (Channel 120).

(41) Strain (μin./in.) in the longitudinal wall reinforcement at the south edge of the base of the second story south wall (Channel 90).

(42) Strain (μin./in.) in the longitudinal wall reinforcement at the center of the base of the second story south wall (Channel 91).

(43) Strain (μin./in.) in the longitudinal wall reinforcement at the north edge of the base of the second story south wall (Channel 92).

(44) Strain (μin./in.) in the longitudinal wall reinforcement at the south edge of the top of the second story north wall (Channel 124).

(45) Strain (μin./in.) in the longitudinal wall reinforcement at the center of the top of the second story north wall (Channel 125).

(46) Strain (μin./in.) in the longitudinal wall reinforcement at the north edge of the top of the second story north wall (Channel 126).

(47) Strain (μin./in.) in the longitudinal wall reinforcement at the south edge of the top of the second story south wall (Channel 96).

(48) Strain (μin./in.) in the longitudinal wall reinforcement at the center of the top of the second story south wall (Channel 88).

(49) Strain (μin./in.) in the longitudinal wall reinforcement at the north edge of the top of the second story south wall (Channel 89).

(50) Strain (μin./in.) in the south end of the bottom transverse reinforcement in the first story of the north wall (Channel 127).

(51) Strain in μin./in. at the north end of the bottom transverse reinforcement in the first story of the north wall (Channel 128).

(52) Strain (μin./in.) at the center of the transverse reinforcement at the mid-height of the first story of the north wall (Channel 129).

(53) Strain (μin./in.) at the south end of the top transverse reinforcement in the first story of the north wall (Channel 130).

(54) Strain (μin./in.) at the north end of the top transverse reinforcement in the first story of the north wall (Channel 131).

(55) Strain (μin./in.) at the south end of the bottom transverse reinforcement in the first story of the south wall (Channel 99).

(56) Strain (μin./in.) at the north end of the bottom transverse reinforcement in the first story of the south wall (Channel 100).

(57) Strain (μin./in.) at the center of the transverse reinforcement at the mid-height of the first story of the south wall (Channel 101).

(58) Strain (μin./in.) at the south end of the top transverse reinforcement in the first story of the south wall (Channel 102).

(59) Strain (μin./in.) at the north end of the top transverse reinforcement in the first story of the south wall (Channel 103).

(60) Strain (μin./in.) in the top longitudinal reinforcement of the coupling beam, at the top face of the 2nd floor slab, close to the north edge of the north wall (Channel 139).

(61) Strain (μin./in.) in the top longitudinal reinforcement of the coupling beam, at the top face of the roof slab, close to the north edge of the north wall (Channel 137).

(62) Strain (μin./in.) in the bottom longitudinal reinforcement of the coupling beam, at the bottom face of the roof slab, close to the north edge of the north wall (Channel 138).

REFERENCES

1. Noland, J. L., "A Review of the U.S. Coordinated Program for Masonry Building Research," submitted to the National Science Foundation, October 1988.

2. Antrobus, N., "Development and Construction of Masonry Shear Wall Specimens," M.S. Report, The University of Texas at Austin, May 1988.

3. Paulay, T. M., "The Design of Ductile Reinforced Concrete Structural Walls for Earthquake Resistance," ***Earthquake Spectra***, Vol. 2, No. 4, 1986.

4. Paulay, T. M., and Taylor, R. G., "Slab Coupling of Earthquake-Resisting Shearwalls," ***ACI Journal***, V. 78, No. 11, March-April 1981, pp. 130-140.

5. Priestley, M. J. N., "Seismic Design of Concrete Masonry Shearwalls," ***ACI Journal***, V. 83, No. 1, Jan.- Feb. 1986, pp.58-67.

6. Englekirk, R. E. and Hart, G. C., ***Earthquake Design of Concrete Masonry Buildings: Volume 2 Strength Design of One- to Four-Story Buildings***, Prentice-Hall, New Jersey, 1982.

7. Shing, P. B., Klamerus, E. W., Schuller, M. P. and Noland, J. L., "Behavior of Single-Story Reinforced Masonry Shear Walls under In-Plane Cyclic Lateral Loads," ***Proceedings***, Fourth North American Masonry Conference, San Diego, California, October 1988.

8. Hidalgo, P. and Luders, C., "Shear Strength of Reinforced Masonry Walls under Earthquake Excitation," ***Proceedings***, Third U.S. National Conference on Earthquake Engineering, Charleston, South Carolina, August 1986, pp. 1,335 - 1,346.

9. Priestley, M. J. N., "The Role of Research in the Formulation of Masonry Design Procedures," ***Proceedings***, Fourth North American Masonry Conference, Los Angeles, California, August 1987, pp. 3-1 - 3-14.

10. International Conference of Building Officials, ***Uniform Building Code***, 1988 Edition, Whittier, California, 1988.

11. Grimm, C. T., "Appendix XI. Selection and Use of Mortar for Unit Masonry," ***ArE 345k Masonry Engineering Class Notes***, The University of Texas at Austin, Summer 1988.

12. Klingner, Richard E., "CE 397: Modern Topics in Masonry Engineering", ***Class Notes*** (Lectures #1 - #6), The University of Texas at Austin, Fall 1988.

13. International Conference of Building Officials, ***Uniform Building Code***, 1985 Edition, Whittier, California, 1985.

14. Klingner, Richard E., "TCCMAR Task 3.1(c): In- Plane Seismic Resistance of Two Story Concrete Masonry Walls with Openings," ***Interim Report***, presented at Boulder, Colorado, September 11, 1987.

15. ACI Committee 318, ***Building Code Requirements for Reinforced Concrete (ACI 318-83)***, American Concrete Institute, Detroit, 1983.

16. Kingsley Gregory R., Atkinson-Noland & Associates, "Nondestructive Evaluation of Two-Story Shear Wall Specimen 2a, TCCMAR Task 3.1(c)," ***Internal Report***, September 6, 1988.

17. Woodward, Kyle A. and Jirsa, James O., "Design and Construction of a Floor Wall Reaction System", ***CESRL Report No 77-4***, December 1977.

18. ***Manual of Steel Construction, Load and Resistance Factor Design***, 1st Edition, American Institute of Steel Construction, Chicago, 1986.

19. Porter, Max L., "Sequential Phased Displacement (SPD) Loading for TCCMAR Testing," presented at Keystone, Colorado, September 1986.

20. ***PCI Design Handbook, Precast and Prestressed Concrete***, Third Edition, Prestressed Concrete Institute, Chicago, Illinois, 1985.

21. Park, R. and Paulay, T., ***Reinforced Concrete Structures***, John Wiley & Sons, NY, 1975.

22. ***Plastic Design in Steel, a Guide and Commentary***, Joint Committee of the Welding Research Council and the American Society of Civil Engineers, 2nd Edition, ASCE, 1971.

23. Farahany, M., "User-Oriented Computer Program for Flexural Behavior of General Reinforced Concrete Sections," M. Sc. Thesis, The University of Texas at Austin, December 1983.

24. Klingner, R. E., Leiva, G., and Merryman, M., "Status Report: TCCMAR Task 3.1(c): In-Plane Seismic Resistance of Two Story Concrete Masonry Walls with Openings," presented at Salt Lake City, Utah, January 12-13, 1989.

25. Klingner, R. E., Leiva, G., and Merryman, M., "TCCMAR Task 3.1(c) - Specimen 2a Test Results," ***Internal Report***, January 16,1989.

26. Hiraishi, Hisahiro, "Evaluation of Shear and Flexural Deformations of Flexural Type Shear Walls," ***Bulletin of the New Zealand National Society for Earthquake Engineering***, Vol. 17, No. 2, June 1984, pp. 135-144.